DNA and Hydrogels for Sensing and Binding Purine Nucleosides

by

Yuqing Li

A thesis

presented to the University of Waterloo

in fulfilment of the

thesis requirement for the degree of

Doctor of Philosophy

in

Chemistry

Waterloo, Ontario, Canada, 2021

©Yuqing Li 2021

Examining Committee Membership

The following served on the Examining Committee for this thesis. The decision of the Examining Committee is by majority vote.

External Examiner	**Dr. Hongquan Zhang** Associate Professor, Department of Laboratory Medicine & Pathology, University of Alberta, Edmonton, Canada.
Supervisor	**Dr. Juewen Liu** Professor, Department of Chemistry, University of Waterloo, Waterloo, Canada.
Internal Member	**Dr. Vivek Maheshwari** Associate Professor, Department of Chemistry, University of Waterloo, Waterloo, Canada.
Internal Member	**Dr. Xiaosong Wang** Professor, Department of Chemistry, University of Waterloo, Waterloo, Canada.
Internal-external Member	**Dr. Boxin Zhao** Professor, Department of Chemical Engineering, University of Waterloo, Waterloo, Canada.

Author's Declaration

This thesis consists of material all of which I authored or co-authored: see Statement of Contributions included in the thesis. This is a true copy of the thesis, including any required final revisions, as accepted by my examiners.

I understand that my thesis may be made electronically available to the public.

Statement of Contributions

The work presented in this thesis are performed by the author and several collaborators. The resulting publications and contributions of each collaborator are listed below in details.

The work in the Chapter 2 has been published as: Yuqing Li, Biwu Liu, Zhicheng Huang, Juewen Liu, Engineering base-excised aptamers for highly specific recognition of adenosine. *Chemical Science*, **2020**, *11*, 2735-2743. All the experiments were performed by the first author. Biwu Liu and Zhicheng Huang provided valuable suggestions for performing experiments. The manuscript was written by Yuqing Li and Juewen Liu.

The work in the Chapter 3 has been published as: Yuqing Li, Juewen Liu, Highly specific recognition of guanosine using engineered base excised aptamers. *Chemistry-A European Journal*, **2020**, *26*, 13644-13651. All the experiments were performed by the first author. The manuscript was written by the two authors.

The work in the Chapter 4 has been published as: Yuqing Li, Zijie Zhang, Biwu Liu, Juewen Liu, Incorporation of boronic acid into aptamer-based molecularly imprinted hydrogels for highly specific recognition of adenosine, *ACS Applied Bio Materials*, **2020**, *3*, 2568-2576. All the experiments were performed by the first author. Zijie Zhang and Biwu Liu helped for the experimental design and data analysis. The manuscript was written by Yuqing Li and Juewen Liu.

The work in the Chapter 5 has been published as: Yuqing Li, Hang Gao, Zengyao Qi, Zhicheng Huang, Lingzi Ma, Juewen Liu, Freezing-assisted conjugation of unmodified diblock DNA to hydrogel nanoparticles and monoliths for DNA and Hg^{2+} sensing, *Angewandte Chemie*, **2021**, *133*, 2-9. All the experiments were performed by Yuqing Li, Hang Gao and Zengyao Qi. Zhicheng Huang helped for getting TEM data.

Lingzi Ma helped for DNA purification. The manuscript was written by Yuqing Li and Juewen Liu.

Abstract

Purine nucleosides, such as adenosine and guanosine, are important biomolecules to regulate physiological functions, including maintain heart and brain health, exert inflammatory responses, and take part in metabolisms. Abnormal levels of purine nucleosides can lead to serious problems. Therefore, monitoring their concentrations is critical for understanding their biological roles and performing related disease diagnoses. Compared with conventional methods to detect them, such as high-performance liquid chromatography (HPLC) and mass spectrometry, DNA aptamer-based strategies are highly attractive due to their high specificity, binding affinity, low cost, and in situ detection ability. Ideally, the aptamers with any desired specific binding abilities could be isolated by systematic evolution of ligands by exponential enrichment (SELEX); however, currently, some selected aptamers cannot distinguish closely related molecules. For example, the widely used adenosine aptamer is effective in distinguishing it from other nucleosides (G, C, T and U) but not the adenine monophosphate (AMP) and adenine triphosphate (ATP), consequently aptamer-sensing platforms built by this sequence are also limited in molecular recognition. In addition, the DNA aptamers for guanosine are not isolated yet. On the other hand, to further graft aptamers on hydrogel matrix for applications, chemical modifications are also inevitable, leading to the high cost of aptamer engineering. To solve these problems, the primary focus of this thesis is to improve the specificity of aptamer-based sensors for detecting purine nucleosides, and develop a modification-free method for preparing DNA-hydrogels at reduced costs.

Targeting the problem of some SELEX-derived aptamers with intrinsically limited specificity, a novel method is developed in chapter 2 to achieve highly specific recognition of adenosine. Typically, an entire adenine nucleotide was excised from the backbone of the existing adenosine aptamer (mentioned above), in which the resulting vacancy on DNA scaffold allowed highly specific re-binding of free adenosine, this

way realized its molecular recognition and other cognate analytes including AMP, ATP, guanosine, cytidine, uridine, and theophylline are distinguished. This method is termed "base-excision". To characterize the adenosine recognition, SYBR Green I (SGI) fluorescence spectroscopy and isothermal titration calorimetry (ITC) were used. The ITC demonstrated that one A-excised aptamer strand can bind to two adenosine molecules, with a K_d of 17.0 ± 1.9 μM at 10 °C, and entropy-driven binding. Since the wide-type aptamer cannot discriminate adenosine from AMP and ATP, we attribute this improved specificity to the excised site. Finally, the A-excised aptamer was tested in diluted fetal bovine serum (FBS) and showed a limit of detection of 46.7 μM adenosine. This work provides a facile, cost-effective, and non-SELEX method to engineer existing aptamers for new features and better applications.

In chapter 3, the aptamer engineering strategy described in chapter 2 is further used to generate new DNA aptamers for specific recognition of guanosine. Both the Na^+-binding aptamer and classical adenosine aptamer were manipulated as the base-excising scaffold. A total of seven guanosine aptamers were designed, in which a guanine-excised Na^+-aptamer showed the highest binding specificity and affinity for guanosine, with an apparent K_d of 0.78 mM. Both the aptamer scaffold generality and excised-site generality were systematically studied. This work provides a few guanosine binding aptamers by non-SELEX method. It also provides deeper insights into engineering aptamers for molecular recognition.

On the other hand, since the adenosine only differs deoxyadenosine by a 2′-OH and the specific recognition of adenosine from their mixture have not been realized by current methods, in chapter 4, molecularly imprinted polymers (MIPs) and aptamers as two different recognition strategies are combined. A boronic acid-containing monomer, 3-acrylamidophenylboronic acid (AAPBA), was incorporated into the MIPs to specifically target *cis*-diol moiety in the ribose of adenosine. ITC and SYBR Green I staining were used to measure the binding. The AAPBA-containing aptamer-MIP

exhibited a 115-fold high selectivity for adenosine against deoxyadenosine at pH 6.4. The ribose in adenosine may interact with the boronic acid unit and decrease its inhibition effect to the aptamer in the MIP. Whereas for deoxyadenosine, it does not bear a *cis*-diol, and thus cannot rescue the aptamer. This work provides insights into the combination of aptamers with other functional groups in MIPs, which may further broaden applications in ways that free aptamers cannot achieve alone.

From an application perspective, since the current preparations of DNA-hydrogels are heavily relying on acrydite-modified DNA, lowering the cost of grafting DNA on hydrogels is another issue. To this end, a modification-free method is studied in chapter 5. We show that unmodified penta-adenine (A_5) can reach up to 75% conjugation efficiency in 8 h under a freezing polymerization condition in polyacrylamide hydrogels. DNA incorporation efficiency was reduced by forming duplex or other folded structures and by removing the freezing condition. By designing diblock DNA containing an A_5 block, various functional DNA sequences were attached. Such hydrogels were designed for ultrasensitive DNA hybridization and Hg^{2+} detection, with detection limits of 50 pM and 10 nM, respectively, demonstrating the feasibility of using unmodified DNA to replace acrydite-DNA. The same method works for both gel nanoparticles and monoliths. This work reveals interesting reaction products by exploiting freezing and has provided a cost-effective way to attach DNA to hydrogels.

Overall, improved molecular recognition of adenosine and guanosine has been achieved, through engineering existing aptamers for new functions or combining aptamers with other functional molecules in MIPs. To further facilitate the incorporation of DNA aptamers in hydrogel systems for various applications, the modification-free method is also developed. This thesis deepens our understandings in DNA aptamer-based molecular recognition and in nucleic acid chemistry, as well as provides opportunities for researchers to achieve more specific adenosine and

guanosine recognitions in real applications for disease monitoring and diagnosis purpose.

Acknowledgements

First and foremost, I would like to express my deepest appreciation to my supervisor Dr. Juewen Liu. Thank you so much for accepting me as your graduate student four years ago, although we just had a brief interview through Skype at that time. Thank you for your trust. During my studies at the University of Waterloo, your guidance, help, support, and encouragement are always with me, especially when I am in difficulties. I am really appreciated and feel quite lucky to be one of your graduate students. Also, thank you for training me from a beginner in doing research to a PhD student that acquires many basic skills in designing projects, carrying out experiments, analyzing data, writing research papers and delivering presentations. They are all important abilities and skills for my future career. Moreover, I am also greatly affected by your positive personality and good working habits, and I believe these are valuable assets for me as well.

At the same time, I would like to sincerely thank my original committee members Dr. Vivek Maheshwari and Dr. Boxin Zhao and Dr. Xiaosong Wang. Thank you for your professional guidance and suggestions for my research projects, and your warm help for writing reference letters to support my scholarship applications. I am very appreciated for that. Also, I would like to extend my gratitude to my external examiner Dr. Hongquan Zhang from the University of Alberta for taking time to attend my examination and giving valuable suggestions. My gratitude also goes to Cathy and Kim, for their patience and support in helping me complete my PhD program.

I also wish to thank all my friends and colleagues in Liu lab. Special thanks are expressed to Dr. Zijie Zhang, Dr. Biwu Liu, Lingzi Ma, Zhicheng Huang and Mohamad Zandieh. Thank you for your help and care. My happiest memories in Waterloo are being with you. Also, my sincere thanks are extended to Dr. Yibo Liu, Dr. Po-Jung Jimmy Huang, Dr. Runjhun Saran, Dr. Jinyi Zhang, Anand Lopez, Yichen Zhao,

Woohyun J. Moon, Tianmeng Yu and all of our visiting scholars and students. Thank you for your help and suggestions on my experiments.

Last but not the least, I would like to send my love to my parents and my boyfriend including his parents. Although you are not living in Canada, you are being with me in another way to share my experiences, feelings, and emotions. Pursuing a PhD at Waterloo alone pushes me to grow up and to be a more independent person; but without my family, I probably cannot be so brave in exploring my life and studies.

Dedication

I would like to dedicate this thesis to my beloved family.

Table of Contents

List of Figures

List of Tables

List of Abbreviations

A	Adenine
AADPA	Acrylamidophenylboronic acid
AAm	Acrylamide
ADP	Adenosine diphosphate
AMP	Adenosine monophosphate
APS	Ammonium persulfate
ATP	Adenosine triphosphate
BIS	*N,N'*-methylenebis(acrylamide)
C	cytidine
cDNA	complementary DNA
DLS	dynamic light scattering
DMPA	*N*-[3-(dimethylamino)propyl]methacrylamide
DMSO	dimethyl sulfoxide
DNA	deoxyribonucleic acid
FAM	6-carboxyfluorescein
FBS	Fetal bovine serum
G	guanine
GMP	guanosine monophosphate
GTP	guanosine triphosphate
HEPES	4-(2-hydroxyethyl)-1-piperazineethanesulfonic acid
ITC	Isothermal titration calorimetry

MES	2-(N-morpholino)-ethanesulfonic acid
MIP	Molecularly imprinted polymers
NIP	Non-molecularly imprinted polymer
NIPAm	*N*-isopropylacrylamide
SDS	sodium dodecyl sulfate
SGI	SYBR Green I
T	Thymine
TEM	Transmission electron microscopy
TEMED	*N, N, N′, N′*-tetramethylethylenediamine
ThT	Thioflavin T
Tris	tris(hydroxymethyl)aminomethane
U	Uridine

Chapter 1 Introduction

1.1 DNA aptamers

1.1.1 DNA

Deoxyribonucleic acid (DNA) are functional biomacromolecules that are tightly packaged in nucleus and carries genetic information. The conformation of DNA is normally described as a right-handed double helix, in which two strands run opposite and twist with each other (antiparallel, B-form) (Figure 1.1A). The backbone of DNA molecule is built up by sugar-phosphate components, in which phosphodiester bonds are presented in linking two nucleotides (Figure 1.1B). Within the DNA structure, each nucleotide is composed of three parts: a pentose sugar, a phosphate group and a nucleobase. The nucleobases include adenine (A), guanine (G), cytosine (C) and thymine (T); and they can interact by forming canonical Watson-Crick base pairs (A-T and G-C, Figure 1.1C), or through other non-canonical ways.

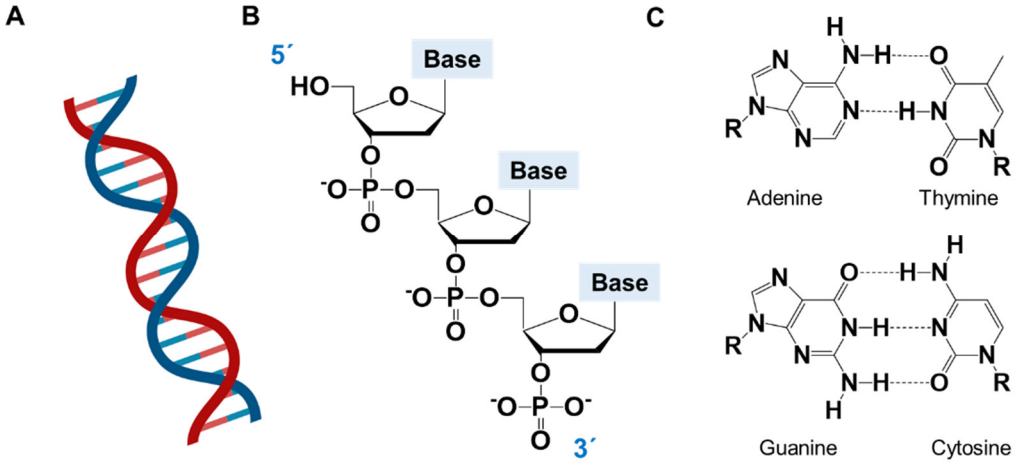

Figure 1.1 Chemical structures of DNA. (A) The helical structure of double-stranded DNA. (B) A single-stranded DNA showing sugar-phosphate backbone. (C) Four types of nucleobases forming Watson-Crick base pairs.

1.1.2 DNA aptamers for binding small molecules

Aptamers are single-stranded oligonucleotides that can specifically bind ligands with high affinity. The term "aptamer" was coined by Ellington and Szostak in 1990,[1] when they isolated RNA sequences for organic dyes such as Cibacron Blue. In the same year, Tuerk and Gold selected an RNA aptamer for recognizing bacteriophage T4 DNA polymerase (gp43),[2] where they named this aptamer isolation strategy to be systematic evolution of ligands by exponential enrichment (SELEX), indicating high-affinity nucleic acid strands for a ligand were isolated and exponentially enriched. After these pioneer works, the aptamer field has taken off. Many different targets have been studied ranging from small molecules, peptides, proteins to even cells. Although antibodies are able to specifically bind analytes with high affinity and specificity, some small-molecule detections have been shown non-specific on antibody-based assays; and at the same time, their high costs, batch-to-batch variation and short shelf life also limit the application of antibodies for on-site biosensing.[3] Therefore, the isolation of aptamers for those small molecules received particular interest. In addition, considering the higher stability of DNA than RNA, DNA aptamers are more preferred in practical applications.

In 1995, Huizenga and Szostak isolated the first DNA aptamer for adenosine and ATP (Figure 1.2A), with an excellent specificity on nucleobase region (K_d ~6 μM adenosine).[4] This aptamer has no affinity to other nucleosides containing G, T, U or C bases, but it is not sensitive to the phosphate part and cannot distinguish adenosine from AMP or ATP. Later, Landry et al. obtained another DNA aptamer for cocaine over its metabolites having 0.4-10 μM cocaine affinity (Figure 1.2B).[5] To transduce binding events to detectable signals for biosensing, these isolated aptamers are often post-modified by a fluorophore to track their ligand-induced conformational changes. Considering that this process requires additional characterization and optimization steps to ensure the original recognition abilities of aptamer are reserved, new selections for signaling aptamers are also discovered. For example, Nutiu and Li isolated a new signaling ATP aptamer, in which the DNA library was designed by having a red domain

hybridized with a quencher-labeled complementary oligonucleotide and two flanked green domains for ligand recognition (Figure 1.2C).[6] In the stem area, a fluorophore-labeled oligonucleotide (denoted in black) was also included in which its fluorescence was initially quenched. Then, upon binding the ATP and a conformational change, the quencher-labeled oligonucleotide may dissociate and trigger fluorescence emission. After selection, the isolated aptamer complex can be directly used as a sensor. On the other hand, to solve the specificity problems for some early obtained aptamers, such as the classic adenosine aptamer isolated by Szostak group having poor ability in distinguishing adenosine and ATP,[4] counterselections[7-9] and some non-SELEX based strategies[10-12] are also developed.

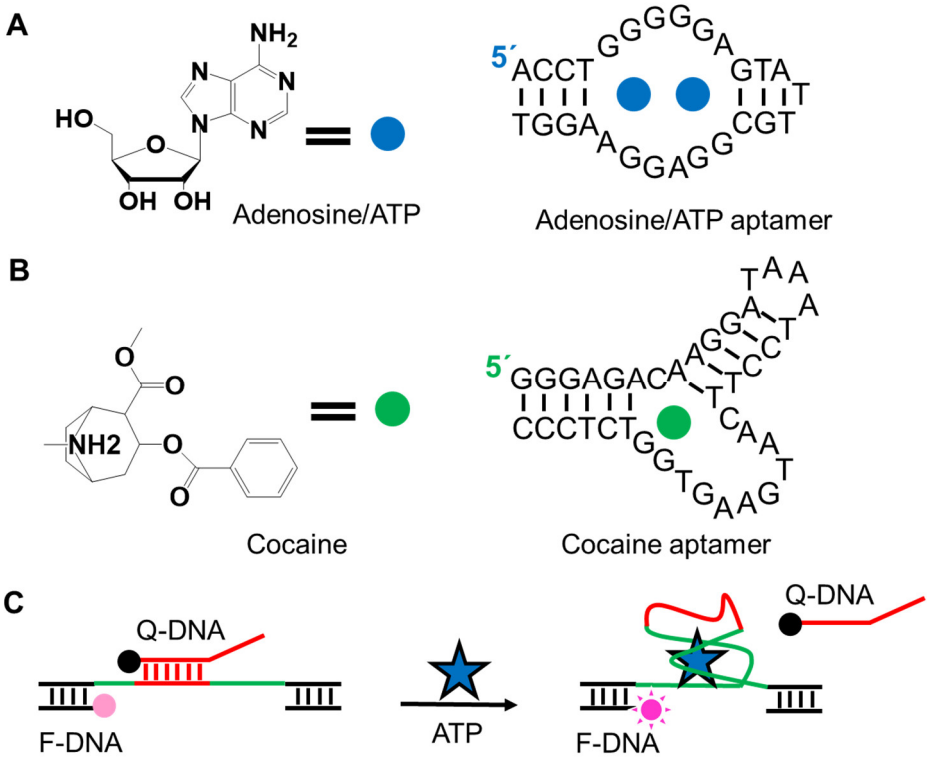

Figure 1.2 The secondary structures of (A) adenosine/ATP DNA aptamer, and (B) cocaine DNA aptamer. (C) A scheme describing the structural switching process induced by ATP in signaling aptamer.

1.2 Detection of adenosine and guanosine

1.2.1 Importance

Purine nucleosides play an important role in normal cellular functions and have become increasingly important in biomedical and bioanalytical fields. Particularly, adenosine is indispensable in modulating functions of heart, brain and kidney, especially when involving inflammation. It is produced from extracellular and intracellular AMP or *S*-adenosylmethionine, taking part in hormones regulation and biological reactions such as *S*-adenosylmethionine-dependent methylation.[13] On the other hand, guanosine, another well-known purine nucleoside, is also important in neuroprotection.[14] After brain injury, the GMP hydrolyses to guanosine around brain tissues to bring neurotrophic effects in central nervous systems, and the guanosine can counteract with some neurotoxins like glutamate at the same time to relieve the brain damage.[15] However, when disorders occur and the self-secreted guanosine cannot regulate the body back to normal, diseases can be caused. For example, an inappropriate guanosine secretion for glutamatergic simulation induces neuronal dysfunction even death.[16] Additionally, in the case of consistently high adenosine levels in blood, sickling, hemolysis and damage to multiple tissues in sickle cell disease (SCD) may happen.[17] Therefore, determine abnormal levels of adenosine and guanosine is significantly important for health monitoring and diseases diagnosis.

Beyond that, although other purine nucleosides such as inosine (deaminated from adenosine and is important for RNA editing)[18] and xanthosine (promoting mammary stem cells *in vivo*),[19] are also biologically valuable, my research is mainly focus on the well-known adenosine and guanosine. Therefore, the following introduction will be mainly related to these two purine nucleosides.

1.2.2 Aptamers for their detection

Conventional methods for qualifying and quantifying adenosine and guanosine rely heavily on chromatographic methods, such as high-performance liquid chromatography (HPLC), gas chromatography, mass spectrometry and microdialysis. They are highly sensitive and selective, but time-consuming, expensive as well as

difficult to operate. In situ detection is also difficult, and samples need to be extracted and processed before measurement. To solve these problems, DNA aptamers-based sensing platforms (termed aptasensors) for adenosine and guanosine are developed.

1.2.2.1 Adenosine

To date, the most aptasensors for detecting adenosine are based on the adenosine aptamer sequence isolated by Huizenga and Szostak in 1995 (Figure 1.2A), ranging from fluorescent sensors to colorimetric and electrochemical sensors.[20-22] Since the sequence was able to binding adenosine and ATP with similar affinity, ATP could be used as an alternative to trigger the sensor response. Some initial ideas of fluorescent sensing rely on labeling a single fluorophore on the aptamer as shown in Figure 1.3A, such as the work carried out by Ellington and coworkers, in which a fluorescein was labeled on 5′-end, on G_7 or between G_7 and G_8 (the later generated 25% fluorescence increase while only 5% for the first two sites).[23, 24] To enhance the signal changes, an external quencher is more often used. For example, the full-length aptamer could be split to two halves, with one strand attached by a fluorophore and the other having a quencher (Figure 1.3B).[25] Upon binding to adenosine, the two strands were brought together and the fluorescence was quenched. Stojanovic *et al*. used a 5′-rhodamine and a 3′-dabcylquencher to screen the binding, achieving 40% fluorescence decrease.[26] Moreover, to achieve signal-on sensing with a lower background and a larger signal increase, the structure-signaling aptamer idea was proposed by Nutiu and Li (Figure 1.3C).[27] When hybridizing a fluorophore-labeled DNA and a quencher-labeled DNA to a long piece containing adenosine aptamer, the fluorescence was quenched in this initial state. Then, adding adenosine released the quencher-contained strand and the fluorescence increased. Using this method, the target binding was able to increase the fluorescence by 13-fold. Besides molecular quenchers, some nanomaterials like graphene oxide are also popular, based on their functions to quench fluorescence by adsorbing DNA moiety on their surfaces (Figure 1.3D).[28-30] Furthermore, cost-effective label-free methods such as by using SYBR Green I (SGI) and thioflavin T (ThT)

staining dyes are also widely accepted, based on the mechanism that adenosine binding can replace the associated dye from aptamers accompanied by a fluorescence decrease (Figure 1.3E).[31] For example, Liu et al. incorporated an acrydite-modified aptamer into hydrogel microparticles, and used a dye named SYTO-13 to screen adenosine binding event.[32] A detection limit of 45 μM was determined.

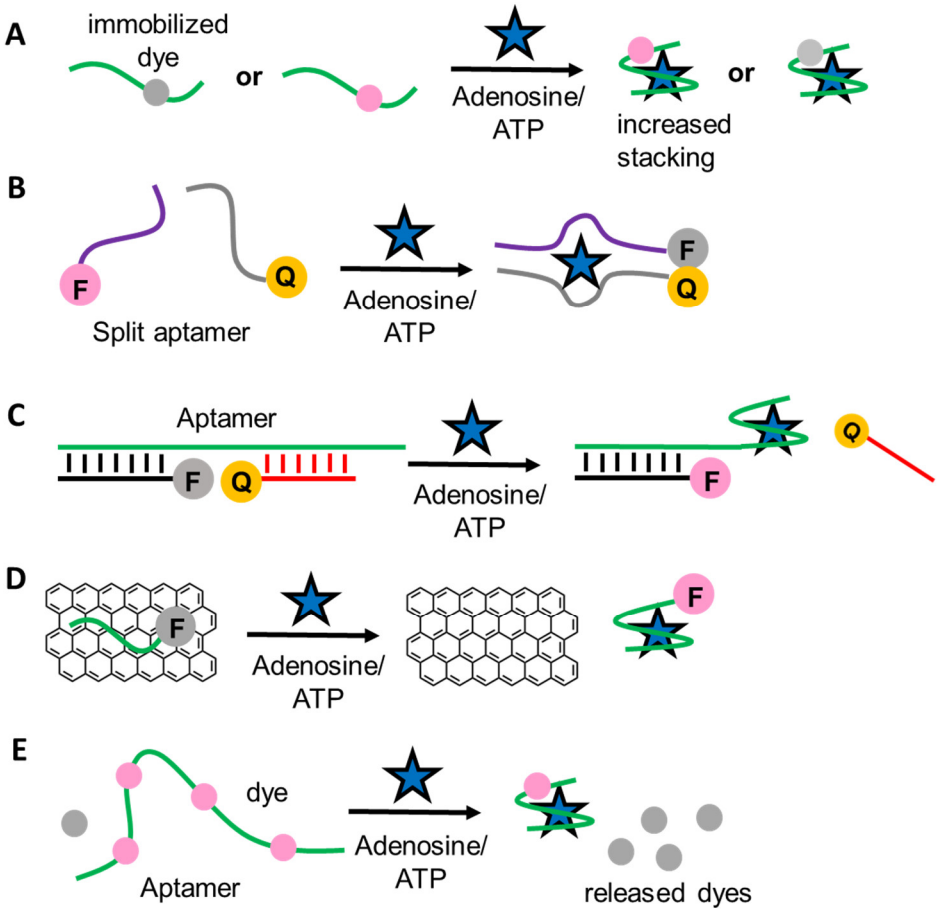

Figure 1.3 Fluorescent sensors for detecting adenosine/ATP based on (A) a covalent labeled fluorophore on the full-length aptamer, (B) split aptamer, (C) structure-switching signaling aptamer, (D) aptamer adsorption on graphene oxide, and (E) a DNA staining dye.

Since colorimetric sensors do not need instruments for detection, they are alternative strategies to achieve cost-effective sensing. Taking advantage of the

distance-dependent color and high extinction coefficient of AuNPs, adenosine binding by its aptamer can be visualized by color changes.[33-35] For example, Liu and Lu employed the adenosine aptamer as a linker to bring the thiol-DNA modified AuNPs together to show a blue color (Figure 1.4A).[33] Adding adenosine induced the aptamer's conformational change, disassembling the AuNPs to turn the color back to red. The detectable range was from 0.3 to 2 mM (Figure 1.4B). Other colorimetric sensors were also designed based on the catalytic oxidation of chromogenic 2,2′-azino-bis(3-ethylbenzthiazoline-6-sulfonic acid) (ABTS) by peroxidase activity,[36] or releasing AuNPs by aptamer-crosslinked hydrogels.[37]

Finally, electrochemical sensors are also attractive in measuring biological samples, due to their ultra-high sensitivity (reaching several nM or even lower).[38-40] For example, Battaglini and coworkers developed an electrochemical split aptamer assay for detecting adenosine.[41] One aptamer fragment was immobilized on electrode surface, and the other was grafted on AuNPs (containing a redox polyelectrolyte for signal transduction) (Figure 1.4C). In the presence of adenosine brought two fragments together and generated current, yielding a limit of detection of 3.1 nM.

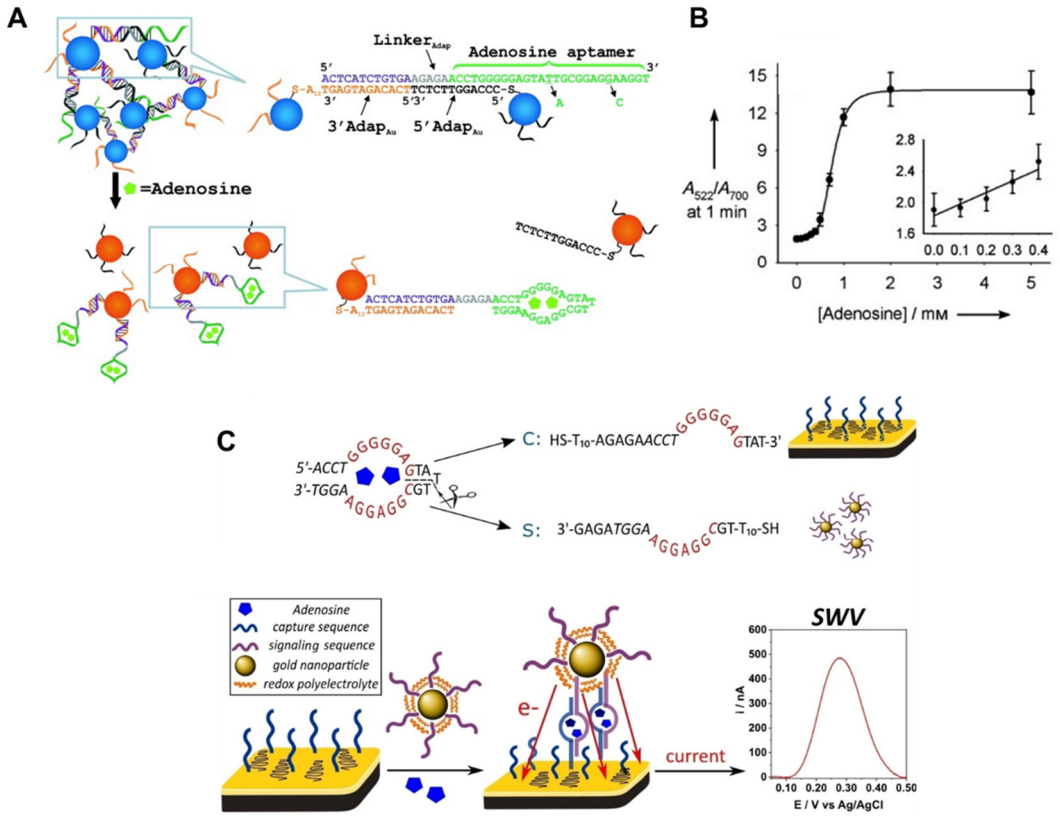

Figure 1.4 (A) Colorimetric sensors based on adenosine binding releasing aggregated AuNPs. (B) Adenosine titrations to DNA-modified AuNPs aggregates. Reproduced with permission.[33] Copyright 2006, Wiley-VCH. (C) Electrochemical split aptamer assays for detecting adenosine. Reproduced with permission.[41] Copyright 2020, Wiley-VCH.

1.2.2.2 Guanosine

Compared to the aptasensors for adenosine, the relevant platforms for guanosine were rarely reported, since the DNA aptamer for guanosine has not been isolated yet. Although Connell and Yarus selected a guanosine binding RNA aptamer (with a K_d of 32 μM guanosine), it was not applied in practical applications probably due to the low stability of RNA molecules. Recently, several non-SELEX-derived DNA sequences for recognizing guanosine have been reported. The Tan group spliced an entire guanine nucleotide from a G-quadruplex, in which a vacancy in its secondary may form (left panel of Figure 1.5A).[10, 42] They found that when this vacancy appeared in top layer of

the G-quadruplex, it was able to bind a few guanine derivatives, such as guanosine, GMP, GDP and GTP (right panel of Figure 1.5A). Since negatively charged phosphate groups tend to be repelled by DNA backbone, the affinities to GMP, GDP and GTP gradually decreased. Other nucleosides cannot bind at all. These binding reactions were evaluated by dimethyl sulfate (DMS) footprinting and DNA melting experiments. The footprinting data in Figure 1.5B shows that guanosine binding was only achieved in the presence of K^+, indicating the formation of a G-quartet.

Later, they further developed this system into a fluorescent sensor by extending this vacancy-bearing G-quadruplex strand with a hybridized domain, and then respectively label the two ends with a fluorophore and a quencher (the left panel in Figure 1.5C). The fluorescence was quenched in the initial stage. After adding guanosine or GMP, under the driving force of forming the G-quadruplex, the loop part switched the structure leading to increased fluorescence.[42] However, apart from GMP, other analytes like xanthosine, 8-oxo-2'-deoxyguanine (a biomarker of DNA damage), and two more guanine-related drugs (Ganciclovir and Acyclovir) all can induce increased fluorescence signals. Yang and coworkers characterized a vacancy-bearing G-quadruplex by NMR, and revealed that the recognition of guanine moiety involved Hoogsteen hydrogen bonding, coordination with K^+ and base stacking. Also, an additional C1′-H1′•••O4′ (a nonconventional CH•••O hydrogen bond) may exist.[43] To further improve the guanosine binding specificity, our group developed a base-excised strategy,[44] in which the non-specific association of GMP, GDP and GTP were all eliminated (studied in the Chapter 3).

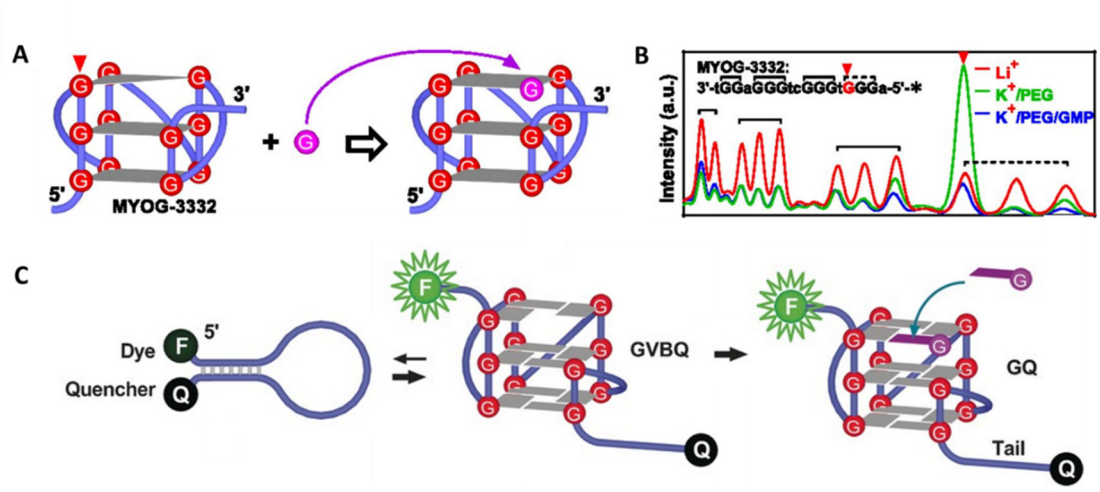

Figure 1.5 (A) Schematic illustration of free guanine-containing ligands fitting into the vacancy in the top layer of the G-quadruplex. (B) Quantification of DMS footprinting results for a vacancy-bearing G-quadruplex upon binding guanine-containing ligands. Reproduced with permission.[10] Copyright 2015, National Academy of Sciences. (C) Schematic illustration of a defective G-quadruplex based fluorescent sensor for specific binding guanine-containing compounds. Reproduced with permission.[42] Copyright 2016, Wiley-VCH.

1.3 DNA-functionalized hydrogels

Hydrogels are crosslinked polymer networks consisting of hydrophilic building units. Their hydration may be affected by various solution stimuli, like pH, temperature, salts, solvent composition and light, thus they have been developed to various stimuli-responsive platforms.[45, 46] For example, poly(*N*-isopropylacrylamide) (PNIPAm) is a temperature-responsive polymer exhibiting a lower critical solution temperature (LCST) behaviour. The PNIPAm is hydrophilic and highly swollen at room temperature, however when heated above to ~32°C, it turns to hydrophobic and shrink sharply, due to thermally induced collapse of the NIPAm units.[47] Therefore, temperature-sensitive systems often include PNIPAm.[48-50] Additionally, polyacrylic acid (PAA) is another pH-sensitive polymer due to its highly negatively charged backbone.[51] The input stimuli toward these responsive hydrogels largely come from the properties of organic

monomers, yet responding to biologically relevant molecules (e.g. small molecule metabolites and nucleic acids) can hardly be realized in this way. To solve this problem, functional biopolymers like proteins and DNA can be grafted to hydrogel backbones to enrich their function.[52-54] We are particularly interested in exploring DNA-functionalized hydrogels, since the DNA molecules are programmable, more thermal-stable, and easy to synthesize and modify.

1.3.1 Preparation and properties

The covalent conjugation of DNA to organic hydrogels often needs chemical modifications. To graft DNA to polymer networks, two strategies are generally used. In the first case, amino-modified oligonucleotides are employed to react with pre-formed polymers containing succinimidyl ester to achieve conjugating through amide bonds (Figure 1.6A). Secondly, acrydite-modified oligonucleotides are also widely used to copolymerize with vinyl monomers, in which the DNA grafting and hydrogel formation process in one-pot (Figure 1.6B). Normally, the amino modification is viable on both the 3′ and 5′-termini of DNA, while that for acrydite is only available on the 5′-end.[45]

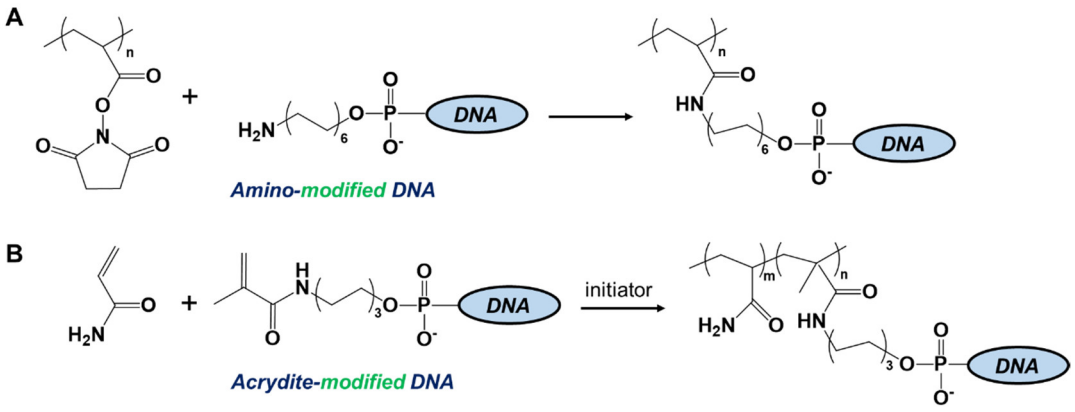

Figure 1.6 Schematic illustrations of two common strategies for preparing DNA-hydrogel conjugates: (A) grafting amino-modified DNA to pre-formed succinimido-polymer; (B) copolymerizing acrydite-modified DNA with acrylamide during free radical polymerization.

The DNA-hydrogels reserve the properties of normal hydrogels, including good biocompatibility and stability; and at the same time, by having the functional DNA, the hydrogels are able to bear additional properties and response to more biorelevant stimuli. When the DNA hybridization is used to crosslink polymer chains and promote gelation, external stimuli like complementary DNA (cDNA) or ligands for aptamer may unwind the hybridized strands and degrade gels to chain polymer. For example, Tan et al. prepared two DNA fragments-functionalized polyacrylamide, which could be further gelled by a longer linker DNA (for both fragments) (Figure 1.7A). Since they engineered part of the linker DNA with adenosine aptamer sequence, the crosslinked networks could be disrupted by addition of adenosine molecules.[55]

Besides to small molecular-responsiveness, the DNA-hydrogels can also be sensitive to enzymes, photons, pH, temperature and magnetic field.[56, 57] For instance, Willner and coworkers designed a pH-responsive DNA-hydrogels through incorporating two guanine- and cytosine-rich sequences into the polyacrylamide (Figure 1.7B). At pH 7.4, both the intermolecular and intramolecular guanine-cytosine pairs were formed based on Watson-Crick interactions, holding the gel backbones together. When pH was lowered to 5.0, due to the protonated cytosine, intramolecular CG•C^+ parallel structures were formed causing the gel degradation.[58] Such sol-gel transition properties of the DNA-hydrogels enable us to visualize the ligand binding- or other stimuli-induced DNA/aptamer conformational changes simply from the status changes of the hydrogels.

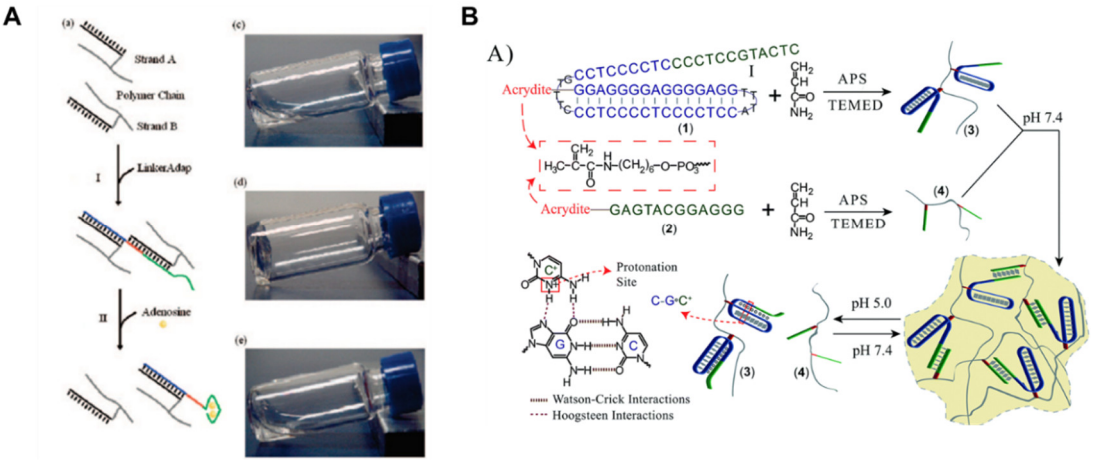

Figure 1.7 (A) DNA-induced gelation and adenosine-induced dissociation of DNA-functionalized polyacrylamide system. Reproduced with permission.[59] Copyright 2008, American Chemical Society. (B) pH-responsive and switchable CG•C^+ triplex-based DNA-hydrogels. Reproduced with permission.[60] Copyright 2015, Royal Society of Chemistry.

1.3.2 Molecularly imprinted hydrogels containing DNA

Molecular imprinted polymers (MIPs) are "artificial antibodies" that can work like natural antibody to accept shape complementary and chemical complementary ligands but are much more stable, robust and cost-effective than natural antibodies. The MIPs are often prepared by copolymerizing functional monomers in the presence of targets. After polymerization and removing the target molecules, complementary cavities for them are exposed for selective recognition (Figure 1.8).[61] When the synthetic monomers are hydrophilic reagents, like acrylamide and NIPAm, the MIPs are imprinted hydrogels exhibiting specific molecular recognition abilities in water phase.[62]

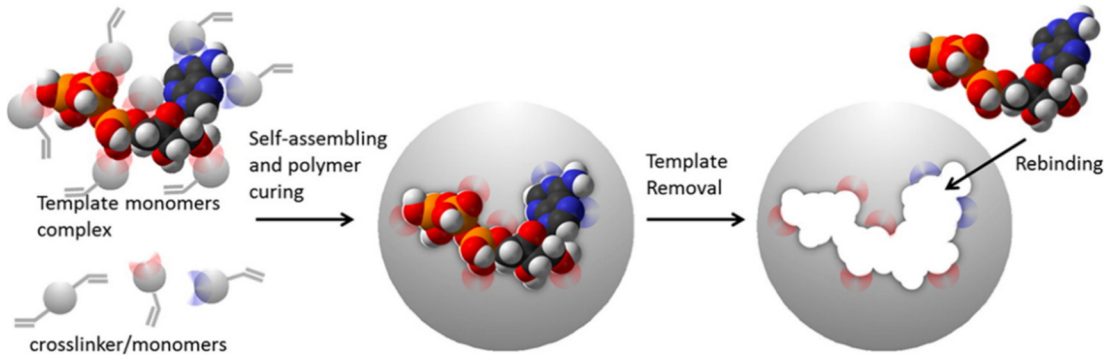

Figure 1.8 Schematic illustration of the general process of preparing MIPs. Reproduced with permission.[61] Copyright 2015, American Chemical Society.

Nevertheless, the binding performance of the traditional molecularly imprinted hydrogels are relatively low, mainly limited by their weak affinity and insufficient specificity. Since the hydrogels can swell significantly in water and deform the imprinting sites for molecular recognition, achieving highly specific ligand binding in hydrogel-based MIPs are often difficult. To solve this problem, DNA is exploited as a macromonomer to functionalize such MIPs, because certain sequence of DNA can achieve precise molecular recognition with improved affinity.[63] The good stability and low cost of DNA also match the properties of MIPs.[63] For example, Spivak et al. modified two different aptamers (29-mer and 15-mer) that target different sites on thrombin (a biomarker in urine for detecting glomerulonephritis) (Figure 1.9A), and then copolymerized with acrylamide and *N,N′*-methylenebisacrylamide (BIS) in the presence of thrombin to prepare the MIP hydrogels (Figure 1.9B).[64] Subsequent removal of thrombin resulted in a notable hydrogel swell, while further rebinding of it led to a shrinkage up to ~8% due to the high thrombin-aptamer affinity (K_d of 0.5 nM and 100 nM for 29-mer and 15-mer fragments respectively).[65] The thrombin MIPs showed good specificity over other proteins like bovine serum albumin (BSA), as no shrinkage was observed at equilibrium. On the other hand, in addition to study aptamer-functionalized hydrogels, Liu and coworkers developed a peroxidase-like G-quadruplex contained MIPs to exploit the DNA catalysis toward a specific substrate.[66]

They incorporated an acrydite-modified G-quadruplex with acrylic monomers to imprint 3,3′,5,5′-tetramethylbenzidine (TMB) during polymerization, then removed the TMB (Figure 1.9C). Consequently, the selective catalysis of TMB in the presence of hydrogel peroxide (also adding hemin as cofactor) was realized, with ~5-fold higher K_{cat}/K_m than converting another type of substrate ABTS. In the case of testing non-molecularly imprinted polymers (NIPs) (i.e. no TMB was added during preparation), the specific catalysis of TMB over ABTS can barely be achieved.

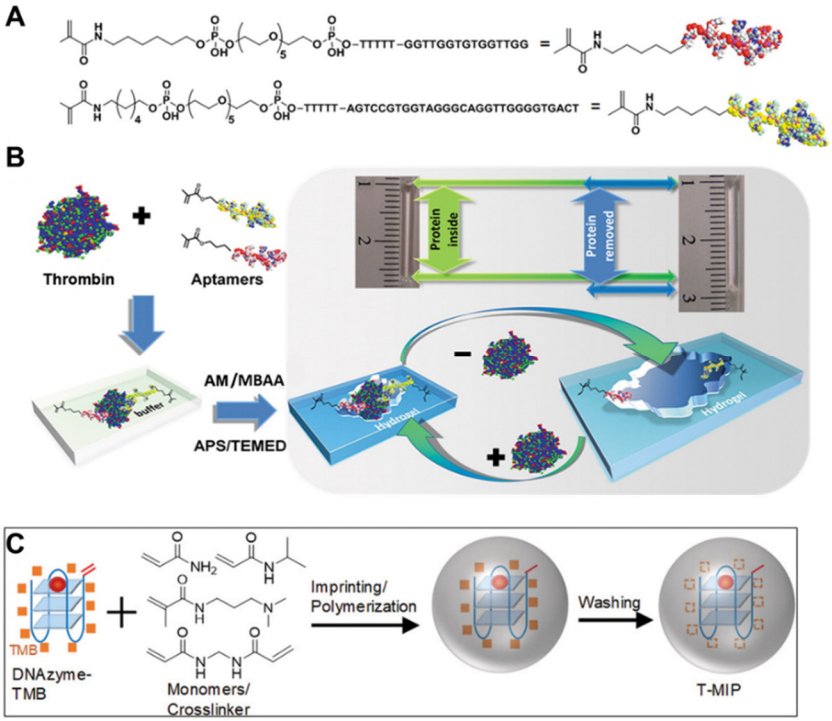

Figure 1.9 (A) Chemical structures of acrydite-modified thrombin aptamers. (B) Schematic illustration of the preparation of thrombin-targeting MIP hydrogels and the visualization of their volume changes binding to thrombin. Reproduced with permission.[64] copyright 2013, American Chemical Society. (C) Schematic illustration of the preparation of DNAzyme-based MIP hydrogels for selectively catalyzing TMB.[66] Copyright 2019, Wiley-VCH.

1.3.3 Examples of applications

1.3.3.1 Biosensing applications

The DNA hydrogels have been widely explored in biosensing and biomedical applications.[67, 68] Firstly, in biosensing field, for noncovalently crosslinked hydrogels by DNA hybridization, the analyte-responsive DNA could be used as the crosslinker and the sol-gel transition induced by ligand-DNA binding could be manipulated for designing the sensor. For example, Tan and colleagues fabricated an acrydite-DNA hydrogel network crosslinking by its complementary DNA, in which two short DNA fragments were individually grafted on linear polyacrylamide polymers while a longer linker was hybridized to both of them acting as a crosslinker (in green, Figure 1.10A).[37] They engineered the linker DNA to cocaine aptamer, and trapped amylose within polymer networks. The amylose was able to bind iodine accompanied by blue color changes. When in the absence of cocaine, the amylose was protected by polymer frameworks, and amylase (can break amylose down to sugar) cannot diffuse into the cage, leaving those blue color unchanged (Figure 1.10B). However, in the presence of cocaine, the gels were degraded due to cocaine-aptamer binding, then the amylose was digested. Consequently, iodine failed to generate any blue color. Other analogues that cannot bind to cocaine aptamer cannot bleach the iodine-stained blue gels (Figure 1.10C). By having this sensor, 20 ng of cocaine was able to be detected.

Moreover, for hydrogel frameworks covalently crosslinked by organic molecules like the BIS,[69] the hydrogels often play a role of the DNA carrier. In biosensing applications, they can enrich the DNA to achieve lower detection limit, and used for separation after centrifugation. For example, Liu and coworkers attached a thymine-rich DNA on polyacrylamide monoliths to selectively detect Hg^{2+}. By staining the DNA by SYBR Green I dye, and comparing the fluorescence changes with and without the Hg^{2+}, the detection limit of Hg^{2+} in a 50 mL water sample was as low as 10 nM.[70]

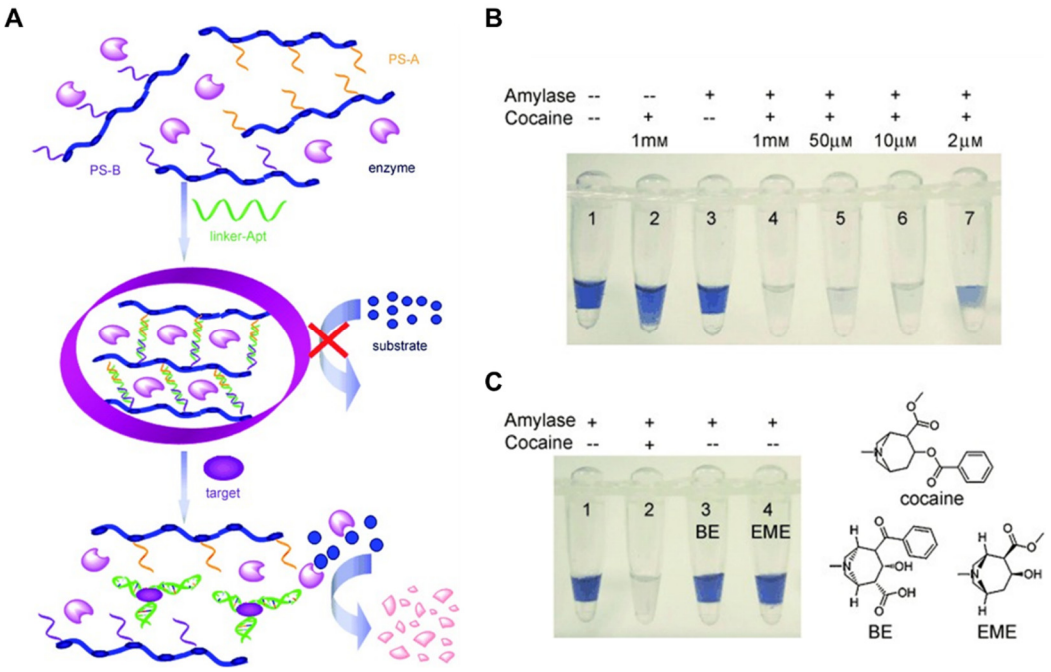

Figure 1.10 (A) Schematic illustration of the DNA cross-linked hydrogel for visual detection of cocaine. Photographs of DNA-gels responding to (B) different concentrations of cocaine and (C) two other analogues in the presence of amylase and iodine. Note that the amylose was embedded in gel matrix. Reproduced with permission.[37] Copyright 2010, Wiley-VCH.

1.3.3.2 Biomedical applications

Since the DNA molecules are easily to be cleaved by nucleases in biofluids, they can be preloaded into protective hydrogel networks for biomedical applications. At the same time, to achieve controlled release of drugs rather than load-off in a burst manner, hydrogel microstructures are also helpful. In these cases, therapeutic agents such as unmethylated cytosine-phosphate-guanine (CpG) oligonucleotides, interfering RNAs (siRNAs) and anticancer drugs like doxorubicin have been applied for immunotherapy, antisense therapy and chemotherapy.[68, 71] For instance, the siRNA-loaded hydrogels are effective for gene knockdown in kidney, ovarian and other cell lines.[72] Recently, Yang et al. incorporated siRNA to DNA hydrogel nanoframeworks by taking advantage of cascade hybridization chain reaction (HCR) (Figure 1.11).[73] The initial DNA scaffolds

(in green) were grafted in hydrogels through acrydite-modification, and then two types of DNA hairpins (named H1 and H2) were added to alternatively extend the DNA length. The siRNA (in dark blue) and an ATP aptamer sequences (in red) were inserted into one of the hairpins. Consequently, when the hydrogel nanoparticles were delivered into cells, due to the high concentration of intracellular ATP (around 5-10 mM), the release of siRNA was specifically triggered. As a result, levels of relevant mRNA and proteins were downregulated, and therapeutic efficacy was achieved.

Moreover, in the case of delivering unmethylated CpG DNA (a potent activator of immune response), Nishikawa et al. intercalated doxorubicin, a model drug for killing cancer cells, into CpG DNA-grafted hydrogels for chemo/immunotherapy.[74] They demonstrated that the CpG DNA hydrogels stimulated cytokine release from murine macrophage-like RAW264.7 cells, and the incorporated doxorubicin was slowly released. After treatment, the growth of murine adenocarcinoma colon26 tumor in mice was effectively inhibited. Overall, the compatibility of DNA hydrogels with nucleic acid drugs solved the difficulties for delivering them into target cells.

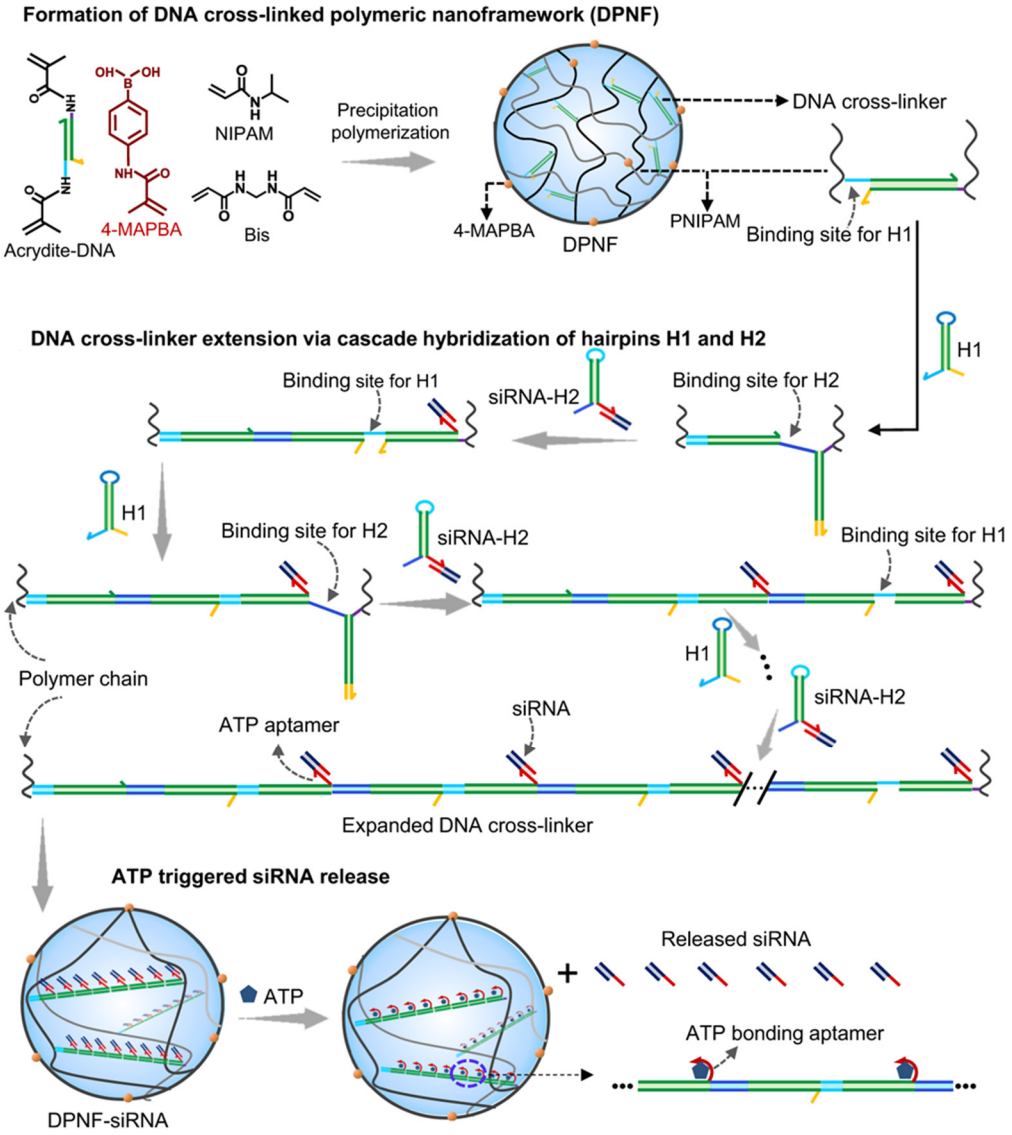

Figure 1.11 Schematic illustration of the DNA-hydrogels for siRNA loading via cascade hybridization of DNA hairpins and ATP-triggered release of siRNA. Reproduced with permission.[73] Copyright 2021, Springer Nature.

1.4 Research goals and thesis outline

Developing highly specific aptamers for sensing small biomolecules are of particular interest,[75] and further combining such functional DNA with hydrogels are attractive for applying them in practical bioanalytical and biomedical applications. However, some most frequently used aptamers still suffer from limited specificity and some other important molecules as “disease indictors” have not been isolated by

SELEX yet (although the SELEX can theoretically generate aptamers for any ligand). Specifically, since the SELEX-derived adenosine aptamer can hardly differentiate it from analogues including deoxyadenosine, AMP, ADP and ATP, my first goal was to develop a highly specific sensing platform for adenosine. In addition, given that DNA aptamers for guanosine have not been selected yet, a specific binding DNA for guanosine is also desirable. Thirdly, based on the fact that current covalent conjugation strategies for directing DNA to hydrogels in biosensing and biomedical applications heavily rely on chemical modifications on oligonucleotides, which can result in a high cost, a modification-free method is also desired. To achieve these goals, the thesis is outlined as the following chapters.

Chapter 2 describes a novel method to engineer base-excised aptamers for highly specific recognition of adenosine. In this work, an adenine nucleotide is excised from the backbone of a one-site adenosine aptamer, leaving a vacancy for specifically rebinding adenosine. The chemical and geometry complementary pockets are expected to form. The binding affinity and recognition mechanism are studied. Single phosphate distinguishing ability between the adenosine and AMP is investigated, and non-specific binding of other cognate analytes including guanosine, cytidine, uridine, theophylline, and ATP are tested, according to the SYBR Green I fluorescence spectroscopy and ITC results. Finally, the adenine-excised aptamer is applied in diluted serum to check its applicability in biofluids.

Chapter 3 followed the work in the chapter 2 using the base-excised strategy to develop a series of DNA aptamers for highly specific recognizing guanosine. Both the Na^+-binding aptamer and classical adenosine aptamer are manipulated as the base-excising scaffolds. Guanosine binding affinity and specificity of the base-excised aptamers is carefully investigated. Also, aptamer scaffold generality and excised-site generality are systematically studied to further demonstrate the feasibility of this aptamer-generation strategy in more systems.

Chapter 4 describes a method to differentiate adenosine from deoxyadenosine (only differ by a -OH) and its *cis*-diol analogues, by using the molecularly imprinted polymers. An acrydite-modified adenosine aptamer and 3-acrylamidophenyboronic acid (AAPBA) are used as functional monomers during the MIPs preparation, respectively targeting nucleobase and sugar part of the adenosine. The adenosine binding affinity and specificity of such (aptamer+AAPBA)-MIPs is evaluated by ITC. Since the boronic acid functions can be modulated by pH, the effect of pH and the mechanism of boronic acid-assisted adenosine recognition is then studied.

Chapter 5 describes a modification-free method to conjugate DNA on hydrogel nanoparticles and monoliths. The intrinsic reactivity of a penta-adenine (A_5) DNA is exploited for covalent conjugation, and freezing is used to promote the reaction efficiency. The importance of freezing, addition of antifreeze and free radicals are studied in detail. In addition, the covalent linking of four homo-DNAs in difference lengths (5, 15 and 30-mer) are studied; and the effects of DNA secondary structures (including duplex, quadruplex and i-motif) are also investigated. To further develop the A_5 to an anchor for any DNA sequence grafting, it is extended to a random sequence denoted as a A_5 diblock DNA. By engineering such A_5 diblock DNA with functional sequences, the detection of complementary DNA and Hg^{2+} ions are demonstrated.

Chapter 6 concludes the conclusions in aforementioned chapters in this thesis, and provides the future plan as well as original contributions.

Chapter 2 Engineering base-excised aptamers for highly specific recognition of adenosine

The results presented in this chapter have been published as:

Yuqing Li, Biwu Liu, Zhicheng Huang, Juewen Liu, Engineering base-excised aptamers for highly specific recognition of adenosine. *Chemical Science*, **2020**, *11*, 2735-2743.

2.1 Introduction

Aptamers are single-strand oligonucleotides that can specifically bind to target molecules.[1, 76, 77] Compared to antibodies, DNA aptamers are much more stable and cost-effective. Some aptamers are naturally found in riboswitches, which can regulate gene expression and interact with metabolites, such as adenine, flavin mononucleotide, and glycine.[78] Most aptamers used for designing analytical biosensors are generated through a strategy called SELEX (systematic evolution of ligands by exponential enrichment).[2, 79] SELEX has be applied to various targets ranging from metal ions,[80, 81] small molecules,[4, 5] peptides,[82] proteins,[83] to whole cells.[84] Duo to these advantages, aptamers are widely used in biosensors,[85, 86] cell engineering,[87] and therapeutics.[88]

The DNA aptamer for ATP or adenosine is one of the most important model aptamers. It was first reported by Huizenga and Szostak in 1995, having excellent selectivity against the other nucleosides or nucleotides.[4] With more than 20 years of research, its structure,[89] highly conserved nucleotides,[90, 91] modification,[77] and single-site binding[92] have been revealed. Nevertheless, this aptamer is limited by its inability to distinguish the substitutions on the 5′ position of adenosine (e.g. cannot distinguish adenosine from AMP and ATP). Since adenosine regulates different cellular processes, and affects the immune, nervous, respiratory, circulatory and urinary systems, abnormal levels of adenosine indicate potential problems in the heart and brain.[93, 94] Therefore, it is important to differentiate adenosine from AMP and ATP.

To improve the aptamer specificity, many efforts have been made. For example, Koizumi and Breaker selected a new aptamer that can differentiate cAMP from ATP, 5′-AMP and 3′-AMP.[95] Through extensive negative selections, the Szostak group isolated an RNA aptamer for ATP, which specifically targeted the triphosphate moiety.[8] Olsen *et al*. obtained an aptamer that can monitor the oscillating concentration of ATP with high resolution, even if the total concentration of adenine nucleotides ([ATP]+[ADP]+[AMP]) was stable.[96] Nutiu and Li re-discovered the ATP DNA aptamer using a new SELEX method,[90] and Ellington *et al*. selected a fluorescein-labeled ATP RNA aptamer.[97] Most recently, Zheng *et al*. reported an ATP aptamer that can be used in cytometric bead assays.[98] Although these SELEX strategies are powerful for guiding the selectivity, still no aptamers are available for highly selective binding of adenosine.

Since DNA oligonucleotides are chemically synthesized, they allow efficient mutation and modification studies.[99-101] Recently, it was reported that after omitting a base on a DNA duplex or G-quadruplex, the scaffold allowed free adenosine or guanosine to re-fit into the vacant site. This was achieved either by introducing an abasic-site in duplex,[12, 102, 103] or by omitting a whole guanine-nucleotide in a G-quadruplex.[10, 104, 105] These DNA complexes can reach a μM K_d, and behave like traditional aptamers. However, they often have a low specificity. Not only the cognate analytes can fit into the vacancy,[104] pseudo-base pairing may also induce binding.[102, 106] This maybe attributed to their recognition largely relying on secondary structural discrimination (simple base pairing).

To achieve more specific recognition, herein we reported an interesting finding of using an aptamer as the scaffold to exclusively recognize adenosine. By deleting a nucleotide in the adenosine aptamer, a new strand breaking point was created, and we called it a base-excised aptamer. Compared with scaffolds consisting of a duplex and G-quadruplex, the base-excised aptamer has more sophisticated 3D structures that may allow more intermolecular forces to take place and enable exclusive adenosine

recognition. Other nucleosides including cytidine, guanosine, uridine, and cognate analytes like AMP, ATP and theophylline all failed to bind. This work provides insights into engineering existing aptamers without the need of new SELEX experiments.

2.2 Materials and Methods

2.2.1 Chemicals

All the DNA samples were purchased from Eurofins (Huntsville, AL). The DNA sequences are listed in Supporting Information Table 2.1. SYBR Green I (SGI), AMP, ATP, theophylline and fetal bovine serum (FBS) were purchased from Sigma-Aldrich. Guanosine, adenosine, cytidine, uridine, sodium chloride, magnesium chloride and 4-(2-hydroxyethyl)piperazine-1-ethanesulfonate (HEPES) were from Mandel Scientific (Guelph, Ontario, Canada). Milli-Q water was used to prepare all of the buffers and solutions.

Table 2.1. The DNA sequences used in this work.

DNA Names	**Sequences (from 5′ to 3′) and modifications**
Wide-type adenosine Apt	ACCTGGGGGAGTATTGCGGAGGAAGGT
One-site Apt	ACCTTCGGGGAGTATTGCGGAGGAAGGT
A10-excised Apt	GTATTGCGGAGGAAGGTTTTTAACCTTCGGGG
Res-A10-Right cut	GTATTGCGGAGGAAGGTTTTTAACCTTCGGGGA
Res-A10-Left cut	AGTATTGCGGAGGAAGGTTTTTAACCTTCGGGG
Duplex-1	GGGGGTATTGCCCCCGCAAGGTTTTTAACCTTG
Duplex-2	GTATTGCGCCCCGAAGGTTTTTAACCTTCGGGG

2.2.2 SGI-based binding assays

An aptamer (50 nM) was first incubated with 2 mM target molecules, including adenosine, AMP, ATP, guanosine, cytidine or uridine, for 5 min in buffer A (20 mM HEPES, pH 7.6, containing 100 mM NaCl, 5 mM $MgCl_2$). The aptamer incubated with the buffer (without target) was used as control. Then, 50 nM SGI (final concentration) was added and the fluorescence spectra were collected (excitation at 485 nm, emission at 535 nm). The fluorescence data were analyzed based on $(F_0\text{-}F)/F_0$, in which F_0 and F stand for the fluorescence without and with the target molecule, respectively. Similarly, a duplex DNA (50 nM) was first incubated with 2 mM cytidine or adenosine for 5 min in buffer A, and then 12.5 nM SGI was added (final concentration). The same sample without adding adenosine or cytidine was used as control.

2.2.3 Isothermal titration calorimetry (ITC)

ITC was performed using a VP-ITC microcalorimeter instrument (MicroCal). All samples were ultrasonicated for 5 min (degassing) prior to applying them for ITC. A 20 μM one-site aptamer, Res-A10-Right cut, and the A10-excised aptamer (in buffer A) were loaded in a 1.45 mL cell at 10 °C, respectively. 1 mM adenosine or AMP in the same buffer was loaded in a 280 μL syringe. After the first injection of 2 μL, the syringe injected 10 μL of the target into the cell each time. Through measuring the heat changes and fitting the titration curves to a one-site binding model, thermodynamic data including association constant (K_a), enthalpy changes (ΔH), entropy changes (ΔS), free energy changes (ΔG), and binding stoichiometry (N) were obtained. The molar ratio was calculated from the ITC data based on the ligand/aptamer concentrations.

2.2.4 Detection in diluted serum

1% FBS was used for this study. The 1% FBS was prepared by diluting the FBS stock in 20 mM HEPES (pH 7.6). Then 50 nM DNA was incubated with or without 2 mM adenosine in 1% FBS, and stained by 50 nM SGI. Additional 100 mM NaCl and 5 mM $MgCl_2$ were then added. To evaluate its specificity, the DNA was also incubated

with 2 mM AMP in the 1% FBS. At last, different concentrations of adenosine (0.28 to 2 mM) were titrated to calculate the K_d value.

2.3 Results and Discussion

2.3.1 Abasic, based-spliced and base-excised DNA

To engineer a vacancy-bearing DNA for specifically refill the vacancy, two strategies have already been reported. One is to create an abasic site by breaking the *N*-glycosylic bond (Figure 2.1A),[107] where the number of phosphodiester bonds remains the same but one of the bases is removed. The other method is to fully remove an entire nucleotide from the original sequence, and join the cleaved strands neatly at the end, which we call the base-spliced strategy (Figure 2.1B).[10, 104] Although rebinding of the deleted parts have been demonstrated in both methods, the specificity remained poor. For example, the abasic-site-contained DNA duplex can bind both adenosine and theophylline based on cytosine recognition,[102, 108] and the vacancy-bearing G-quadruplex can accept guanosine, GMP, GDP and GTP with similar affinities.[104]

In our work here, a new method of DNA engineering is described in Figure 2.1C, in which a whole nucleotide is excised, and a break is created (a new 3′ and a new 5′ end). This is different from the simple splitting (Figure 2.1D), which creates a break but does not remove any base. Besides, the goal of split aptamers is not to detect the removed nucleotide.[109-111] To demonstrate a better specificity of our base-excised aptamer for adenosine, not only the analogues focused on the base part (i.e. guanosine, cytidine, uridine and theophylline), but also the substitutions on the 5′ position like AMP and ATP were carefully tested (Figure 2.1E).

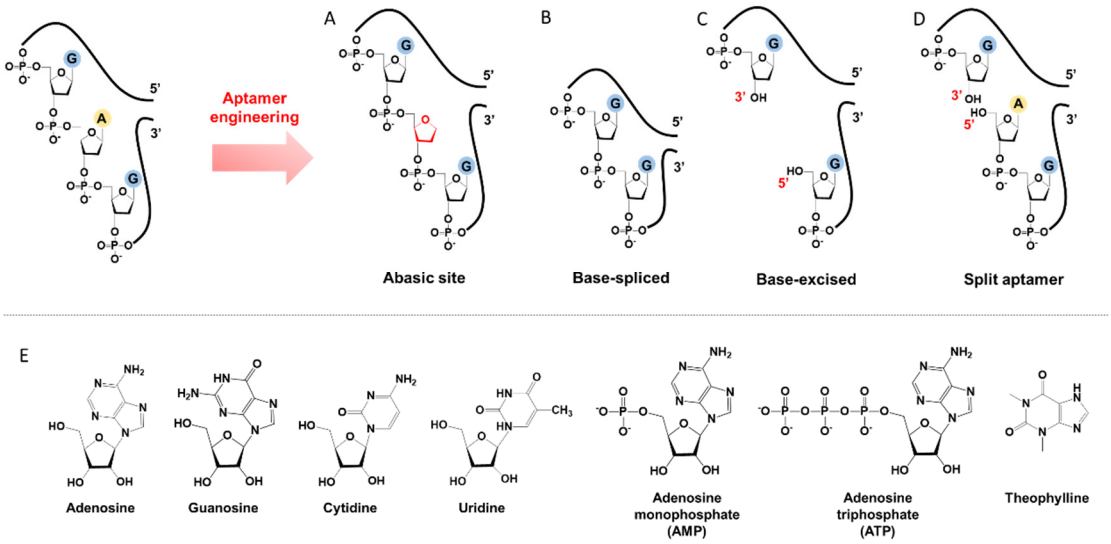

Figure 2.1. A scheme showing the differences between (A) abasic site, (B) based-spliced, (C) based-excised and (D) split aptamers. Note that the 5′ terminus of the purchased DNA was -OH (chemically synthesized), rather than phosphate. (E) Structure of analytes used: adenosine, guanosine, cytidine, uridine, AMP, ATP and theophylline.

2.3.2 Design of the adenine-excised adenosine aptamer

To study the molecular recognition in base-excised DNA, the adenosine aptamer was chosen as a scaffold. The secondary structure of the wide-type aptamer is shown in Figure 2.2A as revealed by Lin and Patel.[89] The red A stands for an adenine-contained ligands, such as adenosine, AMP, ADP and ATP, all of which can be accommodated in the aptamer binding pockets. The binding pockets contain G•A mismatches, and around them are some stacked bases, including the flanked G•G mismatch in one direction and the G•A mismatch in another direction. Therefore, the hydrogen bonding and base stacking are main contributors for target recognition.[91]

We decided to first excise the A10 adenine within the binding pockets because this position is close to the target binding site. Since the original aptamer can bind two adenosine molecules and it may complicate data analysis, we used the one-site aptamer design by sealing the base pairs on the left side of the aptamer (Figure 2.2A, middle

sequence). This one-site aptamer has a similar binding affinity and specificity for adenosine.[92] After excising a whole A10, two strands were generated. To keep the excised-aptamer in one strand, its original 3′ and 5′ ends were joined together, and a new aptamer was generated from the 5′ end near the excised site. The final sequence was named the A10-excised aptamer (Figure 2.2A, right one).

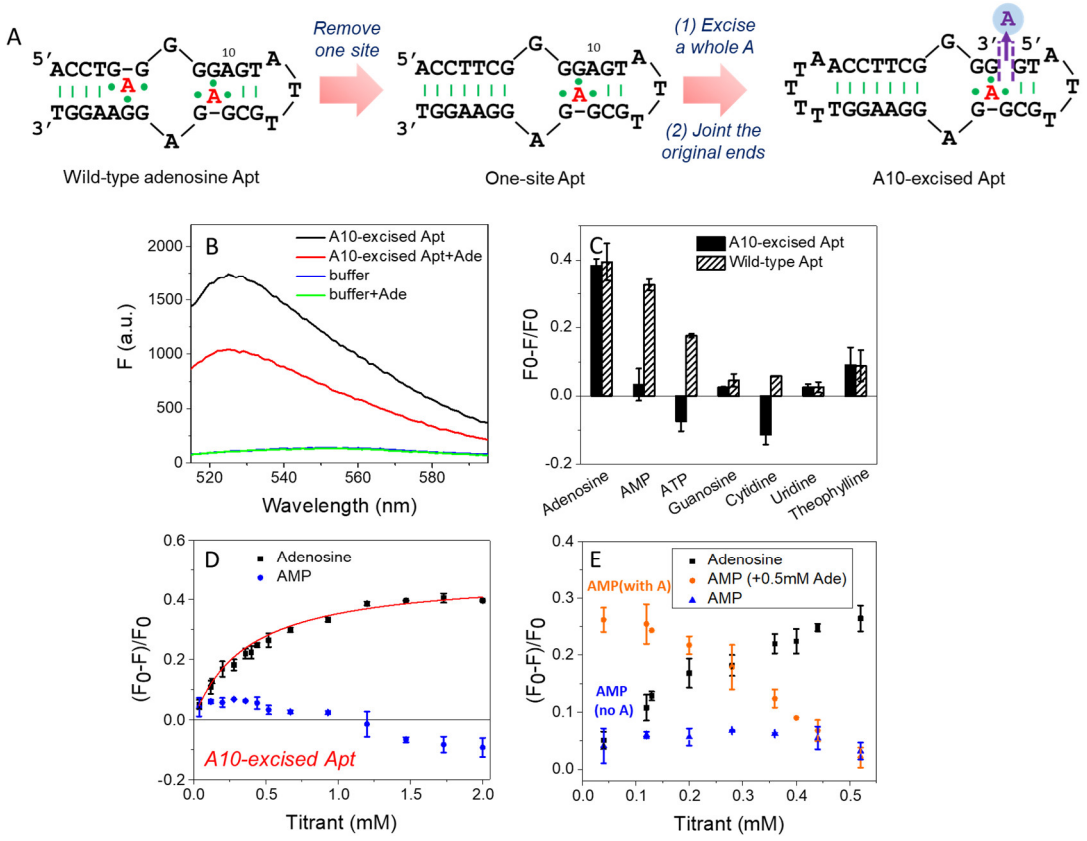

Figure 2.2. (A) The secondary structure of the wide-type adenosine aptamer, the engineered one-site aptamer and the A10-excised aptamer. (B) Fluorescence spectra of 50 nM A10-excised aptamer mixed with or without 2 mM adenosine in buffer A (20 mM HEPES, 100 mM NaCl, 5 mM $MgCl_2$). 50 nM SGI (final concentration) was used. (C) Comparison of the specificity of the A10-excised aptamer with the wide-type aptamer. 50 nM DNA mixed with 2 mM testing molecules, including adenosine, AMP, ATP, guanosine, cytidine and uridine in buffer A with 50 nM SGI. (D) Titrating adenosine or AMP (40 μM to 2 mM) into 50 nM A10-excised aptamer in buffer A. The titration curves were fitted by the equation: $(F_0\text{-}F)/F_0 = a[\text{Adenosine}]/(K_d+[\text{Adenosine}])$.

(E) Titrating Adenosine or AMP (0.04-0.52 mM) into 50 nM A10-excised Apt in buffer A. In orange curve, the DNA was first incubated with 0.5 mM adenosine, then applied to AMP titrations. 50 nM SGI was used to indicate the adenosine or AMP binding to DNA.

2.3.3 Adenosine specifically binds to the A10-excised aptamer

To study the binding performance of the A10-excised aptamer, SGI was used for label-free binding assays.[112-116] First, a 50 nM A10-excised aptamer was incubated with 2 mM adenosine (Figure 2.2B). Compared with the DNA without adenosine, the fluorescence decreased around 40% at 535 nm (excitation at 485 nm), indicating the binding of adenosine. This SGI fluorescence decreasing trend was consistent with previously reported studies, which was attributable to displacement of SGI by adenosine in the binding pockets.[114-116] We then, respectively, incubated AMP, ATP, guanosine, cytidine, uridine and theophylline (2 mM each) with the DNA (Figure 2C, black bars). Interestingly, they all failed to decrease the fluorescence signal, suggesting a lack of binding. For comparison, we also tested the wide-type aptamer with the sequence shown in Figure 2.2A. A descending binding trend was observed with adenosine, AMP and ATP, whereas negligible fluorescence was found for the other three nucleosides and theophylline. Therefore, using this base excised aptamer, the specificity for adenosine drastically improved.

To quantitatively measure binding, we further titrated up to 2 mM adenosine and AMP into the A10-excised aptamer (Figure 2.2D). Adenosine showed a K_d of 0.37 mM, while AMP failed to bind at any of these concentrations. Therefore, our A10-excised aptamer not only distinguished adenosine from C, G and T, but also can distinguished the phosphate part showing no binding to even AMP. This adenosine/AMP distinction has been a main problem of the original aptamer, which has hindered its application in terms of data interpretation, since cellular adenosine pool contains various AMP, ADP, ATP and even cAMP.[117] It could be that the phosphate containing nucleotides are

negatively charged and thus are more repelled by the charges on the phosphate backbone of the DNA, while the neutrally charged adenosine is easier to bind.

Since the original aptamer pocket can accommodate all the adenosine derivatives, we attributed this excellent specificity to the excised site, which may only bind adenosine, but not AMP. The aptamer pocket can only form when this A10 site was filled by adenosine. To test this, we designed a few control experiments. We incubated the A10-excised aptamer with 0.5 mM adenosine (half saturation according to Figure 2.2D), and then titrated AMP (Figure 2.2E). The fluorescence increased, suggesting that AMP competed with adenosine and disrupted the binding complex (orange curve). This suggests that both sites had to bind adenosine, while one AMP and one adenosine were not optimal. Our A10-excised aptamer bears two adenosine binding pockets, with one in backbone and the other in loop. Based on the fluorescence data, the improved specificity for adenosine was due to the excision of the A from the backbone.

2.3.4 Splitting at the A10-site (no base excised)

To further understand the effect of the above design, we then split the aptamer at the A10-site (at the right and left side of A10, respectively), but without any nucleotide excised. We first cut the right-side phosphodiester bond (Figure 2.3A). Interestingly, it showed similar binding specificity to the A10-excised aptamer, in which only the adenosine induced ~42% fluorescence decrease, whereas the AMP, ATP, cytidine and uridine were all failed to achieve a fluorescence signal change (Figure 2.3B). The titration data further confirmed the binding of adenosine, while no AMP binding was observed (Figure 2.3C). Half saturation was achieved at 0.94 mM adenosine, and thus this splitting modification near the aptamer binding pocket also decreased the binding affinity.

In contrast, when cutting the phosphodiester bond on left side (Figure 2.3D), the binding profiles were different (Figure 2.3E). AMP also showed binding, and its fluorescence drop was about two third of that of adenosine. These experiments

indicated that the right-side and the left-side phosphodiester bonds around the A10-site played different roles in helping the loop pockets bind AMP. Breaking the right-side one might change the aptamer local folding, resulting in differentiated binding preference for adenosine and AMP. For both split aptamers, the observed binding was from the original aptamer binding pocket. Therefore, it is not surprising that AMP can also bind in some cases.

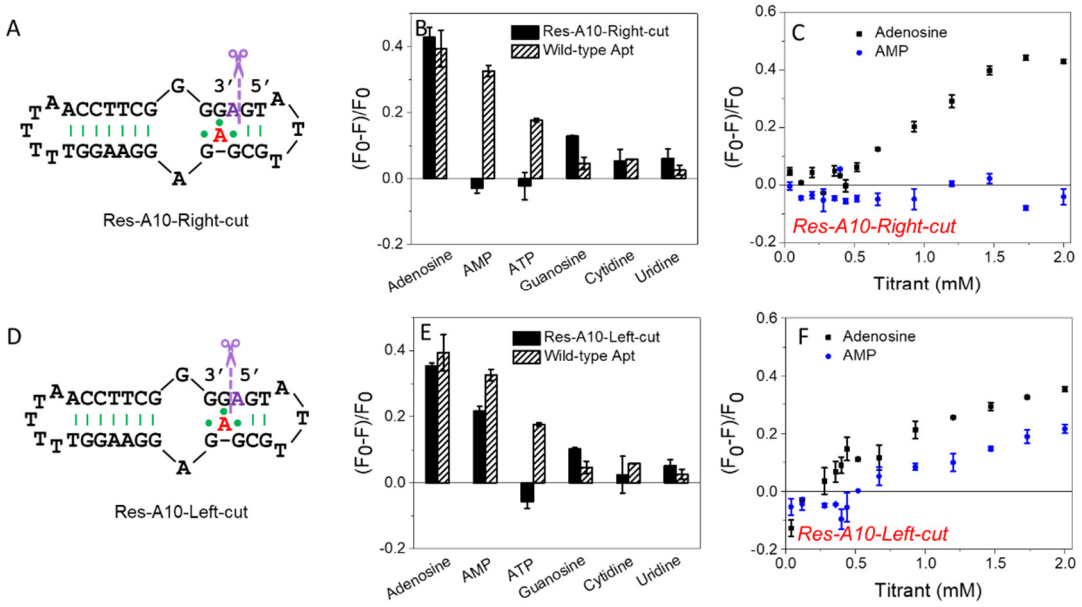

Figure 2.3. (A) Secondary structure of the Res-A10-Right-cut. (B) Comparison of specificity of the Res-A10-Right-cut and the wide-type aptamer. 50 nM DNA mixed with 2 mM testing molecules in buffer A (20 mM HEPES, 100 mM NaCl, 5 mM $MgCl_2$) with 50 nM SGI. (C) Titrating adenosine or AMP (40 μM to 2 mM) into 50 nM Res-A10-Right-cut in buffer A. (D) Secondary structure of the Res-A10-Left-cut. (E) Comparison of specificity of the Res-A10-Left-cut and wide-type aptamer. (F) Titrating adenosine or AMP (40 μM to 2 mM) into Res-A10-Left-cut.

2.3.5 Studying binding thermodynamics using ITC

In addition to studying the aptamer binding using fluorescence spectroscopy, we also employed ITC. ITC can quantitatively measure the heat changes during the binding

process. This can provide rich thermodynamic information, including association constant (K_a), enthalpy changes (ΔH), entropy changes (ΔS), free energy changes (ΔG), and binding stoichiometry (N).[92, 118-120] Figure 2.4A and 2.4B display typical ITC traces of titrating adenosine and AMP into the one-site aptamer, consisting of the upper part of downward spikes and the lower part of the fitted integrated heat. The one-site aptamer was firstly titrated to confirm its similar binding abilities to the wide-type aptamer, which cannot distinguish adenosine with AMP. The K_d of the wide-type aptamer binding to adenosine was reported to be around 6 μM (room temperature) in its original paper,[4] and here the K_d for one-site aptamer binding to adenosine was measured to be 2.8 ± 0.03 μM (10 degree for all titrations, Table 2.2). The K_d for one-site aptamer binding to AMP was at 12.2 ± 1.8 μM. Therefore, the aptamer binds adenosine slightly tighter than AMP.

We then titrated adenosine and AMP to the A10-excised aptamer and the Res-A10-Right-cut respectively (Figure 2.4C-F). Consistent with the fluorescence data demonstrated above, they both only bound to adenosine, whereas they failed to accept AMP. The K_d of the A10-excised aptamer binding to adenosine was at 17.0 ± 1.9 μM, and that of the Res-A10-Right cut was at 11.4 ± 0.2 μM. The K_d of them binding to AMP cannot be obtained from the ITC due to undetectable heat changes. It is interesting to note that the K_d values obtained from ITC indicated tighter binding than those from SGI fluorescence spectroscopy. It could be that SGI might affect the binding. Nevertheless, the conclusion of highly selective binding of adenosine remained true for both methods.

Another important parameter was the binding stoichiometry (N), which indicated how many adenosine/AMP molecules might interact with one aptamer strand. According to Table 2.2, the one-site aptamer binds to adenosine and AMP with a N at 0.8 ± 0.1 and 1.3 ± 0.3, respectively, indicating a 1:1 binding model. After cutting one phosphodiester bond, the Res-A10-Right-cut also bound just one adenosine (N = 0.9 ± 0.2), but it changed to 1.8 ± 0.3 when excised an adenine from the aptamer backbone.

The N obtained from ITC verified our expectations that each A10-excised aptamer was able to accept two adenosine molecules, with one situated in the loop and the other in the backbone pocket.

Moreover, the ΔH and ΔS also provide us some information about the driving force for aptamer binding. In the one-site aptamer, a big difference in binding adenosine and AMP was observed. The ΔH and ΔS for binding adenosine were -13.5 ± 0.4 kcal $mole^{-1}$ and -22.2 ± 1.5 cal K^{-1} mol^{-1}, respectively, indicating enthalpy-driven interaction (base pairing). However, AMP titration changed them to -4.7 ± 0.3 kcal $mole^{-1}$ and 6.0 ± 0.7 cal K^{-1} mol^{-1}. The decreased ΔH and increased ΔS revealed entropy-driven binding force (base stacking). Since the AMP was negatively charged and tended to be repelled by DNA backbone, base-stacking mainly contributed binding. Interestingly, when only cutting one phosphodiester bond at the backbone, the ΔH and ΔS of the Res-A10-Right-cut binding adenosine jumped to -1.0 ± 0.03 kcal $mole^{-1}$ and 19.1 ± 1.2 cal K^{-1} mol^{-1}, which was very different from the one-site aptamer. After removing a whole A, the ΔH and ΔS of the A10-excised aptamer binding adenosine were -1.1 ± 0.1 kcal $mole^{-1}$ and 18.0 ± 0.6 cal K^{-1} mol^{-1}, respectively. Its adenosine binding was mainly driven by base stacking.

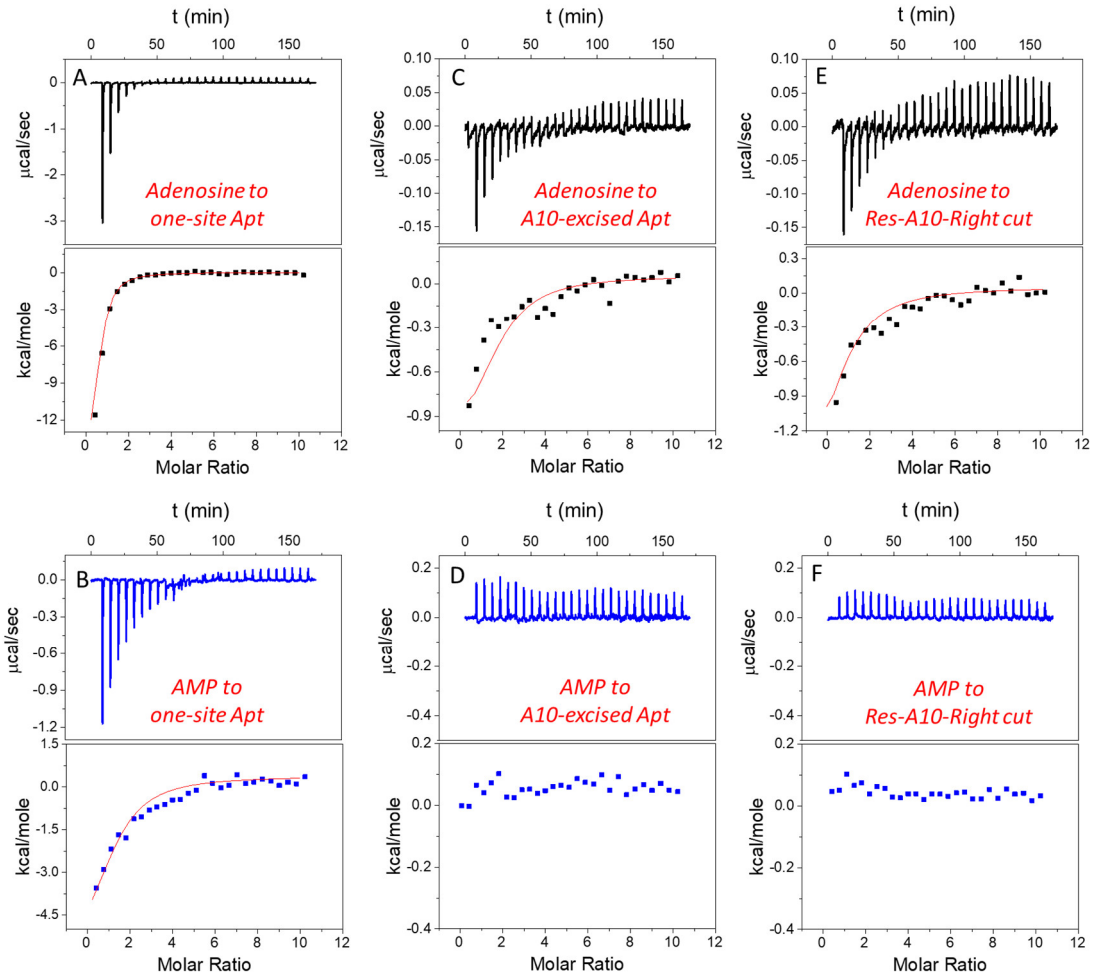

Figure 2.4. ITC traces and integrated heat for 20 µM one-site aptamer titrated by (A) 1 mM adenosine and (B) AMP in buffer A (20 mM HEPES, pH 7.6, 100 mM NaCl, 5 mM $MgCl_2$); 20 µM A10-excised aptamer titrated by (C) 1 mM adenosine and (D) AMP in buffer A; and 20 µM Res-A10 aptamer titrated by (E) 1 mM adenosine and (E) AMP in buffer A. All the titrations were carried out at 10 °C promote aptamer binding, and each titration was repeated at least twice.

Table 2.2. Thermodynamic data of aptamers binding to adenosine and AMP (at 10 °C).

Ligands	**Aptamers**	**N**	**K_a ($\times 10^4$ M^{-1})**	**K_d (μM)**	**ΔG (kcal mol^{-1})**	**ΔH (kcal mol^{-1})**	**ΔS (cal K^{-1} mol^{-1})**
Adenosine	One-site Apt	0.8 ± 0.1	35.8 ± 0.4	2.8 ± 0.03	-7.2 ± 0.1	-13.5 ± 0.4	-22.2 ± 1.5
	Res-A10-Right-cut	0.9 ± 0.2	8.8 ± 0.2	11.4 ± 0.2	-6.4 ± 0.2	-1.0 ± 0.03	19.1 ± 1.2
	A10-excised Apt	1.8± 0.3	5.9 ± 0.7	17.0 ± 1.9	-6.2 ± 0.1	-1.1 ± 0.1	18.0 ± 0.6
AMP	One-site Apt	1.3 ± 0.3	8.3 ± 1.2	12.2 ± 1.8	-6.4 ± 0.8	-4.7 ± 0.3	6.0 ± 0.7
	Res-A10-Right-cut		--[a]				
	A10-excised Apt		--[a]				

[a] Binding was extremely weak and cannot be obtained by ITC. The error is calculated based on fitting by one-site binding model in ITC software.

2.3.6 Investigating binding sites cooperativity

In the wide-type adenosine aptamer, one site can be removed (e.g. the one-site aptamer used in this work) and it even slightly improved adenosine binding.[92] In our A10-excised aptamer, we wanted to understand the relationship between the two adenosine binding sites. For this purpose, two more sequences were designed, named Duplex-1 and Duplex-2, respectively (Figure 2.5A). The Duplex-2 exhibited part of the

same binding pockets (on backbone) as the A10-excised aptamer, but its loop pocket was removed and replaced by complementary base pairs. If Duplex-2 can recognize the target independently, the free adenosine should be able to fit into the vacancy. Since the right-side of the Duplex-2 is very short, Duplex-1 was also designed with the binding site in the middle to ensure formation of the flanked hairpins (confirmed by MFold website server).[121] If adenosine can be independently recognized in Duplex-2, it should also be recognized in Duplex-1. Therefore, we tested the Duplex-1 first.

Figure 2.5B shows that cytidine induced a slight fluorescence increase for Duplex-1 based on the G•C base pairing and stacking (the left black column), but the fluorescence barely changed with adenosine (Figure 2.5B, the left red column). Therefore, the two sites in the A10-excised aptamer very likely worked cooperatively, and removing the one from the loop disrupted the binding ability of the other one on backbone.

For Duplex-2, no fluorescence change was observed regardless of adding cytidine or adenosine. Therefore, this small loop near the 5′-end of the sequence cannot form without the aptamer binding pocket. For comparison, in our A10-excised aptamer, since it showed obvious and strong binding toward adenosine, the aptamer needed to experience a conformational change in its right part.

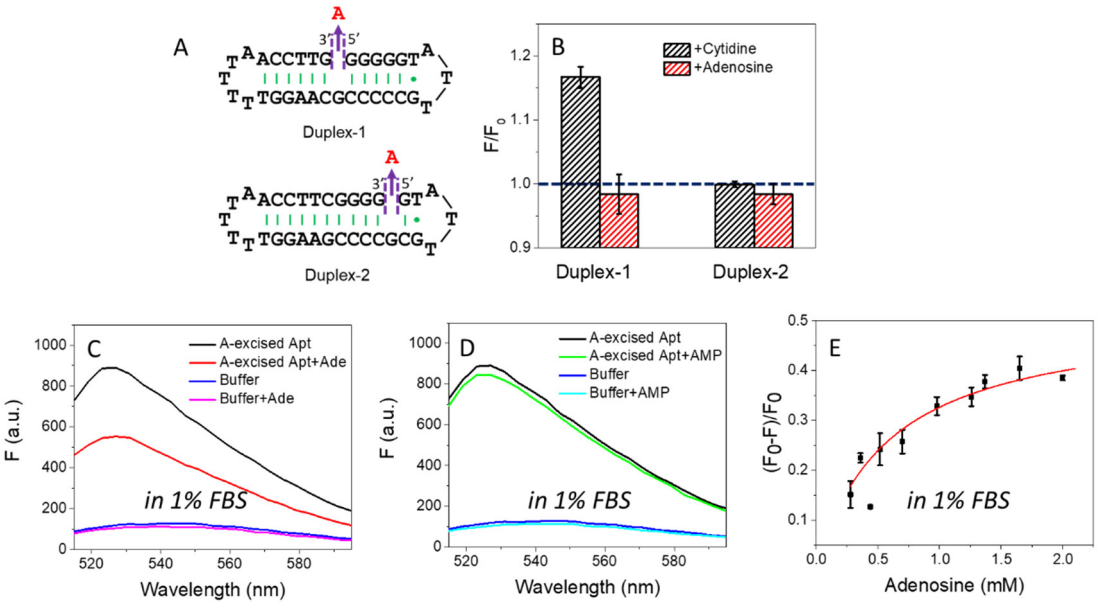

Figure 2.5. (A) The secondary structure of the designed Duplex-1 and Duplex-2. (B) The fluorescence change of 50 nM Duplex-1 and Duplex-2 with 2 mM ligands (adenosine or cytidine) in buffer A. The Duplex-1 and Duplex-2 were stained by 12.5 nM SGI. Fluorescence spectra of the 50 nM A10-excised aptamer mixed with 2 mM (C) adenosine and (D) AMP in 1% FBS (diluted in buffer A). The DNA was stained by 50 nM SGI. (E) Titrating adenosine (0.28 to 2 mM) with the 50 nM A10-excised aptamer in 1% FBS.

2.3.7 Applied the A-excised aptamer in diluted serum

Based on the data in Figure 2.2D, we calculated the detection limit of the A10-excised aptamer to be 46.7 μM adenosine. To demonstrate potential analytical application in a real sample, we then applied the A10-excised aptamer in 1% fetal bovine serum (FBS). Figure 2.5C showed that the aptamer retained adenosine binding, with ~38% fluorescence decrease. AMP still showed no signal (Figure 2.5D). The fluorescence signal change in the diluted FBS was close to that in the clean buffers (~40%, in Figure 2B). Furthermore, we also titrated adenosine with the A10-excised aptamer in 1% FBS, and calculated K_d (Figure 5E). The value was about 0.57 mM, comparable with 0.37 mM in the clean buffers (based on the SGI bind assays). The

experiments demonstrated that our A-excised aptamer was robust. The increased background fluorescence disallowed us to test more concentrated serum. Since many signal transduction methods are available based on the wide-type aptamer to ultra-sensitively detect adenosine, the goal of this work is to achieve highly specific adenosine recognition.

2.4 Summary

Recently, non-SELEX-derived aptamers were reported based on some classic DNA structures, such as a duplex and a G-quadruplex, through introducing a vacant-site on their backbones. Free nucleosides and nucleotides can re-fit into this vacancy. However, the selectivity of this strategy is still limited likely due to its dependence on these simple secondary structures and interactions (base pairing or even pseudo-base pairing). In this work, we employed an aptamer as scaffold, which exhibited a more delicate higher structure than a duplex and a G-quadruplex, allowing highly specific adenosine recognition. When excising an entire A from the adenosine aptamer backbone (termed the A-excised aptamer), only adenosine can fit into the vacancy. Other analogues including AMP, ATP, guanosine, cytidine, uridine and theophylline all failed to bind. SGI binding assays and ITC were used to verify the adenosine binding and investigate related mechanisms. The A10-excised aptamer associated adenosine with a K_d of 17.0 ± 1.9 μM at 10 °C, mainly driven by base stacking. We demonstrated that the A10-excised aptamer can accept two adenosine molecules, with one in the excised site (DNA backbone) and the other in the original binding pocket (loop area). They worked cooperatively to achieve the high specificity. Finally, this engineered aptamer can also work in dilute FBS. This work provides an intriguing example of using existing aptamer sequences for enhanced functions.

Chapter 3 Engineering base-excised aptamers for highly specific recognition of guanosine

The results presented in this chapter have been published as:

Yuqing Li, Juewen Liu, Highly specific recognition of guanosine using engineered base excised aptamers. *Chemistry-A European Journal*, **2020**, *26*, 13644-13651.

3.1 Introduction

Purines are of vital importance for transferring genetic information, participating in cellular processes, and regulating signaling pathways.[122-124] For example, guanosine can regulate glutamate transport and uptake in brain cortical slices,[125] while adenosine can regulate inflammatory responses and limit destruction of inflammatory tissues.[126] Monitoring purines and their derivatives contributes to early diagnosis and treatment of diseases, such as brain damage, immunodeficiency and cancer.[127-130]

Aptamers are ideal to bind and detect small molecules such as purines.[131-135] High quality aptamers were found in the riboswitches for adenine and guanine.[78, 136-138] However, it is difficult to use these large RNA molecules (around 100-mer) as biosensors for applications outside cells.[139-142] While aptamers from SELEX (systematic evolution of ligands by exponential enrichment) can be shorter and many aptamers can bind adenine derivatives,[4, 8, 23, 89, 92, 95, 143, 144] high quality guanosine aptamers, especially DNA aptamers, have yet to be reported.[90, 145-148] Connell and Yarus reported an RNA aptamer that can bind guanosine and guanine nucleotides with similar affinity.[149] Kiga et al. selected a 32-mer RNA aptamer for xanthine, which can bind guanosine with a K_d of 140 μM, but the specificity was poor.[145]

Recently, some non-SELEX derived aptamers were reported. For example, a vacancy-bearing DNA scaffold (like a duplex or G-quadruplex) can act as an aptamer to bind free purine nucleosides.[10, 12, 42, 43, 150] We reported a DNA sequence (32-mer)

with excellent specificity for adenosine using the adenosine/ATP aptamer as a scaffold.[11] We named it a base-excised aptamer, in which an adenine nucleotide near the aptamer binding site was completely removed, and this engineered sequence turned out to have excellent specificity to adenosine (no binding of AMP or ATP).

Inspired by this finding, we wanted to test whether this base excision method can be extended to other scaffolds to achieve high specificity, especially for the specific binding of guanosine, which was never achieved before. In this work, a Na^+-binding aptamer was employed as a scaffold.[80, 81, 151, 152] Both G- and A-excised strands were studied. By exploring both the Na^+ aptamer and the adenosine aptamer, as well as different types of excision sites, we obtained a few highly specific aptamers for guanosine. At the same time, this work provides deeper insights and a more complete picture of the base-excision strategy for molecular recognition.

3.2 Materials and Methods

3.2.1 Chemicals

All the DNA samples were purchased from Eurofins (Huntsville, AL). The DNA sequences are listed in Table 3.1. Thioflavin T (ThT), SYBR Green I (SGI), guanosine monophosphate (GMP), guanosine triphosphate (GTP), adenosine monophosphate (AMP), adenosine triphosphate (ATP), fetal bovine serum (FBS), rubidium chloride, and cesium chloride were purchased from Sigma-Aldrich. Guanosine, adenosine, cytidine, thymidine, 4-(2-hydroxyethyl)piperazine-1-ethanesulfonate (HEPES), sodium chloride, magnesium chloride, lithium chloride, potassium chloride were from Mandel Scientific (Guelph, Ontario, Canada). Milli-Q water was used to prepare all buffers and solutions.

Table 3.1. The DNA sequences and modifications used in this work.

DNA Names	**Sequences (from 5′ to 3′) and modifications**
Substrate	GTCACGAGTCACTATrAGGAAGATGGCGAAA
Ce13d DNAzyme	TTTCGCATAGGTCAAAGGTGGGTGCGAGTTTTTACT CGTTATAGTGACTCGTGAC
Ce13d-del-G16	TGCGAGTTTTCTCGTTATAGTGTTCACTATAGGAAG AACGTCTCGTTAGGTCAAAGGTGG
Ce13d-del-G15	GTGCGAGTTTTCTCGTTATAGTGTTCACTATAGGAA GAACGTCTCGTTAGGTCAAAGGTG
Ce13d-del-G14	GGTGCGAGTTTTCTCGTTATAGTGTTCACTATAGGA AGAACGTCTCGTTAGGTCAAAGGT
Ce13d-del-A10	GGTGGGTGCGAGTTTTCTCGTTATAGTGTTCACTAT AGGAAGAACGTCTCGTTAGGTCAA
Ce13d-del-A9	AGGTGGGTGCGAGTTTTCTCGTTATAGTGTTCACTA TAGGAAGAACGTCTCGTTAGGTCA
Ce13d-del-A8	AAGGTGGGTGCGAGTTTTCTCGTTATAGTGTTCACT ATAGGAAGAACGTCTCGTTAGGTC
Random DNA	GAGGAAGGTTTTTAACCTTCGGGGAGTATTGC
MYOG-3332	AGGGTGGGCTGGGAGGT
Ade apt-del-G19	AGGAAGGTTTTTAACCTTCGGGGAGTATTGCG
Ade apt-del-G18	GAGGAAGGTTTTTAACCTTCGGGGAGTATTGC
Ade apt-del-G9	AGTATTGCGGAGGAAGGTTTTTAACCTTCGGG
Ade apt-del-G8	GAGTATTGCGGAGGAAGGTTTTTAACCTTCGG

3.2.2 ThT-based binding assays for Na^+ aptamer

For the G-excised Na^+ aptamers, 200 nM DNA was incubated with 2 mM target molecules, such as guanosine, GMP, GTP, adenosine, cytidine or thymidine in buffer (50 mM HEPES, pH adjusted by LiOH to pH 7.6, 100 mM NaCl). The same DNA incubated with the buffer but without a target was used as controls. A final of 10 μM ThT was then added to stain the DNA. The fluorescence spectra were measured by exciting the sample at 445 nm. The fluorescence data were analyzed using $(F_0\text{-}F)/F_0$, in which F_0 and F stand for the fluorescence at 490 nm without and with the target, respectively. For the A-excised Na^+ aptamers, the experimental conditions were same except that 4 μM ThT was used. To quantify Na^+ binding specificity, 200 nM DNA was incubated with 2 mM guanosine in the buffer. Then 100 mM LiCl, KCl, RbCl, CsCl or NH_4Cl was individually tested.

3.2.3 Evaluating K_d and binding cooperativity

Different concentrations of guanosine, adenosine and GMP (0.35 to 2.5 mM) were titrated to 200 nM G16-excised Na^+-aptamer in buffer (50 mM HEPES, pH 7.6, 100 mM NaCl) containing 10 μM ThT. The titration curves were fitted by the one-site binding equation (1):

$$(F_0\text{-}F)/F_0 = a + B_{\max}[\text{Ligand}]/(K_d+[\text{Ligand}]) \quad (1)$$

where B_{max} is the maximum fluorescence change, [Ligand] is the concentration of guanosine, adenosine or GMP. For comparison, titration was also performed for a vacancy-bearing G-quadruplex called MYOG-3332. Another experiment was by adding 100 mM Na^+ or Li^+ into the 200 nM G-excised Na^+-aptamer without or with of 2 mM guanosine (adenosine was added for the A-excised sequences). 10 μM ThT was used for staining the G-excised aptamers, and 4 μM ThT was used for the A-excised aptamers. Finally, the $F(Li^+)/F(Na^+)$ was calculated to analyze the specificity for Na^+ binding.

3.2.4 Probing binding by 2AP

1 μM substrate (the rA site replaced by deoxy-2AP) and 2 μM enzyme strand of Ce13p or the G16-excised Ce13p were annealed in buffer (50 mM HEPES, adjusted pH by LiOH, pH 7.6) and gradually cooled to 4°C. Then the samples were transferred to a 96-well plate and the fluorescence was measured at room temperature. 100 mM NaCl or LiCl was added to investigate the fluorescence change. Then, 2 mM guanosine was added to further observe the fluorescence change. The 2AP was excited at 310 nm, and the emission spectra were collected from 365 to 440 nm.

3.2.5 SGI-based assays for the adenosine aptamer

50 nM G-excised adenosine aptamer was incubated with 2 mM adenosine (as the background) and 2 mM target, including guanosine, GMP, GTP, adenosine, cytidine or thymidine in buffer (50 mM HEPES, pH 7.6, 100 mM NaCl and 5 mM $MgCl_2$). The aptamer incubated with the 2 mM adenosine (without target) was used as control. Then, a final of 50 nM SGI was added to stain the DNA. The fluorescence spectra were collected at 535 nm (excitation at 485 nm).

3.2.6 Detection in diluted FBS

5% FBS was prepared by diluting 50 μL of the FBS in 950 μL of 50 mM HEPES (pH 7.6). Then, 200 nM G16-excised Na^+-aptamer with different concentrations of guanosine (0.35~2.5 mM) were incubated in the 5% FBS with addition of 100 mM NaCl. 10 μM ThT was used for staining the DNA, and the fluorescence spectra was measured after 15 min from 475 to 600 nm, with the excitation at 445 nm.

3.3 Results and Discussion

3.3.1 The base-excision strategy

Our base-excision method is illustrated in Figure 3.1A, where an entire purine nucleotide (A or G) is removed from an aptamer backbone. This break generates the

new 3′ and 5′ termini, and we hope this breaking site will be rejoined by binding the excised nucleoside or nucleotide. After excising the A10 in the adenosine aptamer (along with a few other changes to stabilize the engineered aptamer, Figure 3.1B), the sequence was able to specifically bind adenosine,[11] while the original aptamer can hardly differentiate adenosine from AMP and ATP.[4]

In our current work here, a Na^+-specific aptamer was used as a new scaffold (Figure 3.1C), and we wanted to test if we can obtain aptamers for both guanosine and adenosine. We chose this aptamer since it was well characterized.[151-154] The Na^+ aptamer is in the Ce13d DNAzyme, which contains a substrate stand (in green) and an enzyme strand (in red/black). The rA in substrate is the cleavage site. Ce13d requires both a lanthanide such as Ce^{3+} and Na^+ for the cleavage activity, while its enzyme loop (in red) is a major part of the Na^+ aptamer. We picked three consecutive guanines G14, G15, G16, and three consecutive adenines A8, A9, A10 in aptamer loop. They are adjacent to each other, but played different functions. The G15, G16, A9 and A10 are highly conserved, whereas G14 and A8 can be mutated to other nucleotides.

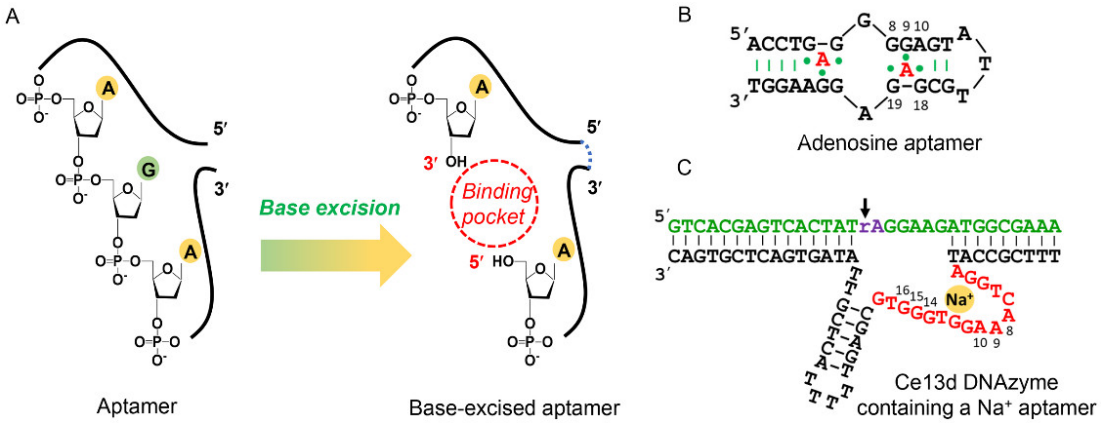

Figure 3.1 (A) A scheme of the base-excision strategy. The secondary structures of (B) the wild-type adenosine aptamer that can bind two adenosine molecules denoted by the red A letters, and (C) the Na^+-aptamer containing Ce13d DNAzyme. The Na^+ ion is bound in the red loop and the purines studied are numbered.

3.3.2 Guanosine specifically binds to the G16-excised Na^+-aptamer

To study aptamer binding, the rA site in the Ce13d DNAzyme was replaced by its DNA analog (dA) to prevent cleavage (Figure 3.2A, left sequence). To further facilitate our study, a shortened circular form was designed in Figure 3.2A (61-nt, the middle sequence). This way, after excising a nucleotide, a 60-nt linear DNA was obtained. In the right panel, an example of excised G16 is shown, where its adjacent T became the new 5′, and G15 became the new 3′ (named Ce13d-del-G16 or ΔG16). Similarly, we designed DNA sequences with G14 and G15 respectively excised (ΔG14 and ΔG15).

Thioflavin T (ThT) was used for a label-free binding assays.[155-157] With 100 mM NaCl, when 2 mM guanosine was added into ΔG16, ~35% fluorescence decrease was observed (Figure 3.2B). In contrast, much less fluorescence decrease was observed for ΔG15, and no change occurred for ΔG14 (Figure 3.2C). Therefore, the ΔG16 appeared to be able to bind guanosine, and this binding displaced some ThT dye to decrease the fluorescence signal.

We then tested the binding specificity of the ΔG16 (Figure 3.2D). Only guanosine induced a fluorescence decrease, whereas adenosine, cytidine and thymidine resulted in no change. Importantly, GMP and GTP showed no change as well. Thus, a single phosphate difference can be effectively distinguished in this Na^+-aptamer scaffold. As a further control, we tested the effect of different monovalent ions. Only Na^+ supported binding of guanosine in ΔG16 (Figure 3.2E), suggesting a driving force of guanosine binding was the formation of the Na^+ binding aptamer.

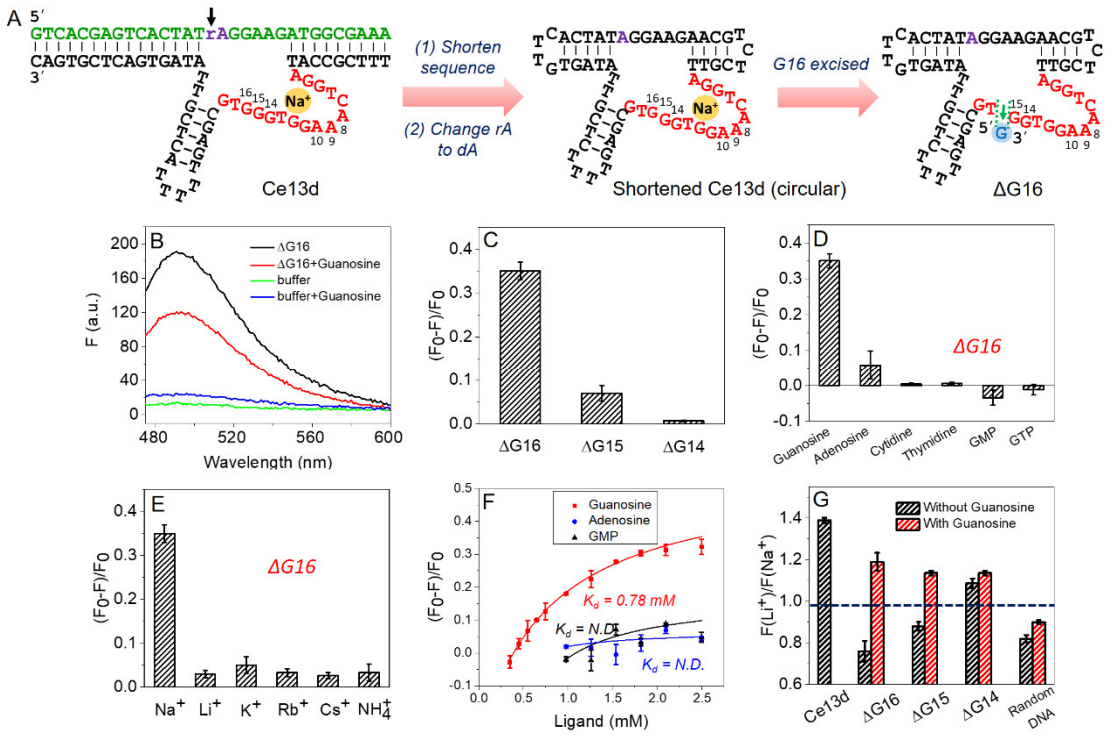

Figure 3.2 (A) The secondary structure of the Ce13d DNAzyme with the rA replaced by dA, a shortened circular Ce13d, and ΔG16, which is a linear DNA with G16 excised from the circular DNA. (B) The fluorescence spectra of 200 nM ΔG16 without and with 2 mM guanosine in buffer (50 mM HEPES, pH 7.6 adjusted using LiOH) containing 100 mM NaCl and 10 μM ThT. The fluorescence intensity of (C) three G-excised Na^+-aptamers bound to guanosine, (D) ΔG16 selectivity, and (E) the effect of metal ions on guanosine binding for ΔG16. (F) Guanosine, adenosine and GMP titrations (0.35 to 2.5 mM) to 200 nM ΔG16. (*N.D.* = not determined). (G) The summary of $F(Li^+)/F(Na^+)$ of 200 nM full-length Ce13d, ΔG16, ΔG15, ΔG14 and random DNA with 100 mM LiCl or NaCl. 2 mM guanosine was used to study the cooperativity with Na^+.

3.2.3 Binding affinity and cooperativity

We gradually titrated guanosine to the ΔG16, and fitted the data by the one-site binding equation yielding a K_d of 0.78 mM guanosine (Figure 3.2F). To test if binding of guanosine and Na^+ was cooperative, we designed the following experiments. Since Li^+ is smaller than Na^+, Li^+ can interact with DNA more strongly via electrostatic

interactions, and condense DNA to a more compact structure, resulting less ThT intercalation.[158] Therefore, for a random DNA stained by ThT, we expected a lower fluorescence in Li^+ than in Na^+ (i.e. $F(Li^+)/F(Na^+) < 1$). For the full-length Ce13d, since Na^+ can specifically fold it, its ThT fluorescence should be lower in Na^+ than in Li^+ (i.e. $F(Li^+)/F(Na^+) > 1$).

After confirming this (Figure 3.2G, the first bar), we tested the ΔG16. When no guanosine was presented, its $F(Li^+)/F(Na^+)$ was smaller than 1, demonstrating non-specific Na^+ binding. However, once guanosine was added, specific Na^+ binding was observed. In the same way, we investigated the ΔG15 and ΔG14. Only ΔG14 retained a moderate Na^+ binding in the absence of guanosine. Our previous dimethyl sulphate (DMS) footprinting and cleavage activity studies indicated that G16 and G15 were highly conserved and involved in Na^+ binding, while G14 was not.[153, 159]

We reasoned that the driving force for binding guanosine was to form the aptamer pocket for Na^+ (folding to a specific tertiary structure). Without Na^+, such driving force did not exist and thus guanosine cannot bind. However, such binding pocket cannot be folded in ΔG16 by Na^+ alone. Guanosine was required to be present (Figure 3.3).

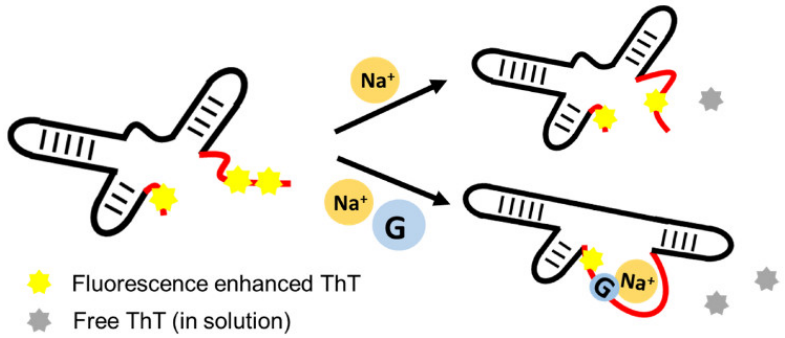

Figure 3.3 Cooperative binding of Na^+ and guanosine in the G-excised Na^+-aptamer.

3.2.4 Adenosine specifically binds to the A10-excised Na^+-aptamer

On the same Ce13d scaffold, we also tested the binding of adenosine. A8, A9, A10 were respectively excised in the same way as indicated in Figure 3.2A, and ΔA8, ΔA9

and ΔA10 were obtained. The secondary structure of the ΔA10 is shown in Figure 3.4A as an example.

By using the ThT assays, about 32% fluorescence decrease was observed for ΔA10 when 2 mM adenosine was added (Figure 3.4B), whereas that drop for ΔA8 and ΔA9 was much smaller (only ~6-10%, Figure 3.4C). Therefore, ΔA10 might be able to bind adenosine. We then tested the specificity of ΔA10 by adding guanosine, cytidine, thymidine, AMP, and ATP (Figure 3.4D), and none of them showed more than 10% signal change. The effect of metal ions on adenosine was also investigated (Figure 3.4E), and the binding of adenosine occurred also only in the presence of Na^+.

In the A-excised aptamers, ΔA10 needed the help of adenosine to support its specific Na^+ binding as well (Figure 3.4F). Our previous study revealed that the A10 is a conserved base and cannot be mutated. Taken together with the highly conserved G16 and the specific guanosine binding of the G16-excised aptamer, we reason the optimal excision sites are also important for Na^+ recognition.

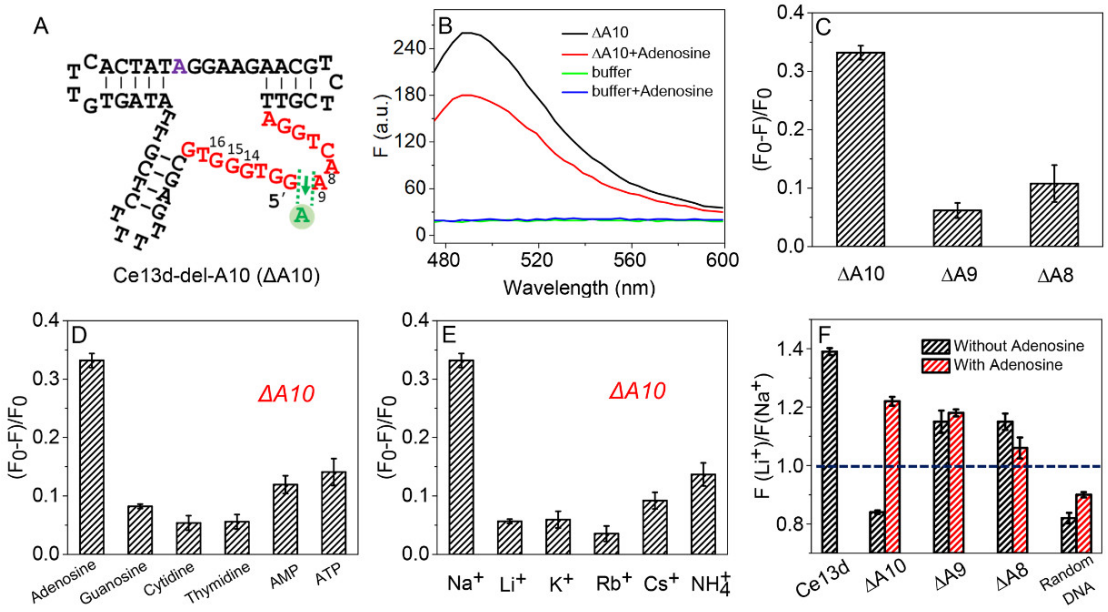

Figure 3.4 (A) The secondary structure of the ΔA10, and the excised adenine is shown in green. (B) The fluorescence spectra of 200 nM ΔA10 without and with 2 mM adenosine in buffer containing 100 mM NaCl and 10 μM ThT. The fluorescence change

of (C) the three A-excised Na^+-aptamers after adding adenosine, (D) ΔA10 selectivity, and (E) the effect of metal ions on adenosine binding for ΔA10. (F) The $F(Li^+)/F(Na^+)$ of 200 nM of the full-length Ce13d, ΔA10, ΔA9, ΔA8 and random DNA in 100 mM LiCl or NaCl without and with 2 mM adenosine.

3.2.5 Probing binding using a covalent 2AP label

The above binding assays were performed using ThT staining. We wanted to have an independent verification to further confirm our observations. For this purpose, the rA on substrate strand was replaced by a deoxy-2-aminopurine (2AP) (Figure 3.5A). 2AP is a fluorescent adenine analog sensitive to its base stacking environment with the nearby nucleotides. Increasing stacking decreases the 2AP fluorescence.[160] Based on our previous findings, the A10C and T20A double mutant (called Ce13p, Figure 3.5B) had a high response to Na^+ binding.[151] Here, we used Ce13p, and its G16 was excised (Figure 3.5C). To distinguish it from ΔG16 which was from the circular Ce13d scaffold, this one was named ΔG16p.

First, we confirmed that the full-length Ce13p only responded to Na^+ (Figure 3.5D) but not to Li^+ (Figure 3.5E). Upon Na^+ binding, the fluorescence of 2AP increased 2.5-fold, indicating relaxation on the 2AP base stacking (Figure 3.5F).[151] Interestingly, in ΔG16p, we found an opposite trend. Na^+ and guanosine together induced about 30% fluorescence decrease (instead of increase, Figure 3.5G), whereas Na^+ alone or Li^+ and guanosine mixture (Figure 3.5H) cannot bring in an obvious fluorescence change. Therefore, Na^+ and guanosine need to be present simultaneously.

We noticed that the initial fluorescence of the Ce13p and ΔG16p in the absence of Na^+ were quite different (Figure 3.5I). After excising G16, the fluorescence of 2AP increased about 1.4 times, indicating that this deletion relaxed the 2AP region (right inset in Figure 3.5I), which was understandable since the overall structure should be floppier after the excision. We reasoned that the binding of Na^+ and guanosine in

ΔG16p reconstructed the original binding pocket, although it probably cannot fold the aptamer to the Ce13p status at the 2AP site (Figure 3.5J).

Selectivity tests were also performed in the 2AP-modified ΔG16p. Na^+ showed 3-fold or more fluorescence decrease than the other metal ions (Figure 3.5K), and only guanosine was able to work with Na^+ to achieve the fluorescence increase (Figure 3.5L). Therefore, this 2AP assay also indicated specific binding of guanosine in the presence of Na^+.

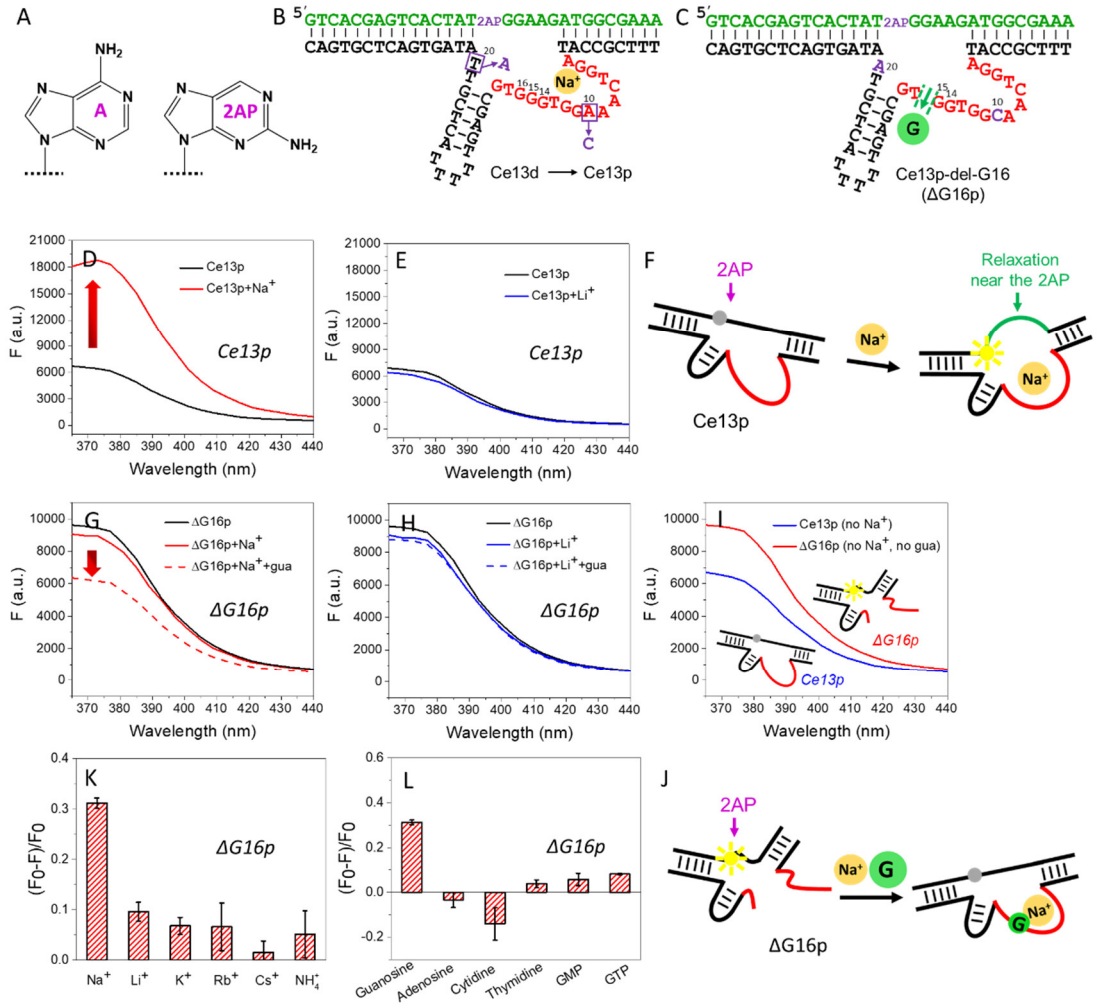

Figure 3.5 (A) The structures of adenine and 2AP. The secondary structures of 2AP-modified (B) Ce13p and (C) ΔG16p. The fluorescence spectra of Ce13p (1 μM 2AP-substrate strand and 2 μM enzyme strand) with (D) 100 mM Na^+ and (E) 100 mM Li^+ in buffer (50 mM HEPES, pH 7.6 adjusted using LiOH). (F) Schematics of the 2AP

fluorescence change of the Ce13p upon Na^+ binding. The fluorescence spectra of ΔG16p (1 μM 2AP-substrate strand and 2 μM each split enzyme strand) with (G) 100 mM Na^+ and (H) 100 mM Li^+, also with 2 mM guanosine. (I) The initial fluorescence of the 2AP-labeled Ce13p and ΔG16p without Na^+ or guanosine. Inset: schematic folding status of the Na^+ aptamers in Ce13p and ΔG16p. (K) The effect of metal ions (100 mM of each) on 2 mM guanosine binding for ΔG16p. (L) The fluorescent decrease of ΔG16p binding to 2 mM nucleosides or nucleotides, in the presence of 100 mM NaCl. (J) Schematics of the 2AP fluorescence change of ΔG16p upon Na^+ and guanosine binding.

3.2.6 The adenosine aptamer scaffold can also detect both adenosine and guanosine

To investigate the generality of guanosine sensing using the base-excision method, the adenosine aptamer was tested as an alternative scaffold. The secondary structure of the wild-type adenosine aptamer is shown in Figure 3.6A (left), in which the red A stands for adenosine, AMP or ATP. The four guanines (i.e. G8, G9, G18 and G19) around the target binding site played different roles in adenosine recognition (including forming G•A mismatches and G•G mismatches).[89] We individually excised these four G nucleotides for specific guanosine recognition. To simplify the binding model, first we removed the left binding pocket to generate an one-site aptamer (middle sequence, Figure 3.6A).[92] We then sealed the two ends by adding a small loop, which was then used for base excision. For example, G19 was deleted in the right panel of Figure 3.6A. The other three guanines were excised in same way. The G19, G18, G9 and G8-excised sequences were named as ΔG19', ΔG18', ΔG9' and ΔG8', respectively.

SGI was used for the binding assays in this part.[115, 116, 161] Figure 3.6B shows that adding adenosine and guanosine together dropped the fluorescence by ~38% for ΔG19', whereas adenosine or guanosine alone could not drop the signal, indicating that they needed to work together to fold the aptamer. In contrast, when adenosine and guanosine were both added, no fluorescence change occurred in the ΔG18', ΔG9' or ΔG8' (Figure

3.6C). Likely G19 in this aptamer is most critical for target binding. Apart from guanosine, other analogues like cytidine, thymidine, GMP and GTP all failed to bring a signal change in ΔG19' (Figure 3.6D). Thus, a single phosphate can be distinguished in the adenosine aptamer scaffold as well.

It is known that G8, G9, G18, G19 and A10 are all highly conserved, and any mutation to them can abolish aptamer binding.[4] Our previous study found that the A10-excised aptamer can specifically recognize adenosine.[11] Taken together the G19-excised aptamer here, and the two more from the Na^+-aptamer, highly conserved purines are more likely to be the optimal excision sites than the non-conserved ones, although not all conserved sites would work. A screening assay is needed to identify best excision sites.

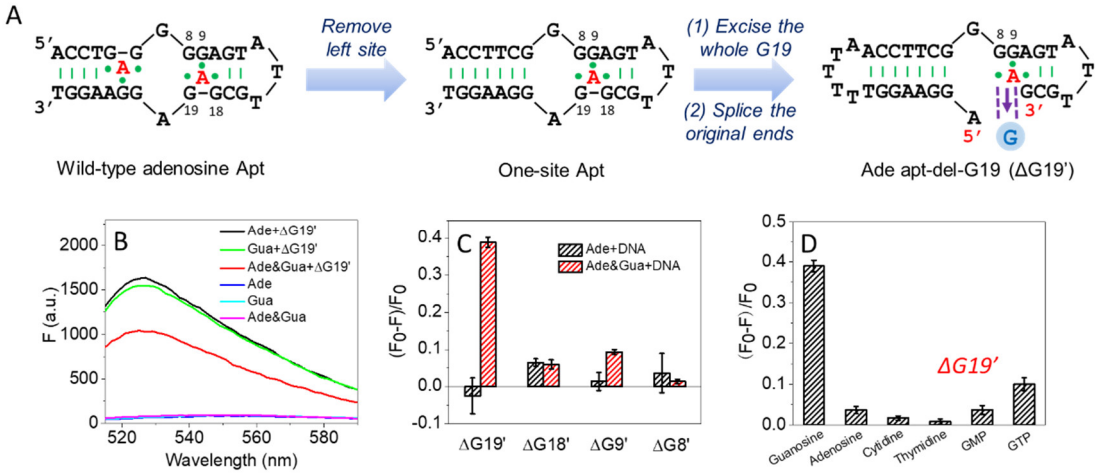

Figure 3.6 (A) The secondary structures of the wild-type adenosine aptamer, the engineered one-site aptamer, and the G19-excised aptamer. (B) The fluorescence spectra of 50 nM ΔG19' incubated with 2 mM adenosine, guanosine, and their mixture in buffer (50 mM HEPES, pH 7.6), with 100 mM NaCl and 5 mM $MgCl_2$. 50 nM SGI was used to stain the DNA. The fluorescence intensity of (C) 50 nM various G-excised aptamers mixed with 2 mM adenosine and 0 or 2 mM guanosine, and (D) 50 nM ΔG19' mixed with 2 mM adenosine (as background) and 2 mM guanosine, adenosine, cytidine, thymidine, GMP or GTP.

3.2.7 Comparing aptamer and G-quadruplex scaffolds

To the best of our knowledge, SELEX-derived guanosine DNA aptamers have not yet been reported. Recently, a few vacancy-bearing G-quadruplexes were found to bind guanosine and induce the formation of G-quadruplexes.[10, 42, 162] For example, a defect G-quadruplex (named MYOG-3332) was characterized to be in a parallel conformation by Tan et al (Figure 3.7A), in which the top layer bears a guanosine binding pocket.[10] A major difference of our design and our base excision design is that we have a break at the intended guanosine binding site and the break generates new termini, while the G-quadruplex scaffolds were continuous at the binding site. Nevertheless, it is still an interesting comparison for these two ideas of detecting the removed base.

We used this MYOG-3332 sequence to compare with our base excised aptamers. ThT was used to probe the G-quadruplex formation.[155] With 100 mM LiCl added, a strong fluorescence was observed, while 100 mM KCl had only about 20% of the intensity (Figure 3.7B). Since the G-quadruplex formation needed the help of K^+, the lower fluorescence in K^+ can be explained by its folding to a G-quadruplex. Upon adding 2 mM guanosine (orange curve, Figure 3.7C), the fluorescence further dropped by 30%, demonstrating stabilization of the full G-quadruplex.

To compare specificity, we then incubated MYOG-3332 with adenosine, cytidine, thymidine, GMP or GTP (Figure 3.7D). Although A, C and U had almost no fluorescence change, GMP and GTP induced a change comparable to guanosine. Therefore, all guanine-bearing molecules can be accommodated by the vacancy through forming the G-quartet via the lock-and-key mechanism (e.g. the quadruplex structure already formed even without the free guanosine).[10] In contrast, our G-excised adenosine aptamer and Na^+-aptamer exhibited the additional ability to distinguish a single phosphate, probably because the aptamer binding involved adaptive recognition,[163] thus more close to "induced-fitting" complementary. Using our method, the apparent K_d values of the MYOG-3332 binding guanosine and GMP were 0.79 mM

and 1.31 mM, respectively (Figure 3.7E). Therefore, the guanosine binding affinity of the MYOG-3332 was comparable with our G16-excised Na^+-aptamer.

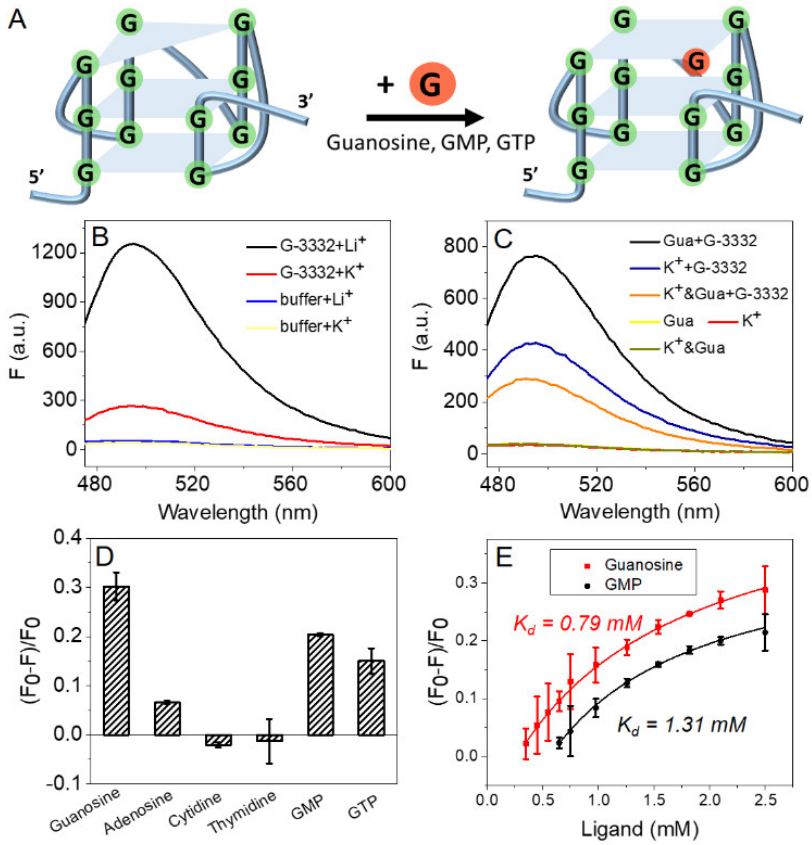

Figure 3.7 (A) A scheme of guanosine filling in a vacancy-bearing G-quadruplex (named MYOG-3332). The fluorescence spectra of (B) 200 nM MYOG-3332 with 100 mM KCl or LiCl in buffer (50 mM HEPES, pH 7.6 adjusted using LiOH), and (C) 200 nM MYOG-3332 with guanosine or K^+ alone and with their mixture. 10 μM ThT was used to stain the DNA. (D) The bar plot of 200 nM MYOG-3332 with 2 mM guanosine, adenosine, cytidine, thymidine, GMP or GTP, with 100 mM KCl added. (E) Guanosine and GMP titrations (0.65 to 2.5 mM) to 200 nM MYOG-3332. The K_d was fitted by the one site binding equation.

3.2.8 Additional discussion

In this work, we used the sodium and adenosine binding aptamers as scaffolds for base excision and guanosine binding. In each example, only one optimal site worked.

Therefore, whether any given aptamer can be used for base excision or not has to be individually tested. In general, the aptamer should bind its target with a well-defined three-dimensional structure and contain important guanines involved in target binding. We previously excised an adenine from a duplex region but that did not allow rebinding of adenosine.[11] Therefore, not all DNA structures can be used either.

3.2.9 Sensing guanosine in serum

The above studies were all carried out in clean buffers. When extending the application of base-excised aptamers to real samples, the matrix effect may appear.[164-166] To investigate the application of our G16-excised Na^+-aptamer, we tested it in 5% fetal bovine serum (FBS). Figure 3.8A showed that ~30% ThT fluorescence decrease was observed in 2 mM guanosine, comparable to the ~35% fluorescence decrease in the buffer. Then, guanosine (0.35~2.5 mM) was titrated to the DNA in 5% FBS (Figure 3.8B), generating a K_d at 0.93 mM. A detection limit of 0.32 mM guanosine was obtained, which was comparable to the detection limit at 0.28 mM in clean buffer (Figure 3.8C). Therefore, in 5% FBS, the Na^+-aptamer was still quite robust.

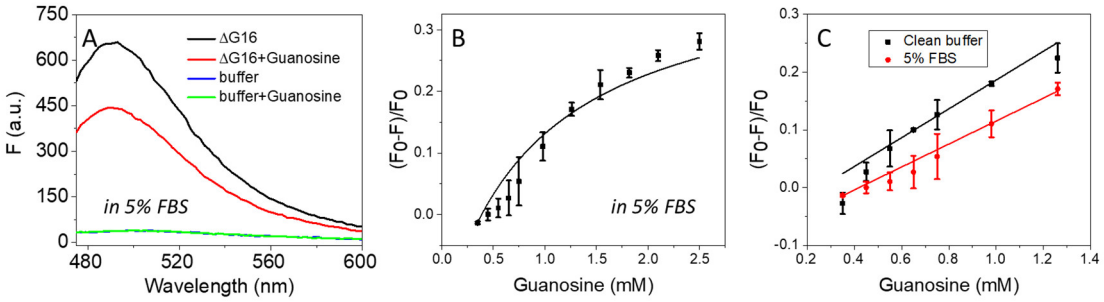

Figure 3.8 (A) The fluorescence spectra of 200 nM ΔG16 DNA without and with 2 mM guanosine in 5% FBS (diluted in 50 mM HEPES, pH 7.6, with 100 mM NaCl). (B) Titrating various concentrations of guanosine (0.35~2.5 mM) to 200 nM ΔG16 Na^+-aptamer in 5% FBS. 10 μM ThT was used to stain the DNA. (C) Linear fitting for titrating guanosine (0.35 to 1.26 mM) into the ΔG16 Na^+-aptamer in buffer (50 mM HEPES, pH 7.6) and 5% FBS (diluted in same buffer) with 100 mM NaCl. 10 μM ThT

was added to stain the DNA. The limit of detection was calculated based on the equation of 3σ/k (σ is the relative standard deviation and k is the slope of the fitted equation).

3.3 Summary

In summary, we have reported highly selective guanosine binding aptamers without performing new aptamer selections. Simply by using the base-excision strategy, a Na^+-specific aptamer and an adenosine binding aptamer were employed as scaffolds. A total of 10 base-excised DNA sequences were studied. Out of these, two optimal sequences were obtained and they only bind guanosine but not GMP or GTP. Combined with previous biochemical studies, highly conserved purines are more likely to be the optimal positions for excision to obtain binding pockets for specific recognition of purine nucleoside. Previous aptamer selection attempts for guanosine has not resulted in high quality DNA aptamers. The binding sites in our aptamers brought the ends of a DNA strand together, which is very difficult to realize in conventional aptamer selection. Other aptamer engineering strategies such as removal of a G base without breaking the strand did not results in exquisite binding of guanosine, since GMP and GTP could also bind. This work provides a useful strategy for engineering guanosine-binding sequences based on existing aptamers.

Chapter 4 Incorporation of boronic acid into aptamer-based molecular imprinting hydrogels for highly specific recognition of adenosine

The results presented in this chapter have been published as:

Yuqing Li, Zijie Zhang, Biwu Liu, Juewen Liu, Incorporation of boronic acid into aptamer-based molecularly imprinted hydrogels for highly specific recognition of adenosine, *ACS Applied Bio Materials*, **2020**, *3*, 2568-2576.

4.1 Introduction

Molecular recognition is critical for sensing, separation, and targeted therapeutics.[167-171] Antibodies[172, 173] and aptamers[92, 163, 174] are specific biopolymers that can bind target molecules with high affinity and specificity. However, they have a high cost and relatively low stability. Molecularly imprinted polymers (MIPs) are prepared by polymerizing various monomers and crosslinkers around a template molecule. After removing the template, the resulting cavities allow specific rebinding of the target.[175-177] MIPs are highly stable and cost-effective, but their binding affinity and specificity are often lower compared to aptamers or antibodies.[178-180]

We are interested in combining these two strategies through the incorporation of biological receptors into MIPs to maximize their advantages.[63] DNA aptamers are oligonucleotide-based ligands,[181, 182] which are more stable than antibodies. DNA-containing MIPs have been reported in a few cases. For example, Spivak et al. used full-length aptamers to imprint thrombin as well as a virus.[64, 183] Bowen et al. designed an aptamer-MIP receptor to detect prostate-specific antigens with a limit of detection of 1 pg/mL.[184] Liu et al. incorporated a glycoprotein aptamer into polydopamine to recognize alkaline phosphatase.[185] Our group recently split a DNA aptamer into two halves, and found that such aptamer fragments were also able to act as macromonomers

to specifically recognize adenosine.[111] Recently, through molecular imprinting, we achieved specificity for a DNAzyme with peroxidase-like activity.[186, 187] An advantage of synthetic polymers is the availability of a wide variety of monomers. By rational choice of monomers, we may enhance aptamer performance via imprinting.

Adenosine is an important model molecule in the aptamer field. The adenosine aptamer can nicely distinguish adenosine (A) from the three other ribonucleosides (G, U, and C), but cannot distinguish adenosine from deoxyadenosine (only differ by a -OH).[4] At the same time, it cannot distinguish adenosine from AMP or ATP either. Efforts have been made in selecting new aptamers for improved discrimination of the phosphate part in these molecules,[8, 96, 98] but distinguishing adenosine and deoxyadenosine has yet to be demonstrated. Adenosine and deoxyadenosine regulate transfer of different genetic information and take part in various cellular processes. Abnormal levels of adenosine indicate unbalanced physiological functions of the heart and brain, and improper regulation of oxygen supply for cell stress. Therefore, selective detection of adenosine from deoxyadenosine helps monitor physiological activities and diagnose the related diseases.[123, 188]

Given that adenosine has a *cis*-diol moiety, which is not present in deoxyadenosine, boronic acid might be useful for its discrimination.[189-192] To date, boronate-affinity imprinting materials have been widely used in recognizing glycoproteins, glycans, saccharides, and nucleotides.[193-196] All of these works took advantage of boronic acid's ability to bind *cis*-diol covalently yet reversibly. Recently, we found that the boronic acid moiety could non-covalently interact with DNA through hydrogen bonding and hydrophobic attractions.[197] In this work, we took advantage of both the non-covalent and covalent binding properties of boronic acid and copolymerized it with the adenosine aptamer to prepare MIPs for enhanced molecular recognition with better selectivity.

4.2 Materials and Methods

4.2.1Chemicals

The DNA samples were purchased from Integrated DNA Technologies (Coralville, IA). 3-Acrylamidophenylboronic acid (AAPBA), acrylamide (AAm), *N*-isopropylacrylamide (NIPAm), *N,N′*-methylenebis(acrylamide) (BIS), *N*-[3-(dimethylamino)propyl]methacrylamide (DMPA), SYBR Green I (SGI), fetal bovine serum (FBS) and sodium dodecyl sulfate (SDS) were purchased from Sigma-Aldrich. Ammonium persulfate (APS) and *N, N, N′, N′*-tetramethylethylenediamine (TEMED) were from VWR. Sodium chloride, magnesium chloride, sodium acetate, 4-(2-hydroxyethyl)-1-piperazineethanesulfonic acid (HEPES), 2-(N-morpholino)-ethanesulfonic acid (MES), adenosine, and deoxyadenosine were from Mandel Scientific (Guelph, Ontario, Canada). All the buffers were prepared in Milli-Q water, and the FBS was diluted in HEPES buffers.

4.2.2 Preparation of imprinted and non-imprinted nanogels

The nanogels were prepared following our previous method with minor modifications.[111, 198, 199] Typically, the template adenosine (1 mM) was first incubated with the aptamer (20 μM) for 1 h. Then AAPBA (7.17 mM), NIPAm (19 mM), AAm (14 mM), BIS (16 mM), and DMPA (0.6 μL) were added in buffer A (20 mM HEPES, pH 7.6, 100 mM NaCl, 5 mM $MgCl_2$, 1 mL), and the sample was purged with N_2 for 1 h. After that, the mixture was stored for 6 h in a 4 °C fridge to form pre-polymerization complexes. Afterwards, SDS (0.8 mg), APS (0.6 mg), and TEMED (0.3 μL) were added to initiate the reaction. After 16 h, the obtained MIPs were collected by centrifugation at 15000 rpm for 10 min, followed by extensively washing them with methanol/acetic acid (90/10, v/v) and Milli-Q water until no adenosine residue appeared in the washing solution. This was confirmed by UV-vis spectroscopy (Agilent 8453A) at 260 nm. Finally, the gels were freeze-dried for further use. The non-molecularly imprinted polymers (NIPs) were prepared in the same way, except no adenosine was added.

4.2.3 Isothermal titration calorimetry (ITC)

ITC was performed using a VP-ITC microcalorimeter instrument (MicroCal). All solutions were degassed in ultrasonication for 10 min prior to measurements. The gel solutions (1 mg/mL), or free aptamer (10 μM) in buffer A was loaded in a 1.45 mL cell at 25 °C. The adenosine, deoxyadenosine, or cytidine (5 mM for gels and 1 mM for free aptamer) solutions in the same buffer was loaded in a 280 μL syringe. After the first injection of 2 μL, the syringe titrated 10 μL of the target into the cell each time. Through measuring the heat changes and fitting the titration curves to a one-site binding model, the enthalpy change (ΔH) and the association constant (K_a) were obtained. The dissociation constant (K_d) and ΔG were calculated by $1/K_a$ and $\Delta G = -RT\ln(K_a)$, respectively. The ΔS was calculated from $\Delta G = \Delta H - T\Delta S$. The molar ratio in the ITC data was calculated based on ligand/aptamer concentration or binding site concentration in gels. Both the aptamer and AAPBA were calculated in binding sites.

4.2.4 SGI fluorescence spectroscopy

To study the optimal staining ratio, different concentrations of SGI (2.5-50 nM) were gradually added into 1 mg/mL aptamer-MIP (contained about 2 μM aptamer) in buffer A (with or without additional 1 mM adenosine), and the fluorescence intensities were compared. Using the optimized condition (7.5 nM SGI), the response of aptamer-MIP (1 mg/mL) towards 1 mM adenosine, deoxyadenosine, adenosine/deoxyadenosine mixture, cytidine, guanosine, thymidine and glucose was respectively tested in buffer A.

4.2.5 TEM and DLS

The hydrodynamic size of gels were measured by dynamic light scattering (DLS) on a Zetasizer Nano ZS90 (Malvern) at 25 °C. 50 μg/mL of the gel particles were dispersed in buffer A. The morphology and the size of the gels were measured by transmission electron microscopy (TEM, Philips CM 10). 200 μg/mL gels were drop-case onto a copper grid and dried overnight at room temperature before imaging.

4.3 Results and Discussion

4.3.1 Free aptamer binding adenosine, deoxyadenosine, and cytidine

The DNA aptamer for adenosine[4] is a well-studied system often used in analytical applications.[200] The original aptamer consists of 27 nucleotides with two target binding pockets (Figure 4.1A). It can bind to a number of adenine derivatives, such as adenosine, deoxyadenosine, AMP and ATP. Before studying the imprinted gels, we first used ITC to quantitatively measure the binding of the free aptamer. ITC is a label-free technique that can provide rich thermodynamic information, such as the association constant (K_a), enthalpy change (ΔH), entropy change (ΔS), free energy change (ΔG), and binding stoichiometry (N).[92, 118-120] Figure 4.1C is a typical ITC trace of gradually titrating adenosine into the free aptamer. The released heat during binding is indicated by the downward spikes in the upper panel of the figure, and the ΔH is recorded as a titration curve in the lower panel. Through fitting the titration curve, the K_a can be obtained.

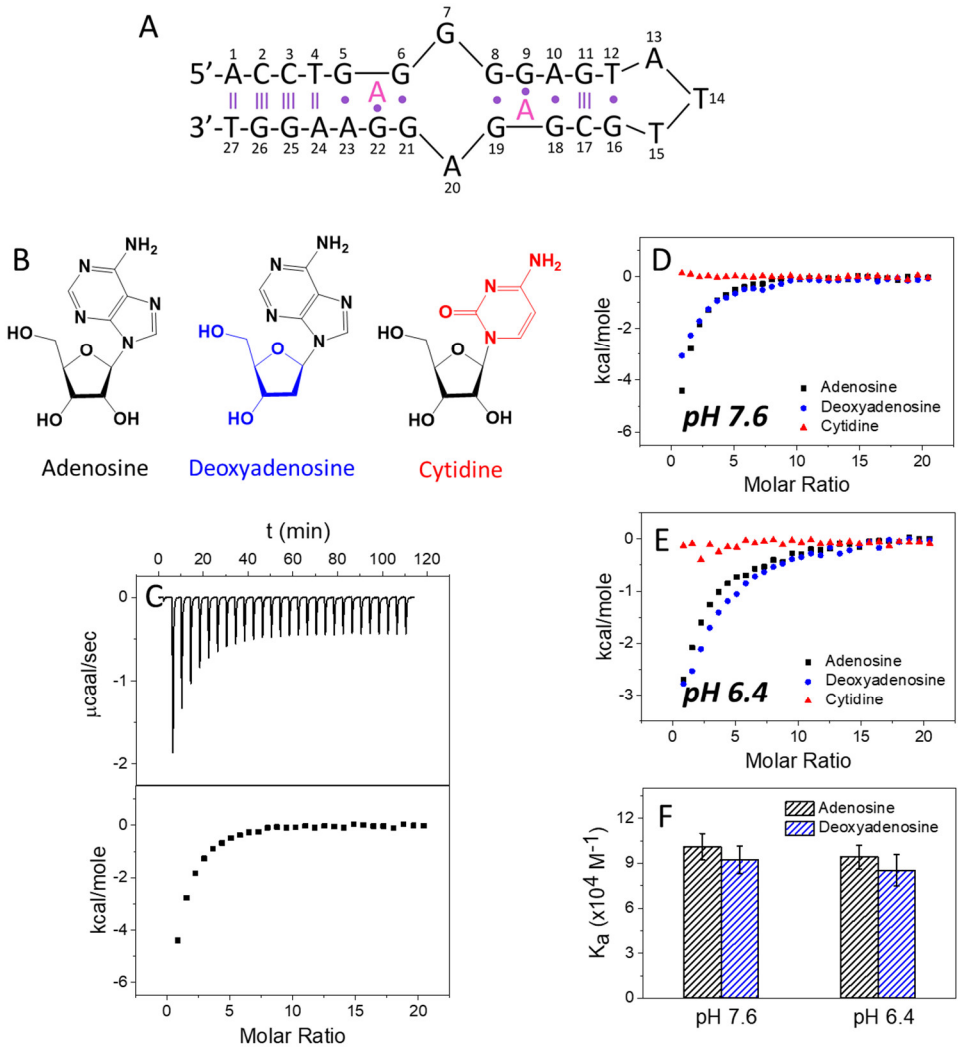

Figure 4.1 (A) The secondary structure of the adenosine aptamer. Each aptamer can bind two adenosine molecules (A in burgundy colored). (B) Chemical structures of adenosine, deoxyadenosine (a different sugar ring), and cytidine (a different base). (C) ITC traces and integrated heat for 10 µM aptamer titrated by 1 mM adenosine at pH 7.6 (20 mM HEPES, with 100 mM NaCl, and 5 mM $MgCl_2$). Comparison of the titration curves for aptamer binding with adenosine, deoxyadenosine, and cytidine at (D) pH 7.6, and (E) pH 6.4 (20 mM MES). (F) The K_a of the free aptamer binding with adenosine and deoxyadenosine at pH 7.6 and 6.4. Cytidine data are not plotted here since it's binding cannot be detected by ITC. Error bars mean standard deviation from at least 2 independent measurements.

First, we titrated the aptamer with adenosine, deoxyadenosine, and cytidine (chemical structures in Figure 4.1B) at pH 7.6 and 6.4, respectively. These two pH conditions were chosen for testing both the aptamer, and boronic acid (*vide infra*). Figure 4.1D and 4.1E are their titration curves, showing that the aptamer can bind to adenosine and deoxyadenosine similarly at these two pH conditions, with a K_a at 10.1 ± 0.9 $\times 10^4$ M^{-1} and 9.4 ± 0.8 $\times 10^4$ M^{-1} respectively (for adenosine, Figure 4.1F), whereas cytidine had no binding at either pH as expected. The K_d of binding adenosine was calculated from $1/K_a$ to be around 9.9 μM. In the original paper for selecting this aptamer, its K_d for adenosine was 6 ± 3 μM based on analytical ultrafiltration.[4] By using different methods, the K_d can vary.[201] For example, electrospray ionization mass spectrometry (ESI-MS) generated a K_d of 5.3 ± 0.6 μM,[202] and equilibrated capillary electrophoresis (CE) measured a K_d at 2.4 ± 0.4 μM.[203] Our value obtained from ITC was comparable with these reported values. The thermodynamic data obtained from ITC for the free aptamer are summarized in Table 4.1.

Table 4.1. Thermodynamic data for the free adenosine aptamer binding to various ligands (adenosine, deoxyadenosine, and cytidine) at pH 7.6 and 6.4.

Ligand	**Aptamer**	**K_a ($\times 10^4$ M^{-1})**	**ΔG (kcal mol^{-1})**	**ΔH (kcal mol^{-1})**	**ΔS (cal K^{-1} mol^{-1})**
Adenosines	Free aptamer (pH7.6)	10.1 ± 0.9	-6.8 ± 0.8	-8.5 ± 0.8	-5.6
	Free aptamer (pH6.4)	9.4 ± 0.8	-6.7 ± 0.6	-2.6 ± 0.6	13.7
Deoxyadenosine	Free aptamer (pH7.6)	9.2 ± 0.9	-6.8 ± 0.5	-5.0 ± 0.5	6.1
	Free aptamer (pH6.4)	8.5 ± 1.0	-6.7 ± 0.4	-2.8 ± 0.4	13.3

Cytidine	Free aptamer (pH7.6)	--[a]
	Free aptamer (pH6.4)	--[a]

[a] Binding was extremely weak or cannot be obtained by ITC.

4.3.2 Binding by boronic acid containing hydrogels (no aptamer)

Since the aptamer cannot distinguish adenosine from deoxyadenosine, and boronic acid can capture *cis*-diols,[204, 205] we expected that introducing a boronic acid may bring in additional molecular recognition chemistry to help the aptamer. Although boronic acid is likely to distinguish adenosine from deoxyadenosine, it alone is unlikely to tell adenosine apart from other ribonucleosides such as cytidine.[206] Thus, it might be necessary to combine boronic acid and the aptamer to form hybrid materials. Before combining them, we prepared hydrogel nanoparticles that only contained a boronic acid monomer (without the aptamer) to check its binding. In addition to 3-acrylamidophenylboronic acid (AAPBA) as a functional monomer to target adenosine (water-soluble), NIPAm and AAm were also added as monomers to build a hydrogel (Figure 4.2A).

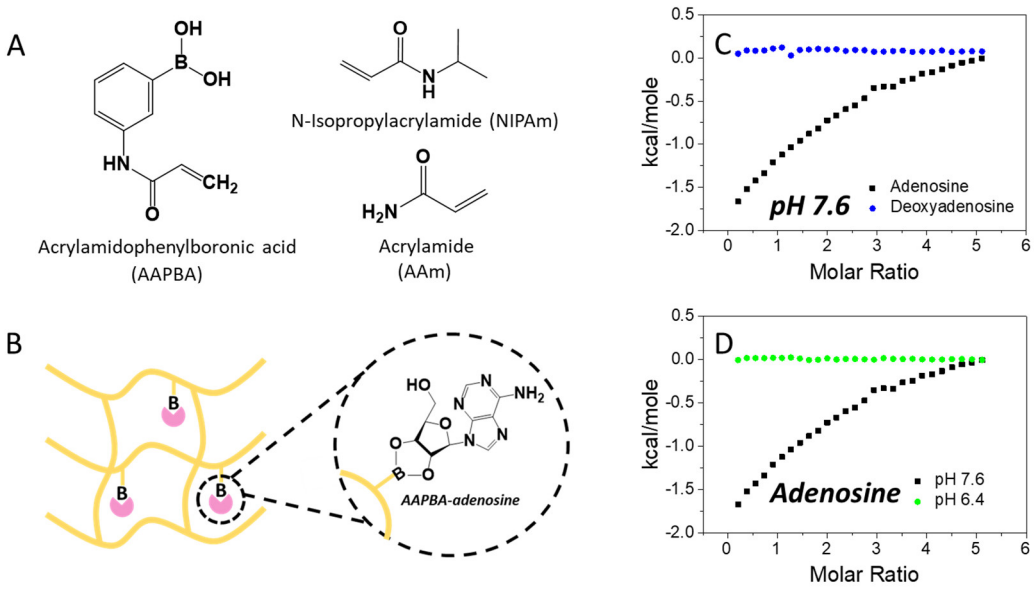

Figure 4.2 (A) Chemical structures of AAPBA, NIPAm, and AAm. (B) A scheme of a boronic acid-functionalized hydrogel binding adenosine. The ITC curves of titrating (C) 5 mM adenosine and deoxyadenosine into 1 mg/mL boronic acid-hydrogels at pH 7.6 (20 mM HEPES, 100 mM NaCl, and 5 mM $MgCl_2$); (D) 5 mM adenosine into 1 mg/mL boronic acid-hydrogels at pH 7.6 and 6.4 (20 mM MES, 100 mM NaCl and 5 mM $MgCl_2$). For each 1 mg/mL boronic acid-hydrogels, it contained around 200 μM AAPBA.

For the boronic acid moiety in AAPBA, its most effective pH range for binding to *cis*-diols was pH = pK_a ± 1 (AAPBA has a pK_a ~ 8.2). Therefore, we checked the binding at pH 7.6 first. Figure 4.2C confirmed its binding to adenosine (K_a = 1.0 ± 0.1 $\times 10^4$ M^{-1}, in Table 4.2), while it failed to bind deoxyadenosine. This indicated that the boronate/*cis*-diol chemistry was responsible for the binding of adenosine (Figure 4.2B). The hydrogel also bound cytidine with a K_a at 0.9 ± 0.1 $\times 10^4$ M^{-1} (Table 4.2), as cytidine also has a *cis*-diol.

We then dropped the pH to 6.4 (Figure 4.2D), which was outside the optimal pH range of AAPBA, and the adenosine binding was largely lost (green line). Although a

more acidic condition could further inhibit *cis*-diol binding by AAPBA, since the aptamer preferred to work near neutral pH, no further lowering of pH was tested.

Table 4.2 Thermodynamic data for AAPBA-hydrogels binding adenosine, deoxyadenosine and cytidine.

Ligand	**Hydrogels**	**K_a ($\times 10^4$ M^{-1})**	**ΔG (kcal mol^{-1})**	**ΔH (kcal mol^{-1})**	**ΔS (cal K^{-1} mol^{-1})**
Adenosine	AAPBA-hydrogel (pH7.6)	1.0 ± 0.1	-5.4 ± 0.1	-2.1 ± 0.1	11.3
	AAPBA-hydrogel (pH6.4)	--[a]			
Deoxyadenosine	AAPBA-hydrogel (pH7.6)	--[a]			
Cytidine	AAPBA-hydrogel (pH7.6)	0.9 ± 0.1	-5.3 ± 0.1	-0.9 ± 0.1	14.7

[a] Binding was extremely weak or cannot be obtained by ITC.

4.3.3 Aptamer-MIPs can distinguish adenosine from deoxyadenosine

So far, we know that the aptamer alone can distinguish the base part, while boronic acid can distinguish the sugar rings. The question then is if we can selectively recognize both parts by using the aptamer and boronic acid together. To test this, we first incorporated 8.33 mM AAPBA and 20 μM aptamer to prepare the imprinted gels, denoted as aptamer-MIPs. We chose to use 20 μM aptamer based on our previous work of preparing the aptamer-contain hydrogels,[111] and 8.33 mM AAPBA.[197] The number of boronic acid moieties was far more than that of the aptamer since its binding affinity was lower and a higher concentration was needed to achieve saturated binding (*vide infra*).

To create shape-complementary binding pockets in MIPs, the acrydite-modified aptamer, AAPBA and the other monomers were incubated with adenosine for 6 h before initiating the polymerization reaction. Afterwards, the imprinted adenosine was removed by extensive washing to generate the binding pockets (Figure 4.3A). For comparison, non-imprinted polymers (NIPs) were prepared in the same way, except no adenosine was added during polymerization. The hydrodynamic sizes of the gels were measured by DLS to be around 400 nm (Figure 4.3B). From TEM, their size was between 300 and 400 nm (Figure 4.3C). The gels measured by DLS were fully swelled, but the TEM samples were dried and appeared slightly smaller. These experiments confirmed that we have successfully prepared hydrogel nanoparticles.

For each 1 mg/mL aptamer-MIP used for ITC titrations, it contained around 200 μM AAPBA, and 2 μM aptamer (calculated based on UV-vis and SYBR Green I stained fluorescence spectroscopy). To our surprise, this MIP fully distinguished adenosine from deoxyadenosine (Figure 4.3D), despite that the aptamer was present in the gel. The respective K_a values for adenosine and deoxyadenosine were $3.3 \pm 0.3 \times 10^4$ and $0.03 \pm 0.01 \times 10^4$ M^{-1}, respectively (Table 4.3). To evaluate whether an K_a is reliable, it must be satisfied by the relationship of $0.1<K_a[M]_T<1000$, where $[M]_T$ is the total concentration of the titrated molecules.[115] In our case, when titrating 5 mM ligands into gels, the reliable K_a should fall between 0.002×10^4 M^{-1} and 20×10^4 M^{-1}. Thus, a K_a larger than 20 M^{-1} was still measurable (e.g. the above K_a of deoxyadenosine of ~30 M^{-1} is still an acceptable value).

To evaluate the specificity of the MIP, we calculated the K_a(adenosine)/K_a(deoxyadenosine). The ratio for the aptamer-MIP gels reached 110. Yet for the free aptamer (no imprinting), the ratio was just 1.07 (calculation based on Table 4.1), indicating that the incorporation of AAPBA into the aptamer-containing hydrogels improved specificity by around 100-fold. The very weak binding of deoxyadenosine implied that the aptamer might be inhibited by the gel matrix.

Therefore, whether adenosine was bound by the gel matrix (e.g. the boronic acid), or by the aptamer, or both, has yet to be determined.

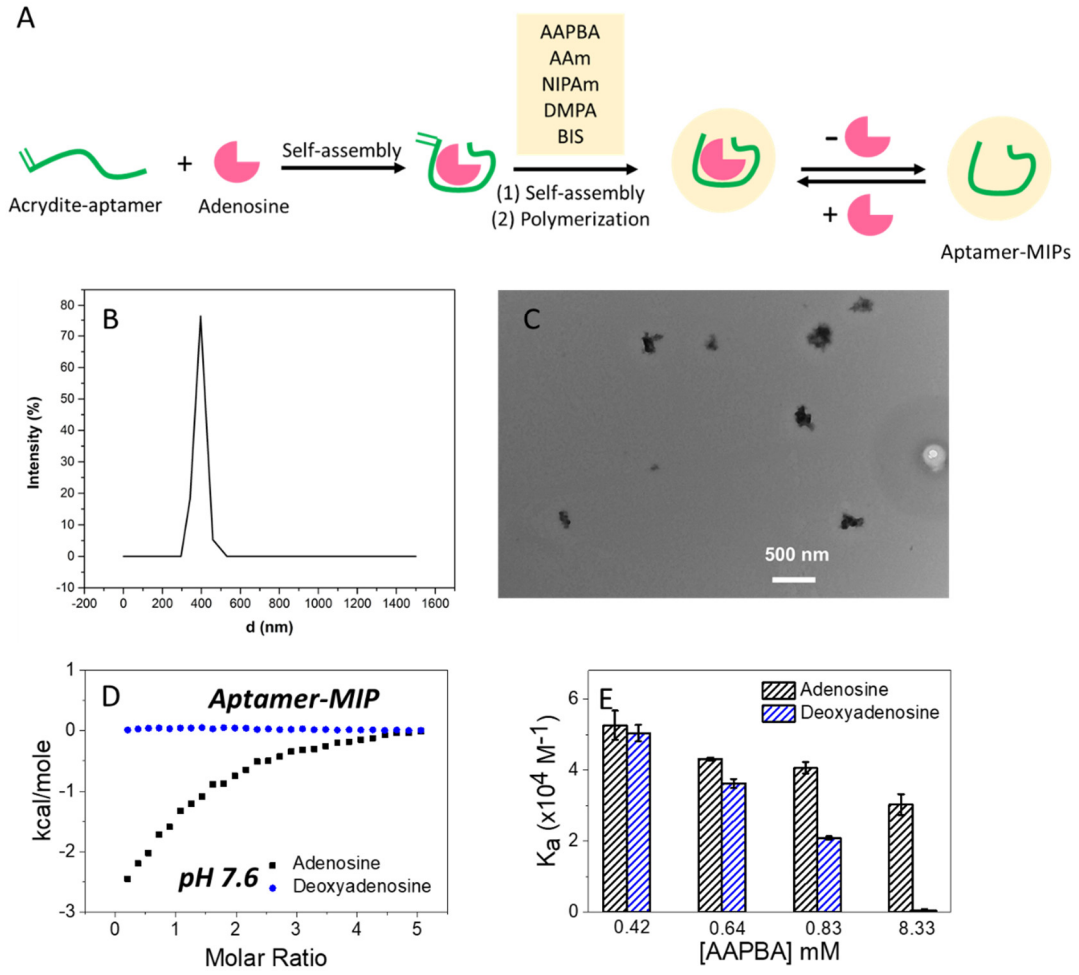

Figure 4.3 (A) A scheme for preparing aptamer-MIPs (containing AAPBA). (B) The hydrodynamic size of the aptamer-MIPs (50 μg/mL, dispersed in 20 mM HEPES, pH 7.6, 100 mM NaCl, 5 mM $MgCl_2$). (C) A TEM micrograph of the aptamer-MIPs. (D) The ITC curves of gradually titrating adenosine and deoxyadenosine (5 mM) into the aptamer-MIPs (1 mg/mL, containing 200 μM AAPBA and 2 μM aptamer) at pH 7.6 (20 mM HEPES, 100 mM NaCl, and 5 mM $MgCl_2$). (E) The K_a of the aptamer-MIPs (with 0.42, 0.64, 0.83, and 8.33 mM AAPBA during preparation of the gel) for adenosine and deoxyadenosine at pH 7.6.

Table 4.3. Effect of AAPBA concentration on aptamer-MIPs binding to adenosine and deoxyadenosine at pH 7.6. The incorporation of AAPBA enhanced binding specificity to adenosine.

Ligand	**Aptamer-MIPs**	**K_a ($\times 10^4$ M^{-1})**	**ΔG (kcal mol^{-1})**	**ΔH (kcal mol^{-1})**	**ΔS (cal K^{-1} mol^{-1})**
Adenosine	Aptamer-MIP with 0.42 mM AAPBA	5.3 ± 0.4	-6.1 ± 0.2	-0.7 ± 0.2	18.0
	Aptamer-MIP with 0.64 mM AAPBA	4.3 ± 0.1	-5.7 ± 0.1	-0.7 ± 0.1	16.7
	Aptamer-MIP with 0.83 mM AAPBA	4.1 ± 0.2	-5.2 ± 0.2	-0.6 ± 0.2	15.6
	Aptamer-MIP with 8.33 mM AAPBA	3.3 ± 0.3	-7.1 ± 0.2	-3.0 ± 0.2	13.9
	Aptamer-NIP with 8.33 mM AAPBA	0.9 ± 0.2	-4.5 ± 0.2	-2.0 ± 0.2	8.4
Deoxyadenosine	Aptamer-MIP with 0.42 mM AAPBA	5.0 ± 0.2	-5.8 ± 0.1	-0.5 ± 0.1	17.5
	Aptamer-MIP with 0.64 mM AAPBA	3.6 ± 0.1	-5.6 ± 0.1	-0.3 ± 0.1	18.0
	Aptamer-MIP with 0.83 mM AAPBA	2.1 ± 0.1	-5.6 ± 0.1	-0.2 ± 0.1	18.2
	Aptamer-MIP with 8.33 mM AAPBA	0.03 ± 0.01[a]			

[a] Binding was extremely weak or cannot be obtained by ITC.

To further confirm that the inhibiting effect of AAPBA, we then decreased its concentration from 8.33 mM to 0.83, 0.64, and 0.42 mM during preparation of the MIPs. Figure 4.3E (summarized from Table 4.3) show a gradually increased affinity to deoxyadenosine with these gels. When only 0.42 mM AAPBA was added, the aptamer-MIP bound to adenosine and deoxyadenosine with a similar K_a around 5×10^4 M^{-1}, while the difference increased with increasing AAPBA concentration. This experiment further verified the inhibiting role of AAPBA.

After imprinting, the binding pockets in the MIP exhibited higher affinity than the NIP ($0.9 \pm 0.2 \times10^4$ M^{-1}, Table 4.3). The NIP data further confirmed the inhibition role of the gel matrix, likely due to the boronic acid interacting with the aptamer.[197] By comparing the MIP and NIP data (Figure 4.4A), the effect of imprinting was clear. The K_a (aptamer-MIP)/K_a (aptamer-NIP) was around 3.67, demonstrating that imprinting process created shape-complementary binding pockets for adenosine, and further improved the material binding affinity.

We then removed the AAPBA monomer, and only used the aptamer with NIPAAm and AAm to imprint adenosine. In this case, the gel failed to differentiate adenosine from deoxyadenosine (Figure 4.4B). Compared to the free aptamer, which had a K_a (adenosine)/K_a (deoxyadenosine) of 1.07, the imprinting process only improved the ratio to 1.93. This demonstrated that AAPBA was indispensable for distinguishing adenosine from deoxyadenosine, and its role might be related to its inhibition effect.

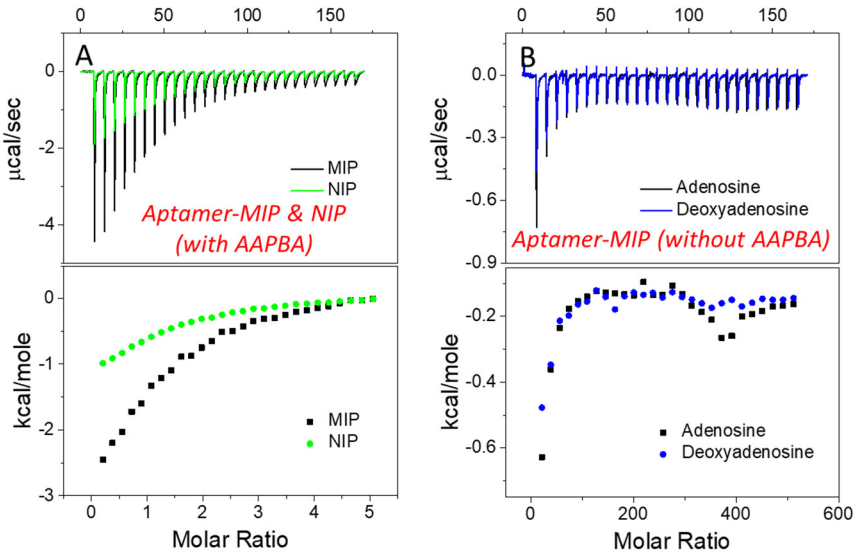

Figure 4.4 ITC traces and integrated heat for (A) 1 mg/mL Aptamer-MIP or Aptamer-NIP (both with AAPBA) titrated by 5mM adenosine at pH 7.6. Imprinting process doubled the adenosine binding due to more specific binding sites formed in MIP. (B) 1 mg/mL Aptamer-MIP (without AAPBA) titrated by 5 mM adenosine and deoxyadenosine at pH 7.6. The aptamer cannot tell adenosine from deoxyadenosine in MIP without the help of AAPBA .

4.3.4 pH modulated boronic acid function: aptamer achieved higher specificity at acidic pH

The above work focused on distinguishing adenosine from deoxyadenosine. It verifies that boronic acid can inhibit the aptamer function, thus an interesting question is whether this system can still distinguish adenosine from other ribonucleosides, such as cytidine. Figure 4.5A shows obvious cytidine binding from the AAPBA-containing aptamer-MIP (red curve). Since cytidine also bears a ribose (structure in Figure 4.1B), it is important to decrease the binding between boronic acid and ribose. We lowered the pH to 6.4, at which AAPBA largely lost its binding ability while the aptamer could still work.

To our surprise, at pH 6.4, the aptamer-MIP exhibited better specificity (Figure 4.5B and 4.5C): only adenosine binding was observed, while the heat for deoxyadenosine and cytidine binding was almost ignorable. Binding of adenosine at pH 6.4 (K_a = 4.6 ± 0.6 ×10^4 M^{-1}) was even stronger than that at pH 7.6 (K_a = 3.3 ± 0.3 ×10^4 M^{-1}) (summarized in Table 4.4). The K_a(adenosine)/K_a(deoxyadenosine) was 115 and 110 at pH 6.4 and 7.6, respectively. The discrimination against cytidine at pH 6.4 also reached 230-fold based on K_a(adenosine)/K_a(cytidine). Overall, at pH 6.4, this system can tell adenosine apart from both deoxyadenosine and cytidine.

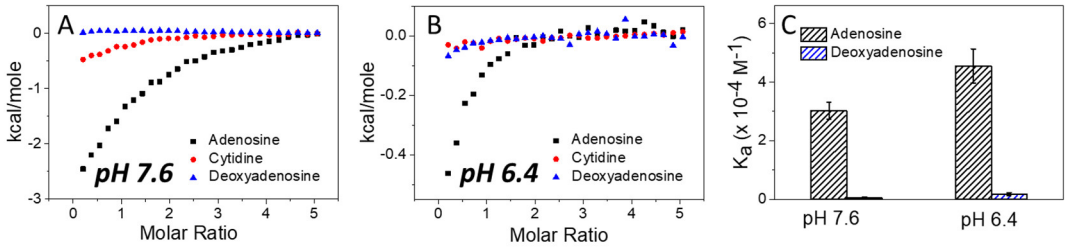

Figure 4.5 The ITC curves of gradually titrating 5 mM adenosine, deoxyadenosine, and cytidine into 1 mg/mL aptamer-MIP (containing 2 μM aptamer and 200 μM AAPBA) at (A) pH 7.6 (20 mM HEPES), and (B) pH 6.4 (20 mM MES), both also contained 100 mM NaCl and 5 mM $MgCl_2$. (C) The K_a values for the aptamer-MIP binding to adenosine and deoxyadenosine at pH s7.6 and 6.4.

Table 4.4. Effect of pH on aptamer-MIPs (with AAPBA). At pH 6.4, non-specific binding of cytidine was decreased.

Ligand	**Aptamer-MIPs**	**K_a (×10^4 M^{-1})**	**ΔG (kcal mol^{-1})**	**ΔH (kcal mol^{-1})**	**ΔS (cal K^{-1} mol^{-1})**
Adenosine	Aptamer-MIP with 8.33 mM AAPBA (pH7.6)	3.3 ± 0.3	-7.1 ± 0.2	-3.0 ± 0.2	13.9

	Aptamer-MIP with 8.33 mM AAPBA (pH6.4)	4.6 ± 0.6	-6.4 ± 0.1	-0.5 ± 0.1	19.6
Deoxyadenosine	Aptamer-MIP with 8.33 mM AAPBA (pH7.6)	0.03 ± 0.01[a]			
	Aptamer-MIP with 8.33 mM AAPBA (pH6.4)	0.04 ± 0.02[a]			
Cytidine	Aptamer-MIP with 8.33 mM AAPBA (pH7.6)	1.0 ± 0.2	-5.3 ± 0.1	-0.4 ± 0.1	16.4
	Aptamer-MIP with 8.33 mM AAPBA (pH6.4)	0.02 ± 0.01[a]			

[a] Binding was extremely weak or cannot be obtained by ITC.

4.3.5 Aptamer-MIP binding measured with SYBR Green I

The aforementioned ITC data indicated that incorporating AAPBA into the aptamer-functionalized MIP, hundred-fold specificity improvement was achieved for adenosine. Here, we want to use an independent method to study the binding of the aptamer moiety in these gels by using a DNA staining dye, SYBR Green I (SGI).[206, 207] First, we fixed the concentration of the gel to be same as that for ITC (1 mg/mL, contained about 2 μM aptamer), and the concentration of SGI was optimized to be 7.5 nM.

We then used this method to measure the aptamer-MIP (contained AAPBA) binding to adenosine (Figure 4.6A), deoxyadenosine (Figure 4.6B) and their mixture (Figure 4.6C) at pH 7.6. These spectra show that the aptamer-MIP only bound to adenosine, even if the ligand was in a mixture. Other nucleosides (cytidine, guanosine and thymidine) and glucose were also checked (at pH 6.4, Figure 4.6D, and they barely showed any binding. This fluorescence result that the aptamer-MIP can exclusively bind to adenosine which was pretty consistent with our ITC data.

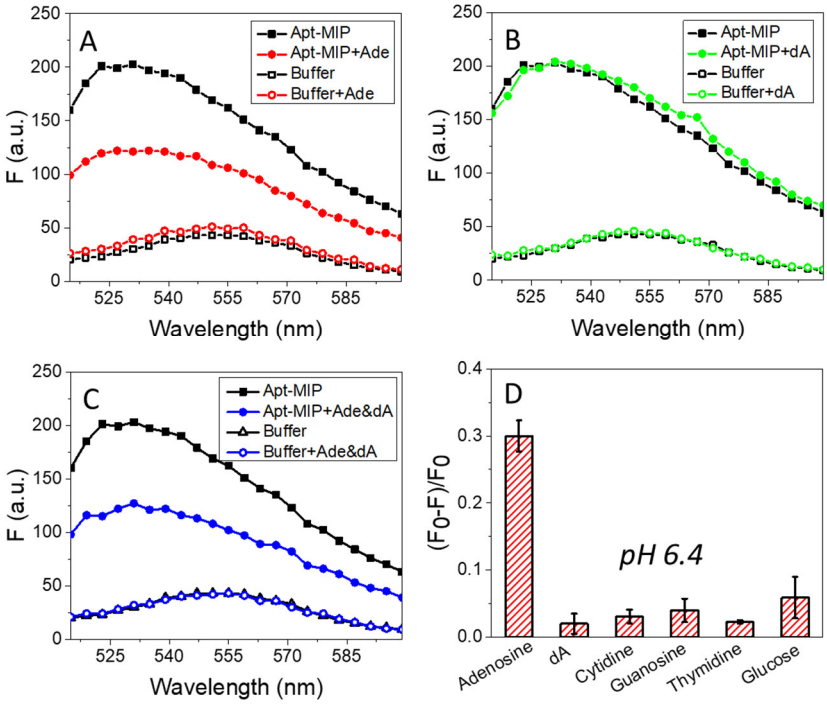

Figure 4.6 Fluorescence spectra of 1 mg/mL of the aptamer-MIP mixed with (A) 1 mM adenosine, (B) 1 mM deoxyadenosine, and (C) 1 mM adenosine and 1 mM deoxyadenosine in 20 mM HEPES (pH 7.6) with 7.5 nM SGI. (D) The specificity of the aptamer-MIP (in 20 mM MES, pH 6.4).

4.3.6 Probing the effect of boronic acid on the aptamer

In this part, we wanted to understand the mechanism of the improved specificity for adenosine. Since the aptamer can bind to adenosine and deoxyadenosine with almost no difference, and a high concentration of AAPBA was required to achieve high

specificity, we suspected that the mechanism might be through an interaction between AAPBA and the aptamer. Our previous study already indicated non-covalent interactions between DNA oligonucleotides and boronic acid.[197] To test this, we then added glucose (containing a *cis*-diol) to block the boronic acid on AAPBA. In the presence of glucose, when titrating deoxyadenosine to aptamer-MIPs (Figure 4.7A and Table 4.5), an obvious binding was observed at both pH 7.6 and 6.4. The K_a of binding deoxyadenosine recovered to 6.3×10^4 M^{-1} and 5.4×10^4 M^{-1}, respectively. Since adenosine also contained a *cis*-diol, it may play the role of glucose, and the ribose can block the boronic acid from the aptamer, and thus activate aptamer binding (Figure 4.7B). Whereas for deoxyadenosine, it does not have a *cis*-diol and thus the aptamer is more strongly inhibited. At pH 7.6, it is easy to understand that AAPBA can bind to the ribose in adenosine, leaving the un-occupied aptamer binding to its base part.

Another question is why such high specificity can also be achieved at pH 6.4? Since glucose still worked for recovering deoxyadenosine binding at pH 6.4, a boronic acid-diol binding equilibrium must also exist (Figure 4.7C). AAPBA can start to form the covalent bond at ~pH 6.5,[189] but the binding was too weak to be detected by ITC. We can consider this reversible binding in the time domain, and boronic acid/*cis*-diol binding/unbinding interactions were in dynamic equilibrium. Although the bond could not be stable for a long time at pH 6.4, this interaction might be sufficient for breaking the non-covalent boronic acid/aptamer interactions. In summary, a slightly acidic pH (pH 6.4) was preferred when using an aptamer-MIP to completely distinguish adenosine from deoxyadenosine and cytidine.

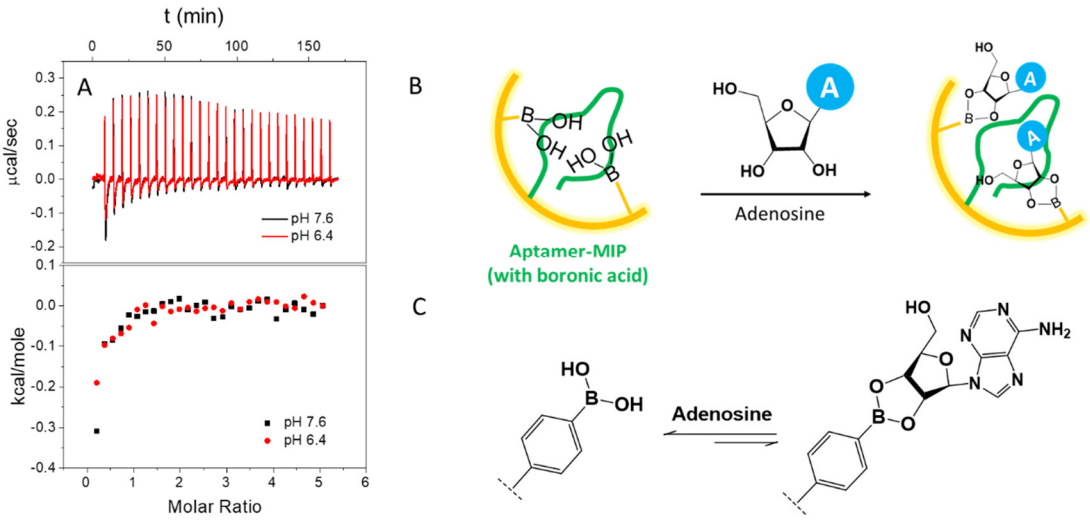

Figure 4.7 (A) ITC traces and integrated heat for 1 mg/mL aptamer-MIP (containing 2 µM aptamer, with 1 mM glucose) titrated by 5 mM deoxyadenosine at pH 7.6 (20 mM HEPES) and 6.4 (20 mM MES), both with an additional 100 mM NaCl and 5 mM $MgCl_2$. Schemes of (B) adenosine replacing the boronic acid moiety from an aptamer-MIP and (C) the covalent bonding between boronic acid and adenosine at pH 6.4.

Table 4.5 Effect of glucose on aptamer-MIPs (with AAPBA) binding to deoxyadenosine at pH 7.6 and pH 6.4. Glucose recovered deoxyadenosine binding at both pH conditions.

Ligand	**Aptamer-MIPs**	**K_a ($\times 10^4$ M^{-1})**	**ΔG (kcal mol^{-1})**	**ΔH (kcal mol^{-1})**	**ΔS (cal K^{-1} mol^{-1})**
Deoxyadenosine	Aptamer-MIP with 8.33 mM AAPBA (pH7.6)	0.03 ± 0.01[a]			
	Aptamer-MIP with 8.33 mM AAPBA (pH6.4)	0.04 ± 0.02[a]			

Aptamer-MIP with 8.33 mM AAPBA (+glucose, pH7.6)	6.3 ± 0.9	-6.5 ± 0.1	-0.4 ± 0.1	20.7
Aptamer-MIP with 8.33 mM AAPBA (+glucose, pH6.4)	5.4 ± 0.8	-6.5 ± 0.1	-0.2 ± 0.1	21

[a] Binding was extremely weak or cannot be obtained by ITC.

4.4 Summary

Adenosine has been a model analyte for developing aptamer-based biosensors for many years. While this aptamer has excellent ability to distinguish the base part, it has limited specificity when comes to the sugar ring. Aside from its inability to tell adenosine apart from AMP and ATP, it can hardly differentiate adenosine from deoxyadenosine, which only differ by a –OH group. Through incorporating boronic acid with this aptamer in molecularly imprinted polymers (MIPs), a hundred-fold higher specificity for adenosine was achieved. The K_a(adenosine)/K_a(deoxyadenosine) for the free aptamer was only 1.07, for aptamer-MIP (without boronic acid) just increased to 1.93, but it soared to 110 when a boronic acid unit was incorporate in the aptamer-MIP at pH 7.6. By lowering the pH to 6.4, the ratio further increased to 115, and non-specific boronic acid/diol interactions with other *cis*-diol containing molecules such as cytidine was also inhibited since stable boronic acid/*cis*-diol interactions only took place at high pH (around the pK_a of boronic acid). When adding glucose to screen the effect of boronic acid, the deoxyadenosine binding was recovered. Therefore, much

of the selectivity was from the aptamer binding by the boronic acid moiety noncovalently. This work demonstrated an interesting example of using an aptamer with MIP to achieve highly specific molecular recognition.

Chapter 5. Conjugating unmodified DNA on hydrogel nanoparticles and monoliths

The results presented in this chapter have been published as:

Yuqing Li, Hang Gao, Zengyao Qi, Zhicheng Huang, Lingzi Ma, Juewen Liu, Freezing-assisted conjugation of unmodified diblock DNA to hydrogel nanoparticles and monoliths for DNA and Hg^{2+} sensing, *Angewandte Chemie*, **2021**, *133*, 2-9.

5.1 Introduction

DNA as a functional polymer has been used in various nanostructures and smart soft materials.[208-211] Particularly, DNA-based hydrogels have been actively explored due to their biocompatibility, programmability, and stimuli-responsive properties enabling various applications such as drug delivery, controlled release, and biosensing.[46, 54, 68, 211, 212] To reduce the cost and introduce other functions in hydrogels, DNA is often conjugated with synthetic polymers such as polyacrylamide and poly(*N*-isopropylacrylamide) (polyNIPAm).[37, 45, 63, 181, 213, 214]

To achieve covalent conjugation, both amino[215] and acrydite[57, 216, 217] modified DNA strands were used. The former strategy is mainly for functionalizing pre-formed succinimido-gels and DNA is attached to the gel surface, while the latter is through copolymerization allowing a high DNA loading also in the interior (Figure 5.1A). Other more sophisticated modifications such as adding a C-5 alkene on 2′-deoxyuridine residues were also reported.[218, 219] While these modified DNA worked well, using unmodified DNA is preferred for cost and synthetic considerations. While unmodified DNA strands were reported to functionalize gold nanoparticles,[34, 220-222] graphene oxide,[182, 223] and other materials,[182, 224] attaching unmodified DNA to hydrogels has yet to be demonstrated.

In fact, the nucleobases are reactive with hydrogel monomers. For example, DNA could form adducts with acrylamide by adding its nitrogen atoms to the β-carbon of the acrylamide (known as Michael addition).[225-229] DNA is also vulnerable to various radicals,[230, 231] such as reacting with hydroxyl radicals (•OH) to form adenine-OH adducts.[232] We reason that such reactions might be exploited for conjugating unmodified DNA to hydrogels. Herein, we report that penta-adenine (A_5) can serve as a conjugation block to graft DNA on acrylamide- and NIPAm-based hydrogels using a freezing-mediated gelation method (Figure 5.1B),[101] where up to 75% of DNA immobilization was achieved in 8 h. Comparisons were made with acrydite-modified DNA, and representative applications including the detection of complementary DNA (cDNA) and Hg^{2+} were demonstrated.

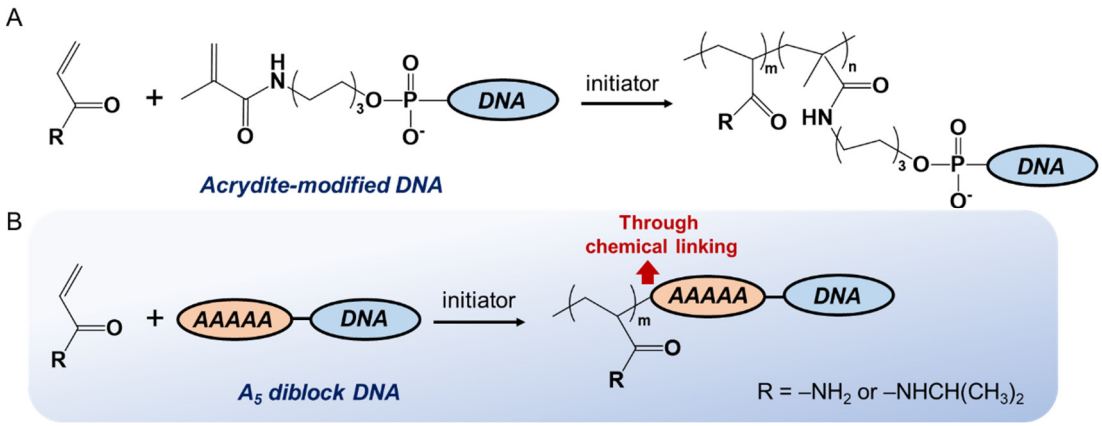

Figure 5.1 Schematic illustrations of two strategies for preparing DNA-hydrogel conjugates: (A) copolymerizing acrydite-modified DNA during free radical polymerization; and (B) reacting an unmodified diblock DNA containing a A_5 block to form addcuts with polymers such as polyacrylamide and polyNIPAm.

5.2 Materials and Methods

5.2.1 Chemicals

All DNA samples were from Integrated DNA Technologies Inc. (Coralville, IA, USA). The DNA sequences and modifications are listed in Table 5.1. Acrylamide, *N*-

isopropylacrylamide (NIPAm), *N,N'*-methylenebis(acrylamide) (BIS), sodium dodecyl sulfate (SDS), mercury acetate, copper chloride, zinc chloride, manganese chloride, cobalt chloride, lead acetate, magnesium chloride, calcium chloride, silver nitrate and iron chloride were purchased from Sigma-Aldrich. Ammonium persulfate (APS) and *N,N,N′,N′*-tetramethylethylenediamine (TEMED) were from VWR. Sodium chloride, potassium chloride, lithium chloride, sodium nitrate, sodium carbonate, sodium bicarbonate, tris(hydroxymethyl)aminomethane (Tris), 4-(2-hydroxyethyl)piperazine-1-ethanesulfonate (HEPES), ethylene glycol, ethanol and dimethyl sulfoxide (DMSO) were from Mandel Scientific (Guelph, Ontario, Canada). 10000× SYBR Green I (SGI) was purchased from Invitrogen (Carlsbad, CA).

Table 5.1. The DNA sequences and modifications used in this work.

DNA Names	**Sequences (from 5′ to 3′) and modifications**
A_5 DNA	AAAAA
A_{15} DNA	AAAAAAAAAAAAAAA
T_{15} DNA	TTTTTTTTTTTTTTT
FAM-A_5	[FAM]AAAAA
FAM-A_{15}	[FAM]AAAAAAAAAAAAAAA
FAM-A_{30}	[FAM]AAAAAAAAAAAAAAAAAAAAAAAAAAAAAA
FAM-T_5	[FAM]TTTTT
FAM-T_{15}	[FAM]TTTTTTTTTTTTTTT
FAM-T_{30}	[FAM]TTTTTTTTTTTTTTTTTTTTTTTTTTTTTT
FAM-C_5	[FAM]CCCCC

FAM-C_{15}	[FAM]CCCCCCCCCCCCCCC
FAM-C_{30}	[FAM]CCCCCCCCCCCCCCCCCCCCCCCCCCCCCC
FAM-G_5	[FAM]GGGGG
FAM-G_{15}	[FAM]GGGGGGGGGGGGGGG
A_5DNA1-FAM	AAAAATATGCGGAGGAAGGT[FAM]
Acryl-T_5DNA1-FAM	[Acrydite]TTTTT[6FI]TATGCGGAGGAAGGT
cDNA1	ACCTTCCTCCGCATA
A_5DNA2	AAAAACCCAGGTTCTCTTCACAGATGCGT
cDNA2	ACGCATCTGTGAAGAGAACCTGGG
FAM-cDNA2	[FAM]ACGCATCTGTGAAGAGAACCTGGG
FAM-Control DNA	[FAM]GCATATCGCCCCCCCCCCCCGATATG
A_5DNA3	AAAAACTTCTTTCTTCCCCTTGTTTGTTG
A_5DNA4	AAAAACAACAAACAAGGGGAAGAAAGAAG
cDNA3	CAACAAACAAGGGGAAGAAAGAAG
cDNA4	CTTCTTTCTTCCCCTTGTTTGTTG

5.2.2 Preparation of DNA-hydrogel conjugates

First, 100 nM DNA was mixed with 20 mM acrylamide, 20 mM NIPAm and 16 mM BIS in 1 mL buffer A (20 mM HEPES, pH 7.6, 4% glycerol). The total monomer concentration was 56 mM or 0.6% (w/v). The mixture was purged with N_2 for 30 min to remove oxygen, after which, the sample was placed in an ice bath (~4°C) for 1 h.

When it was completely cooled, 20 μL of 60 mg/mL SDS, 20 μL of 10% w/v APS and 0.6 μL TEMED were added successively. After initiating the polymerization (in ice bath, ~1 min), the tube was quickly transferred to a freezer (-20°C), and the reaction proceeded overnight (>16 h). After that, the tube was thawed in tap water for ~3 min, and the generated hydrogels were vortexed (~1 min) and sonicated (~2 min) to be dispersed. Next, 20 mM HEPES (pH 7.6) was used to wash the products for three times by centrifugation at 15000 rpm for 10 min. Finally, the gels were dried by vacuum centrifugation (Vacufuge, Eppendorf) for further use.

5.2.3 Quantification of DNA in hydrogel nanoparticles

To calculate the DNA incorporation percentage in hydrogel nanoparticles, FAM-labeled DNA was used during gel preparation. After polymerization, the DNA-hydrogel conjugates were first centrifuged at 15000 rpm for 10 min, and the supernatant was collected. After that, 20 mM HEPES was used to wash the pellets for three times and each supernatant was collected as well. Next, the four supernatants were individually measured by exciting at 485 nm and the emission at 535 nm was recorded (Infinite F200 Pro, Tecan). The fourth supernatant had almost no fluorescence. Based on the fluorescence of 100 nM free FAM-DNA in 20 mM HEPES (pH 7.6, no additional salt), the DNA incorporation (%) in hydrogel conjugates was calculated.

5.2.4 Gel electrophoresis

The 6× gel loading buffer (stock) was diluted to 1× in 8 M urea. Then 10 μL of the 1× loading buffer was mixed with 10 μL of freshly prepared gel particle solutions (containing 100 nM FAM-DNA). 100 nM free FAM-DNA (no gel nanoparticles) was used as a control. To quantify the non-covalently attached DNA, the gel nanoparticles were not washed. The final DNA concentration for gel electrophoresis was 50 nM (in 10 mM HEPES, pH 7.6). Next, 8 μL of the mixture was loaded to 15% denaturing polyacrylamide gel and ran at 200 V for 30 min. The results were analyzed by a ChemDoc MP imaging system (Bio-Rad).

5.2.5 Comparing A_5 and acrydite-modified DNA

Fluorophore-labeled DNA with an A_5 block or with an acrydite group was used. They were named A_5DNA1-FAM and Acryl-T_5DNA1-FAM, respectively (Table 5.1). First, to rule out the influence of other nucleobases, 5 μM A_5DNA1-FAM or Acryl-T_5DNA1-FAM was hybridized with 7.5 μM complementary DNA1 (cDNA1) in 20 mM HEPES and 100 mM NaCl. 20 μL of the duplex was added to 1 mL monomer solution containing 20 mM acrylamide, 20 mM NIPAm, 16 mM BIS and 100 mM NaCl in buffer A. The final concentration of the A_5DNA1-FAM or Acryl-T_5DNA1-FAM was 100 nM. After overnight polymerization at -20°C, the hydrogel nanoparticles containing the A_5DNA1-FAM or Acryl-T_5DNA1-FAM were obtained, and they were washed by 20 mM HEPES for three times to remove the unreacted reagents. The DNA incorporation (%) was determined by fluorescence spectroscopy as described in part 5.2.3.

5.2.6 A_5 diblock DNA containing hydrogels for cDNA capturing

A DNA containing a 24-mer random sequence and an A_5 extension, named A_5DNA2 (Table 5.1), was used. First, 150 μM A_5DNA2 was annealed with 300 μM 24-mer cDNA2 in 20 mM HEPES containing 100 mM NaCl. Then, 20 μL of the duplex was added to 1 mL monomer solution containing 20 mM acrylamide, 20 mM NIPAm, 16 mM BIS and 100 mM NaCl in buffer A. The final concentration of A_5DNA2 used during polymerization was 3 μM, and the concentration of covalently grafted DNA on hydrogel nanoparticles was estimated to be ~1 μM (based on ~35% incorporation efficiency indicated in Figure 5.7C). After polymerization, the cDNA2 was removed by hot NaOH (0.1 mM, pH 10, 90°C treatment for 1 min). The NaOH treatment was performed three times to fully remove the cDNA2, and Milli-Q water was then used to further wash the residual NaOH. Finally, the products were dried by vacuum centrifugation. To measure the binding of FAM-cDNA2, 20 mg/mL gel nanoparticles containing ~500 nM A_5DNA2 were incubated with various concentrations of FAM-

cDNA2 (from 50 pM to 2 μM) for 10 min, and then centrifuged at 15000 rpm for 10 min. The quantification of bound FAM-cDNA2 was based on the fluorescence change in the supernatants.

5.2.7 Hg^{2+} detection

Similar to the experimental procedure in part 5.2.6 that 150 μM A_5DNA3 was first annealed with 300 μM cDNA3 in 8 mM Tirs-nitrate (pH 8.0, with 150 mM $NaNO_3$). Then 20 μL of the duplex was added to 1 mL monomer solution for gel preparation in the Tirs-nitrate buffer, with 150 mM $NaNO_3$ and 4% glycerol. After polymerization and removing the cDNA3 by hot NaOH (0.1 mM, pH 10), the products were dried by vacuum centrifugation. Then, 20 mg/mL A_5DNA3 containing hydrogel nanoparticles (containing ~500 nM DNA) were incubated with 5 μM Hg^{2+} in 8 mM Tris-nitrate buffer (pH 8.0, with 150 mM $NaNO_3$) for 5 min. Next, 200 nM SGI was added to stain the DNA in the hydrogel nanoparticles (excitation at 490 nm and emission at 535 nm). A sample without Hg^{2+} was used as a control, and the selectivity was studied based on measuring the binding of 5 μM other metal ions (Zn^{2+}, Co^{2+}, Cu^{2+}, Mn^{2+}, Pb^{2+}, Mg^{2+}, Ca^{2+}, Ag^{+} and Fe^{3+}).

5.2.8 DNA conjugation and Hg^{2+} binding in monolithic gels

First, 50 μM FAM-cDNA2 was annealed with 100 μM A_5DNA2 or the same sequenced DNA without an A_5 block to form a duplex in 20 mM HEPES (containing 100 mM NaCl). The diblock DNA was added in excess to ensure that all the FAM-cDNA2 strands were hybridized. Then, 20 μL of the duplex was added to 1 mL monomer mixture containing 60 mM acrylamide, 60 mM NIPAm, 48 mM BIS and 100 mM NaCl in 20 mM HEPES. Note that no glycerol was added in this experiment. After incubating the mixture in an ice bath (~4°C) for 1 h, 20 μL of 10% w/v APS and 0.6 μL TEMED were added successively, followed by quickly transferring 75 μL solution to each well of a transparent 96-well plate. The plate was placed in a freezer (-20°C) for overnight reaction (>16 h), and the generated monolithic gels were transferred and

soaked in 20 mM HEPES (containing 100 mM NaCl) for at least three times to remove unincorporated DNA duplex and unreacted chemicals. Each soaking took 3 h in 1.5 mL buffer. Since the soaking buffer also contained salt, the FAM-cDNA2 remained hybridized with A_5DNA2 in the monolithic gels. Finally, the DNA-monolithic gel conjugates were examined by a blue light transilluminator with 470 nm excitation and by a ChemDoc MP imaging system (Bio-Rad) respectively to verify that the A_5 anchor must be included for DNA attachment to the gels.

To study the function of the DNA in the monolithic gel system, the A_5DNA3 (i.e. the A_5 extended T-rich DNA) was used during the gel preparation steps. Specifically, 20 μL of 150 μM A_5DNA3 complex (already hybridized with 300 μM cDNA3) was added to 1 mL monomer mixture containing 60 mM acrylamide, 60 mM NIPAm, 48 mM BIS and 150 mM $NaNO_3$ in 8 mM Tris-nitrate buffer (pH 8.0, with 150 mM $NaNO_3$). The total monomer concentration was 168 mM and calculated to be 2% (w/v). No glycerol was added. After incubation in ice for 1 h, 20 μL of 10% w/v APS and 0.6 μL TEMED were added successively. The sample was quickly transferred to a 96-well plate by taking 75 μL aliquots. The plate was placed in a freezer (-20°C) for overnight reaction. After that, the cDNA3 was removed by hot NaOH treatment (0.1 mM, pH 10, 90°C) for 1 min and 0.1 mM NaOH soaking for 1 h. This process was repeated five times. Milli-Q water was used to further remove the residual NaOH. Then, 5 μM Hg^{2+} was incubated with the DNA-monolithic gel conjugates in 8 mM Tris-nitrate (containing 150 mM $NaNO_3$) for 10 min, and 1 μM SGI was used to stain the gels. The same sample without Hg^{2+} was used as a control. Both the blue light transilluminator with 470 nm excitation and a ChemDoc MP imaging system (Bio-Rad) were used to confirm Hg^{2+} binding.

5.2.9 DLS and TEM

The hydrodynamic size of A_5 DNA-hydrogel conjugates were measured by dynamic light scattering (DLS) on a Zetasizer Nano ZS90 (Malvern) at 25°C. For this,

50 μg/mL gel particles were dispersed in 20 mM HEPES (pH 7.6). The morphology of such dried gels was measured by transmission electron microscopy (TEM, Philips CM 10). 200 μg/mL gels were drop-cast onto a copper grid and dried overnight at room temperature before imaging.

5.3 Results and Discussion

5.3.1 Freezing-promoted DNA attachment

To prepare hydrogel nanoparticles, we chose acrylamide and NIPAm as monomers, BIS as a crosslinker, and APS as an initiator along with 100 nM penta-adenine (A_5) DNA in 20 mM pH 7.6 HEPES buffer with 4% glycerol. We wished to form gel nanoparticles with covalently attached DNA (Figure 5.2A).[233] The polymerization reaction was performed at -20°C, and the sample froze under this condition. After the reaction and thawing the tubes, the previously clear monomer solution turned to a milky dispersion, suggesting the formation of hydrogel nanoparticles (Figure 5.2B).

We found that adding 4% glycerol generated a high yield of hydrogel particles that could be well dispersed and easily precipitated by centrifugation (the right tube in Figure 5.2B; and Figure 5.2C). The average hydrodynamic size of the 4% glycerol sample was around 340 nm by dynamic light scattering (DLS) (Figure 5.2D). The gels were also characterized with TEM, showing features of dried gel nanoparticles (Figure 5.2E). A lower glycerol (0-2%) resulted in bulky gels instead of nanoparticles, while 6% glycerol reduced the yield (Figure 5.2C). Glycerol decreased the ratio of the ice/non-ice phases and may affect polymerization in the non-ice phase.[234-236]

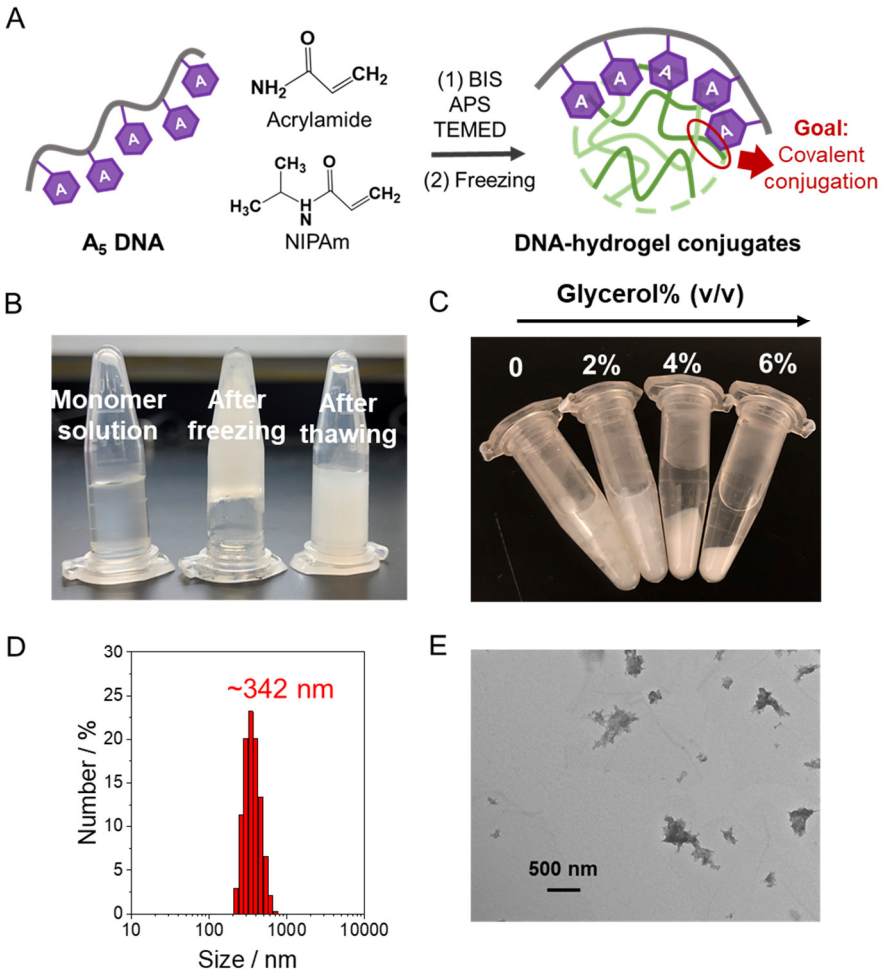

Figure 5.2 (A) Schematic illustration of preparing A_5 DNA-hydrogel conjugates via freezing radical polymerization. (B) A photograph showing the monomer solutions before and after freezing polymerization, and after thawing at room temperature. The gels were prepared in buffer A (20 mM HEPES, pH 7.6, 4% glycerol). (C) Effect of glycerol concentration (v/v%) on gel yield observed after centrifugation. (D) The average hydrodynamic size of A_5 DNA-gel particles measured by DLS. (E) A TEM micrograph of dried A_5 DNA-gel particles.

After confirming formation of gel nanoparticles, we then used a 5′-carboxyfluorescein (FAM) labeled A_5 DNA (FAM-A_5) to monitor DNA incorporation. After the freezing polymerization, we washed away the free DNA by centrifugation, and only the pellet was fluorescent (Figure 5.3A), suggesting that the DNA was

associated with the gel nanoparticles. The percentage of DNA incorporation was calculated based on the fluorescence intensity remained in the supernatants after centrifugation. Using this method, we then optimized the reaction time. The kinetics of DNA incorporation were fitted to a first order reaction yielding a rate constant of 2.5 h^{-1} (black curve in Figure 5.3B). Notably, as much as ~75% FAM-A_5 strands were incorporated after an 8 h polymerization, which was comparable to that using acrydite-modified DNA (~83%).[237] The saturation after 8 h may due to the exhaustion of free radicals, which were indispensable for the conjugation (*vide infra*). Interestingly, when the polymerization was carried out at 4°C, no more than 10% of the DNA incorporated even after 48 h (red curve in Figure 5.3B). Therefore, freezing was critical for DNA attachment.

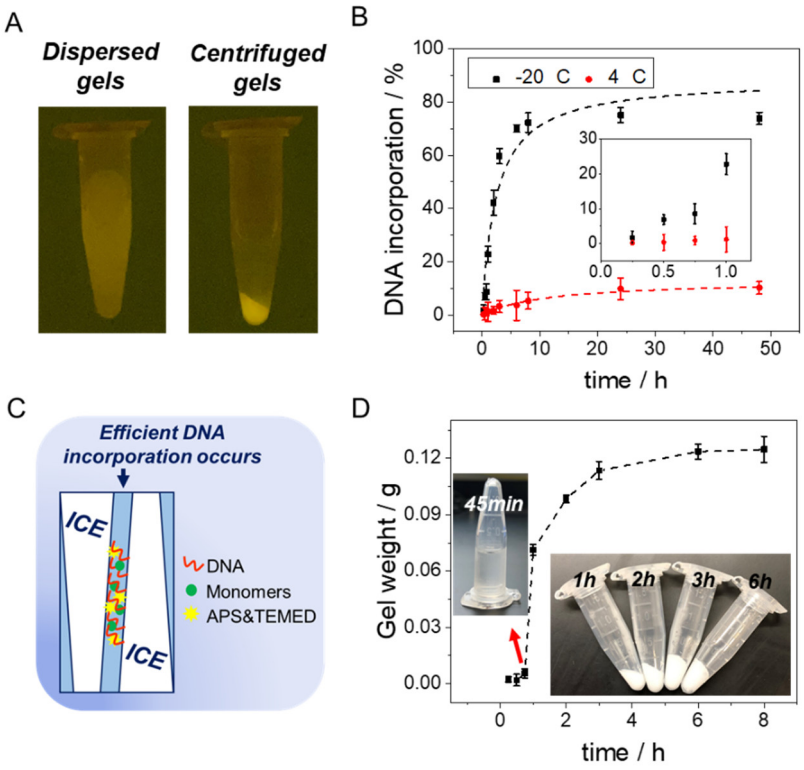

Figure 5.3 (A) Fluorescent photographs of the dispersed and centrifuged FAM-A_5 containing hydrogel nanoparticles. (B) The FAM-A_5 incorporation kinetics at -20°C and 4°C. Inset: the data within 1 h. (C) Schematic presentation of solutes concentrated in micropockets after freezing, leading to efficient DNA attachment. (D) The weight of

swelled gels as a function of reaction time. No precipitate appeared until 1 h. Insets: the photographs of samples at different time points after centrifugation.

To ensure hydrogel nanoparticles instead of monoliths were produced, our monomer concentration was only 0.6% (w/v).[238-242] During freezing, a portion of the water crystallized to form ice, leaving the solutes in the remaining non-ice regions where the monomers and DNA were likely to be concentrated (Figure 5.3C).[243] Such a concentration effect can accelerate reactions,[244-246] which may favor DNA attachment and gelation. To study the relationship between freezing and gel yield, we weighed the gels (formed at -20°C). No gels precipitated at the point of 45 min (left inset in Figure 5.3D). After 1 h, the sample fully froze and after thawing, white precipitates started to appear, reaching a plateau after 6 h (Figure 5.3D). These experiments demonstrated that freezing was essential to promote gelation. The 45 min delay for the hydrogel growth was also observed for DNA incorporation (inset in Figure 2B), indicating the importance of freezing for capturing the DNA strands.

To confirm that the DNA was covalently attached instead of physically trapped, we then analyzed the FAM-A_5 containing hydrogel nanoparticles by gel electrophoresis.[247, 248] This way, only the non-covalently associated DNA would migrate in the electric field. As shown in Figure 5.4A, lane 1 contained the free DNA as a control, and lane 2 had the gel monomers but without the initiators (prepared by freezing), where the same amount of free DNA was observed. In lane 3, the unwashed gel particles were loaded. By comparing the intensity of the free DNA band in lane 3 with that in lane 1, ~70% DNA was incorporated in the gels, consistent with the above washing-based result. The band trapped in the well was assigned to be the DNA in the gel nanoparticles, which could not migrate. However, for the sample prepared at 4°C, the band of the free FAM-A_5 did not change much (comparing lane 6 and lane 4 in Figure 5.4A), confirming that freezing was critical for DNA attachment. In addition,

we also reacted the FAM-A_5 with each acrylic monomer respectively, and found that the acrylamide, NIPAm and BIS could all react to form DNA conjugates (Figure 5.4B).

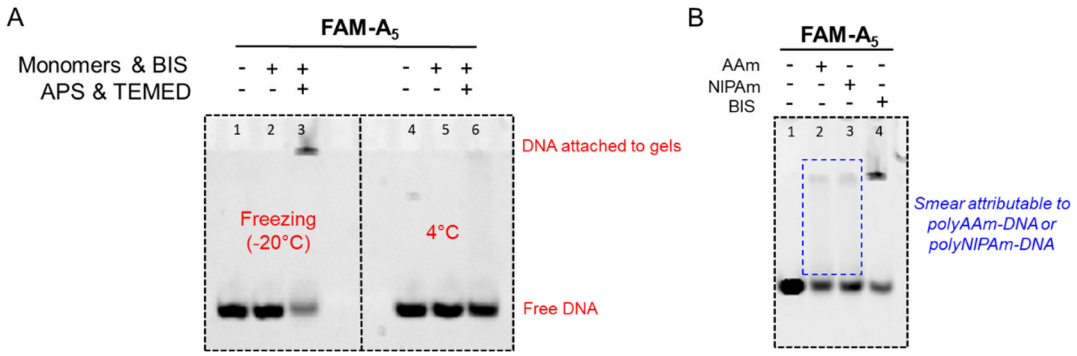

Figure 5.4 Gel micrographes of 50 nM FAM-A_5 reacted under different conditions.

5.3.2 Radical-mediated DNA conjugating

When the initiator APS was omitted, no gel formed and the DNA failed to attach even with freezing (lane 2 of Figure 5.4E), indicating that radicals were critical for DNA conjugation. The optimized APS amount was 2 mg when working with 0.6 μL TEMED as an accelerator at -20°C (Figure 5.5A-D). In our system, the radicals mainly came from APS and they can be transferred to the vinyl group in acrylic monomers. Steeken et al. reported that the reaction between adenine and HO• radicals mainly happened on the double bond regions of adenine.[232] We reason that the reaction between A_5 DNA and the vinyl radicals in our system might also occur in similar regions.

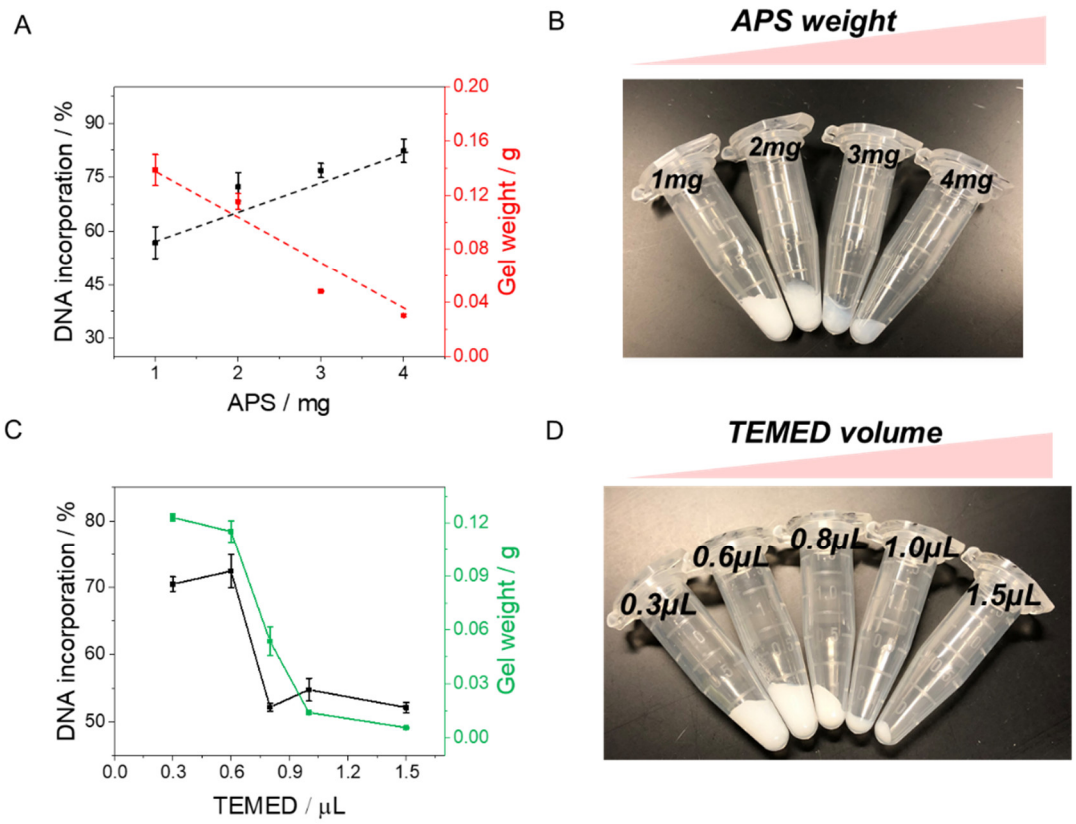

Figure 5.5 (A) The effect of APS amount (from 1 to 4 mg) on the FAM-A_5 incorporation % and the gel weight. 0.6 μL TEMED was added for all the samples in buffer A (20 mM HEPES, pH 7.6, with addition of 4% glycerol). (B) Photograph for the samples in (A). (C) The effect of TEMED volumn (from 0.3 to 1.5 μL) on the FAM-A_5 incorporation % and the gel weight. 2 mg APS was added to all these samples. (D) Photograph for the samples in (C). 100 nM FAM-A_5 was added to these experiments. Given that more initiators can result in more free radicals, appropriate amount of APS or TEMED could promote polymer formation. However to much of them generated many shorter polymer chains, thus eventually lowered the gel yield. Based on the data, 0.6 μL TEMED and 2 mg APS were optimal for our 1 mL reaction system.

5.3.3 A_5 is an optimal anchoring sequence

To understand the generality of this method, we further studied the effect of DNA sequence, length, and conformation. First, four FAM-labeled homo-DNAs of different

lengths (5, 15 and 30-mer) were respectively used to prepare gel particles. Using the washing method, the incorporation efficiency decreased for poly-A and poly-G DNA when their length was increased (Figure 5.6A). It might be that longer DNA tended to fold on its own especially under the low reaction temperature condition, which may shield the bases for reacting with acrylamide. Very short 5-mer DNA might not form stable internal structures even under the freezing condition.[249] Poly-T incorporated more for the longer DNA (from 4.3% to 33.2%), while the incorporation of poly-C was length-independent (~15%). Since thymine was not previously reported to covalently react with acrylamide, we attribute its incorporation to physical entrapment, which was confirmed by gel electrophoresis (Figure 5.6B). Overall, A_5 had the highest incorporation efficiency.

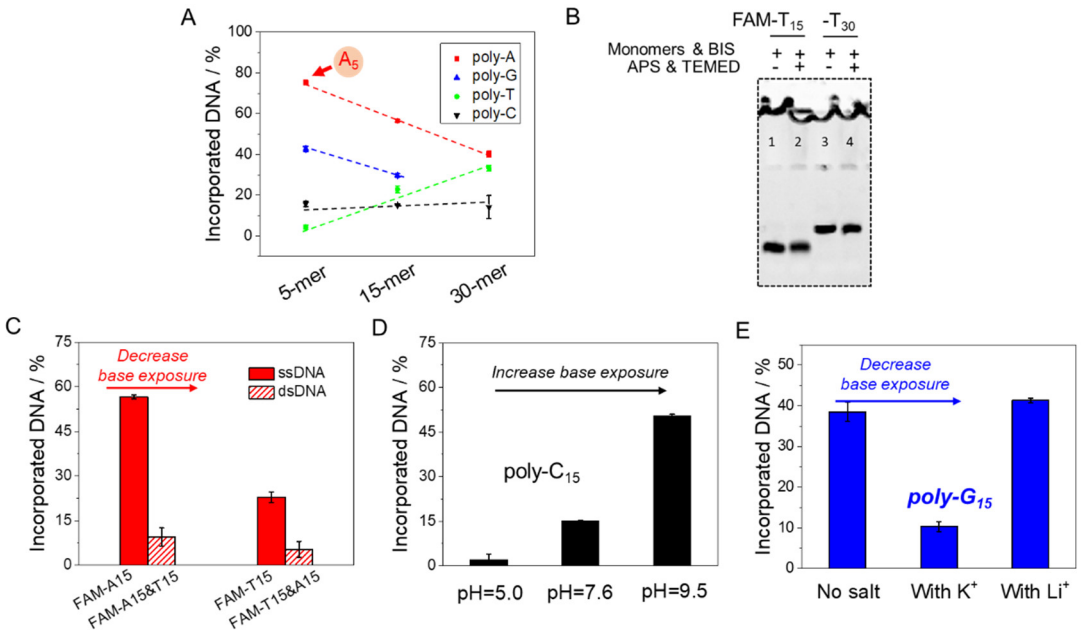

Figure 5.6 (A) Incorporating efficiency of 100 nM FAM-labeled homo-DNAs of different lengths prepared by freezing. (B) Gel micrographs of free FAM-T_{15} and FAM-T_{30} and their hydrogel conjugates prepared by freezing in buffer A. (C) Comparing the incorporation efficiency of double- and single-stranded DNA during gel preparation. 100 nM FAM-DNA was hybridized with 150 nM non-label DNA. (D) Incorporation of FAM-C_{15} in hydrogels prepared at pH 5.0 (20 mM acetate), 7.6 (20

mM HEPES) and 9.5 (20 mM carbonate). (E) The incorporation percentage of FAM-G_{15} in hydrogels prepared with or without addition of 10 mM KCl during freezing polymerization (in 20 mM Li-based HEPES, pH 7.6, 4% glycerol). 10 mM LiCl was also used to confirm the importance of adding K^+.

5.3.4 Non-structured DNA attaches more favorably

Since the nucleobases are important for the attachment, we then tested duplex DNA, for which the bases are shielded. By hybridizing FAM-A_{15} with non-labeled T_{15}, the incorporated FAM-A_{15} dropped by 6-fold (<10% incorporated, Figure 5.6C), confirming nucleobase-driven DNA grafting. Interestingly, the incorporated FAM-T_{15} also dropped by 4.3-fold in the presence of A_{15}, likely due to the decreased entrapment due to rigid duplex formation. In addition, we prepared gels with FAM-C_{15} under different pH. The DNA incorporation dropped from 50.3% at pH 9.5 to 10.1% at pH 7.6 and further to 2.0% at pH 5.0 (Figure 5.6D). Since poly-C DNA tends to adopt an i-motif structure at acidic pH,[250, 251] a low pH shielded cytosine bases for the reaction. Similarly, placing the FAM-G_{15} in a K^+-containing buffer (10 mM KCl) encouraged the formation of G-quadruplex,[252, 253] thus decreasing guanine exposure and the incorporation of G-rich DNA (Figure 5.6E). These results together demonstrated that the attachment efficiency can be controlled by tuning DNA sequence, length and conformation.

5.3.5 Comparing A_5 and acrydite-modified DNA

Given the high conjugation yield of A_5, we then developed a diblock DNA strategy using A_5 as an anchoring block. We designed a 20-mer DNA with an A_5 block on its 5′ end and a 15-mer block of random sequence containing a FAM label (named A_5DNA1-FAM in Figure 5.7A). For comparison, the same 15-mer sequence with a 5′ acrydite was used with a T_5 spacer (named Acryl-T_5DNA1-FAM). To protect the 15-mer block, its 15-mer cDNA was hybridized with both DNA before gel preparation (lower panel in Figure 5.7A). Since we demonstrated that duplex DNA is disfavored for the reaction,

the attachment should occur mainly via the A_5 block or the acrydite. After freezing polymerization and washing, both products emitted intense fluoresence (Figure 5.7B), indicating DNA conjugation. After washing, about 35% A_5 diblock DNA and 43% acrydite DNA were retained in the gels (left bars in Figure 5.7C). Although A_5 DNA alone achieved ~75% incorporation (Figure 5.6A), appending a rigid duplex may lower the incorporation efficiency possibly by the slower diffusion and steric hindrance from the bulky duplex structure hindering the motion of the A_5 for reaction.[216, 218] Without hybridization to the cDNA during gelation, ~10% more incorporation was observed for both (right bars in Figure 5.7C). Finally, through testing different DNA concentrations (from 50 nM to 200 nM), we found that the incorporation efficiency was quite consistent, all being a few percent below that of the acrydite DNA (Figure 5.7D).

Most previous work using acrydite-DNA was performed at room temperature. As demonstrated in this work, their conjugation via DNA bases was low at non-freezing conditions, and the reactions mainly proceeded via the acrydite. Under the freezing condition, conjugation via DNA bases was promoted. Overall, A_5 diblock DNA performed well for grafting unmodified oligonucleotides to hydrogel nanoparticles.

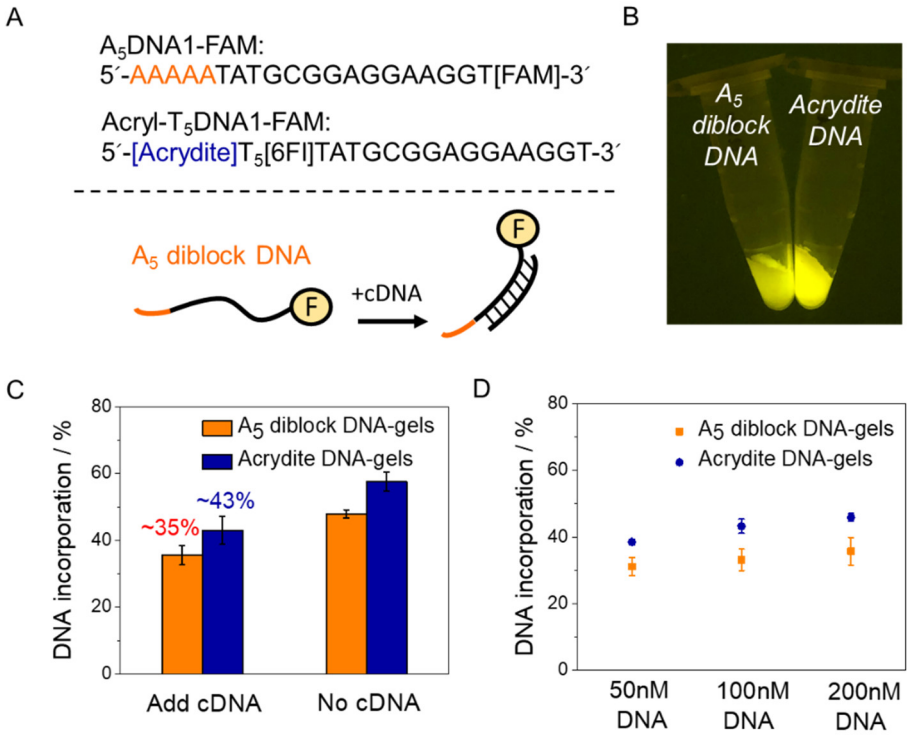

Figure 5.7 Comparing DNA grafting between a fluorescent A_5-containing diblock DNA and an acrydite-modified DNA. (A) The upper panel: DNA sequences used. The lower panel: cDNA shielding and exposure of the A_5 block during gel synthesis. (B) A photograph of the gels prepared with the two DNA strands. (C) Comparison of the incorporation percentage of the two DNA without and with the cDNA during gel synthesis. (D) The effect of DNA concentration on the incorporation efficiency.

5.3.6 A_5 diblock DNA-functionalized hydrogels for cDNA capture

After achieving conjugation of unmodified DNA, we then explored the applications of such conjugates. Acrydite-DNA functionalized hydrogels have been widely used for various applications, and DNA hybridization is a key reaction.[46, 57, 63, 254, 255] Herein, we aimed to test whether such applications can also be realized by A_5 diblock DNA. We designed a 24-mer random sequence and extended its 5′-terminus by A_5 (named A_5DNA2 in Figure 5.8A). During gel preparation, we hybridized it with its 24-mer cDNA (named cDNA2 in Figure 5.8A) to protect the recognition block (left panel in Figure 5.8B). After the reaction, the cDNA was washed away under denaturing conditions, leaving behind the A_5 containing DNA (right panel in Figure 5.8B).

We then tested the gels for capturing its cDNA. To do this, 20 mg/mL gels, containing ~500 nM A_5DNA2, were incubated with 50 nM FAM-cDNA2 or with a random control sequence. After centrifugation, based on the decrease of the fluorescence in the supernatants, only the FAM-cDNA2 was specifically captured (Figure 5.8C and 5.8D). To quantitatively determine cDNA capture, we gradually titrated it to the conjugates. Figure 5.8E shows that 2 μM FAM-cDNA2 saturated the binding. Initially, 90% of the cDNA can be captured (inset of Figure 5.8E). If this was used as a sensor, the detection limit would be 50 pM (3σ/slope). Therefore, the DNA has retained its hybridization function. However, when the cDNA was omitted during gel preparation, the generated nanoparticles had an obviously lower cDNA binding capacity (Figure 5.8F), and the saturated cDNA capturing capacity was only about one

third, indicating that the cDNA must be added during gel preparation to ensure that efficient conjugation occurred only via the A_5 block.

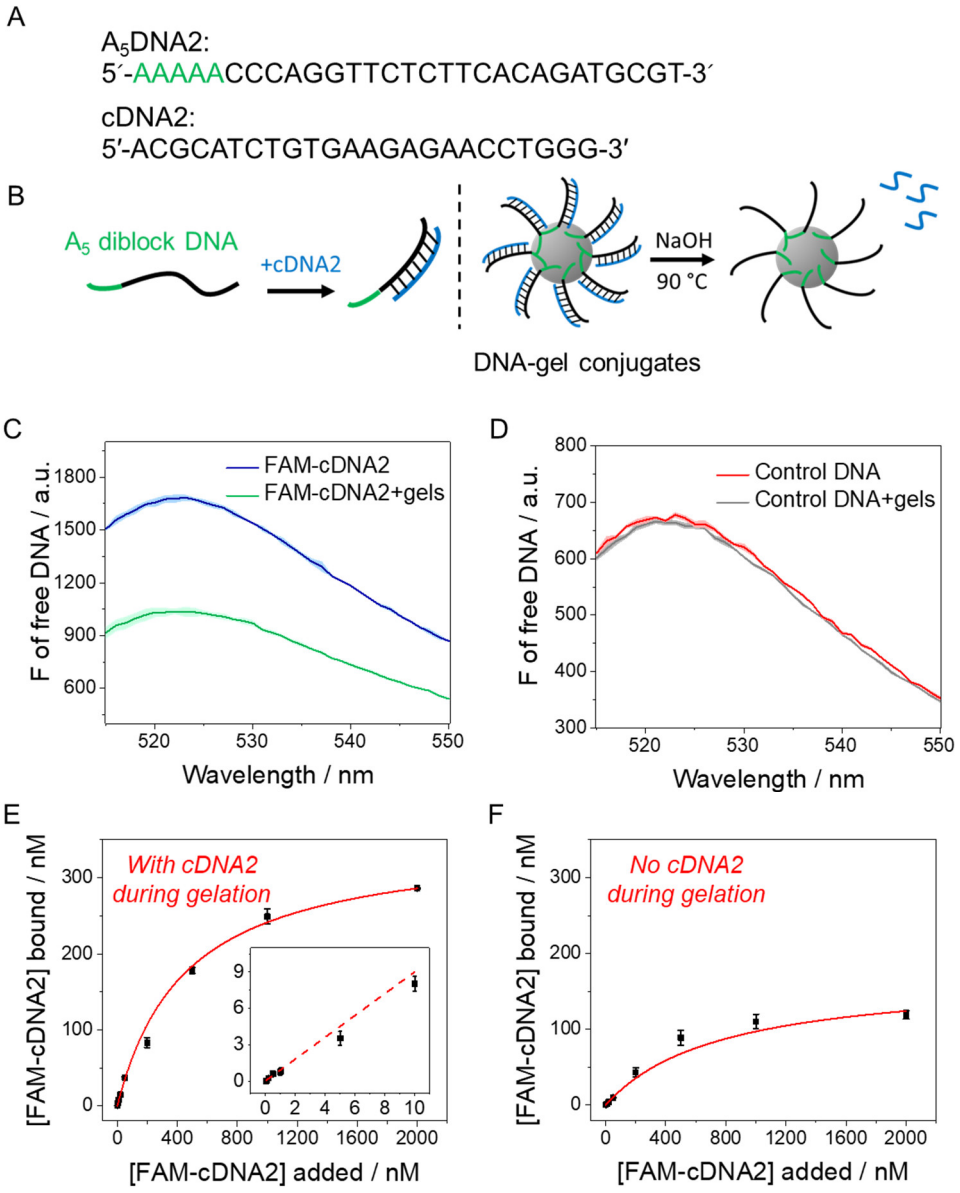

Figure 5.8 DNA capturing by A_5 diblock DNA-hydrogel conjugates. (A) DNA sequences used. (B) Left panel: schematic of forming duplex to only expose the A_5 segment in diblock DNA for conjugating. The right panel: schematic of removing cDNA2 by 0.1 mM NaOH at 90°C for 1 min. Fluorescent spectra of the A_5 diblock DNA-hydrogel conjugates binding to (C) FAM-cDNA2 and (D) FAM-control DNA in 20 mM HEPES (pH 7.6, with 100 mM NaCl). Titrating various concentrations of FAM-

cDNA2 to gel conjugates prepared (E) with and (F) without the cDNA2. Inset of (E): response at low FAM-cDNA2 concentrations showing nearly 90% capturing efficiency.

5.3.7 Detection of Hg^{2+}

DNA-functionalized hydrogels have been widely used in analytical applications such as disease and environemental monitoring.[68, 71, 256, 257] The detection of Hg^{2+} is a particularly interesting example, since the gel can help enrich Hg^{2+}, protect the DNA, and allowing drying and long-term storage.[70, 258, 259] In our work, to explore non-hybridization-based applications, the detection of Hg^{2+} was also studied. We appended a thymine-rich sequence commonly used for Hg^{2+} sensing with a 5′ A_5 block (Figure 5.9A, named A_5DNA3). After Hg^{2+} mediated formation of T-Hg^{2+}-T to fold the DNA into a hairpin, SYBR Green I (SGI) can stain this structural change with a large fluorecence enhancement.[260] We expected that the A_5DNA3 would also function for Hg^{2+} binding within hydrogels (Figure 5.9B). We then added 5 μM Hg^{2+} to 20 mg/mL gels (~500 nM DNA). Nearly 4-fold fluorescence increase was observed (Figure 5.9C). Replacing the thymine to adenine in the sequence failed to bring much signal change (Figure 5.9D), verifying that Hg^{2+} binding was indeed from the T-rich region. Due to the small gel size, the signaling kinetics were also very rapid (Figure 5.9E, within 1 min). Titrating the Hg^{2+} to the hydrogels achieved a detection limit of 10 nM (Figure 5.9F), and the sensor also had high specificity for Hg^{2+} (Figure 5.9G).

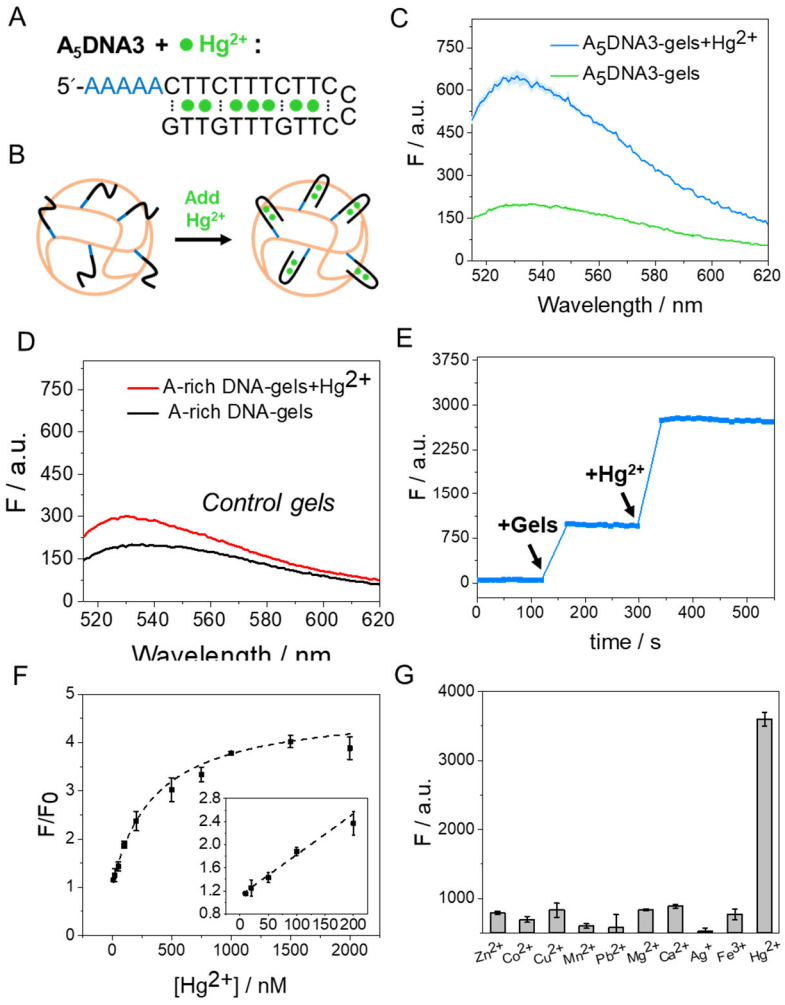

Figure 5.9 Hg^{2+} sensing by A_5 diblock DNA-hydrogel conjugates. (A) The sequence of the A_5DNA3. (B) Schematic of Hg^{2+} binding to A_5DNA3 containing hydrogel nanoparticles. Fluorescence spectra of 5 μM Hg^{2+} binding to 20 mg/mL (C) A_5DNA3 containing hydrogels and (D) A-rich DNA (named A_5DNA4 in Table 5.1) containing hydrogels. Hg^{2+} binding was stained by 200 nM SGI in 8 mM Tris-nitrate (pH 8.0), with 150 mM $NaNO_3$. (E) Kinetics of 20 mg/mL A_5DNA3 containing hydrogels binding to 5 μM Hg^{2+}. (F) Titrating various concentrations of Hg^{2+}. Inset: the initial linear response. (G) The selectivity of the Hg^{2+} sensor with 5 μM of each metal ion.

5.3.8 Monolithic gel conjugates

The above work was all performed using hydrogel nanoparticles. For some applications, monolithic gels were used.[261-267] We then tested whether the A_5 anchor

could also be used to prepare DNA conjugates in monolithic gels by increasing the monomer concentration from 0.6% to 2%. At the same time, freezing polymerization was also performed to promote DNA attachment, and glycerol was omitted to encourage forming monolithic gels. We prepared the monoliths in a 96-well plate to generate a cylinder shape (Figure 5.10A).

Using the DNA sequences in Figure 5.8A, we hybridized the two DNA to expose the A_5 block. As a control, the same DNA but without the A_5 block was also used. After polymerization and washing, the A_5 containing sample exhibited stronger fluorescence than the A_5-free one (left panel in Figure 5.10B). Subsequent imaging by a gel documentation system showed that the A_5 bearing duplex had approximately 4-fold stronger fluorescence (right panel in Figure 5.10B). To explore the DNA functionality in monolithic hydrogels, we used the A_5DNA3 during the preparation for binding Hg^{2+}. As expected, in the presence of 1 μM SGI, adding 5 μM Hg^{2+} resulted in strong fluorescent (Figure 5.10C), but Hg^{2+} did not bring a change in the A-rich DNA (A_5DNA4) sample (Figure 5.10D). Together, these experiments proved that our method for grafting the unmodified DNA to hydrogels can be general from gel nanoparticles to monoliths.

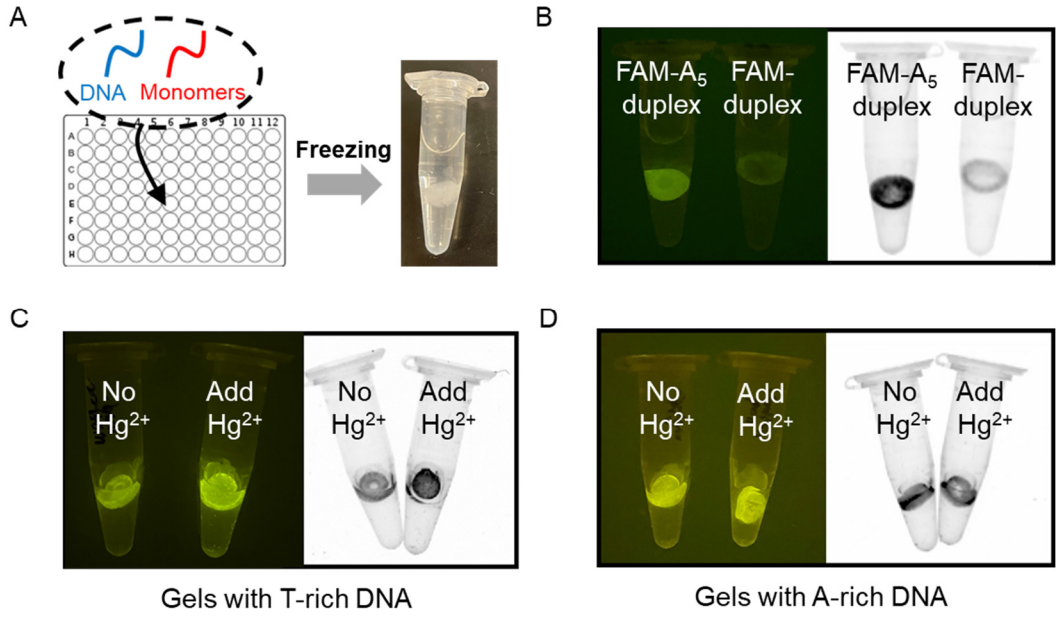

Figure 5.10 (A) Schematic illustration of preparing A_5 diblock DNA-monolithic gel conjugates in a 96-well plate using freezing polymerization. (B) The incorporation of FAM-labeled duplex without and with an A_5 block in monoliths imaged by a digital camera (left) and by a gel documentation system (right). 5 μM Hg^{2+} binding by A_5 containing (C) T-rich DNA and (D) A-rich DNA in monoliths, and the DNA was stained by 1 μM SGI in 8 mM Tris-nitrate buffer (pH 8.0, with 150 mM $NaNO_3$).

5.4 Summary

In summary, we have developed a simple method to covalently incorporate unmodified DNA oligonucleotides to hydrogel nanoparticles and monoliths by exploiting A_5 as an anchoring block. A_5 was found to be the optimal choice among other DNA sequences and lengths due to the highest reactivity of adenine. By studying DNA conformation, unfolded DNA with exposed bases had the highest incorporation efficiency. In this system, DNA incorporation and hydrogel formation were completed in one-pot in a few hours. A key to the success is the freezing reaction condition to ensure sufficient DNA immobilization. Notably, A_5 DNA showed ~75% incorporating efficiency, and a longer 20-mer A_5 diblock strand also exhibited nearly 40% incorporation. The DNA-hydrogel conjugates could be applied for ultrasensitive cDNA capturing and Hg^{2+} detection, replacing the traditional acrydite-modified DNA. Together, this work provides deeper insights in DNA/hydrogel systems and offers opportunities for more researchers to develop DNA-based soft materials at a much lower cost.

Chapter 6 Conclusions and Future work

6.1 Conclusions and original contributions

Functional DNA and DNA-hydrogels have been extensively explored for sensing bio-relevant small molecules in analytical and biomedical applications. Nevertheless, the limited specificity for some SELEX-derived aptamers (e.g., the adenosine aptamer) and the lack of aptamers for important "disease indictors" (e.g., guanosine) have left some room for improvement. Additionally, the current strategies for grafting DNA on hydrogels require chemical modification of DNA, which increases the cost of using them in applications. In this thesis, the programmability, binding specificity, and chemical properties of functional DNA are actively exploited to address these issues.

In chapter 2, I designed a novel "base-excised aptamer" to achieve highly specific recognition of adenosine. In this strategy, an entire A nucleotide is excised from the adenosine aptamer backbone to create a vacancy for specifically accepting a free adenosine. Other analogues including AMP, ATP, guanosine, cytidine, uridine and theophylline, none of them can fit into such a pocket. SYBR Green I binding assays and ITC were used to verify the specific adenosine binding. Mechanism studies (by ITC) show that the adenosine recognition is mainly driven by base stacking, and one adenine-excised aptamer can accommodate two adenosine molecules, with one in the excised site (DNA backbone) and the other in the original aptamer binding pocket (loop area). These two sites work cooperatively to achieve the high specificity. Finally, I also demonstrated the application of the A-excised aptamer in dilute FBS. This work provides an interesting method of using existing aptamer sequences for enhanced functions.

In chapter 3, to further demonstrate the generality of the base-excised strategies proposed in the chapter 2, a Na^+-specific aptamer and the original adenosine aptamer are also employed as the scaffolds for base deleting and guanosine recognition. I design a total of 10 G-excised DNA sequences are studied in this work. Among them, two

optimal sequences are obtained, and they only bind guanosine but not GMP or GTP, verifying that the sequences can be used as a specific guanosine aptamer. Importantly, highly conserved purines are found to be more reasonable excision-positions than less conserved ones for specific recognition. This work shows the generality our strategy, and generates new guanosine aptamers for application purpose.

In chapter 4, based on the fact that the adenosine only differs deoxyadenosine by a -OH and the specific recognition of adenosine from their mixture can hardly be realized by existing aptamers, I develop a polymer-based strategy through incorporating boronic acid with the original adenosine aptamer in MIPs. A hundred-fold higher specificity for adenosine over deoxyadenosine is achieved in this case. The ITC provides the K_a(adenosine)/K_a(deoxyadenosine) ratio of our MIPs to be 110 (at pH 7.6), while that of free aptamer is only 1.07. By lowering the pH to 6.4, the ratio further increases to 115, and non-specific cytidine binding is also inhibited. Mechanism studies further reveal that much of the selectivity is from the aptamer binding by the boronic acid moiety noncovalently. This work demonstrates an alternative strategy of using an existing aptamer with tailored MIPs to achieve highly specific molecular recognition.

In chapter 5, I developed a modification-free method to covalently conjugate DNA on polyacrylamide-based hydrogels, by taking using of the intrinsic reactivity of an A_5 DNA. Freezing is used to promote the reaction efficiency from 10% at 4°C to ~75% at -20°C. A_5 is found to be the optimal choice among other DNA sequences and lengths; and by exploiting A_5 as an anchoring block, any random sequence and functional DNA containing the A_5 moiety can be incorporated to hydrogels for application purposes. Ultrasensitive cDNA capturing and Hg^{2+} detection have been demonstrated by this unmodified A_5 diblock DNA, showing its practicability in replacing the traditional acrydite-modified DNA. This work provides deeper insights in DNA/hydrogel systems and offers opportunities for more researchers to develop DNA-based soft materials at a much lower cost.

6.2 Future work

The results presented in this thesis provide two new strategies to achieve highly specific recognition of adenosine and guanosine, in which the first one is through engineering base-excised aptamers and the other combines existing adenosine aptamers with a functional monomer, boronic acid, in MIPs. To further facilitate the application of functional DNA in sensing applications, and in particular, to lower its cost, the freezing-assisted conjugation method for grafting unmodified DNA to polyacrylamide-based hydrogels is developed. Based on these studies, future works could be carried out in following aspects.

First, since the non-SELEX strategies cost much less and more time-efficient than SELEX, deeper mechanism studies can be performed to better understand the base-excised strategies; this way, the field of generating non-SELEX derived aptamers is further developed. For example, the structure characterization of our engineered base-excised aptamers could be carried out to reveal how the binding pockets distinguish the adenosine from its analogues. Based on these, more insights are gained for rational and efficient sequence design in other aptamers.

Second, the preparation of the imprinted hydrogels needs to be improved for achieving more specific and tighter molecular recognition from the polymer matrix. The current specificity of our MIPs largely comes from the functional monomers used (i.e. aptamers and boronic acid), while the binding affinity and specificity of the polymer matrix itself is relatively weak. To solve this problem, the preparation of MIPs may be performed in lower temperatures, in which the ligand-MIPs binding could be promoted. The formulation of MIPs could be optimized as well to improve the specificity of the binding pockets.

Finally, more chemical properties and applications of the unmodified DNA-hydrogel conjugates need to be explored. In addition to their reported applications in sensing (for cDNA and Hg^{2+} detection), other aspects such as stimuli-responsiveness,

recognition of small molecules and drug delivery are also important to be studied. More research in this new conjugation strategy may provide evidence showing that it indeed can rival the traditional acrydite-DNA based conjugation method.

Letters of Copyright Permission

For paper published in chapter 3:

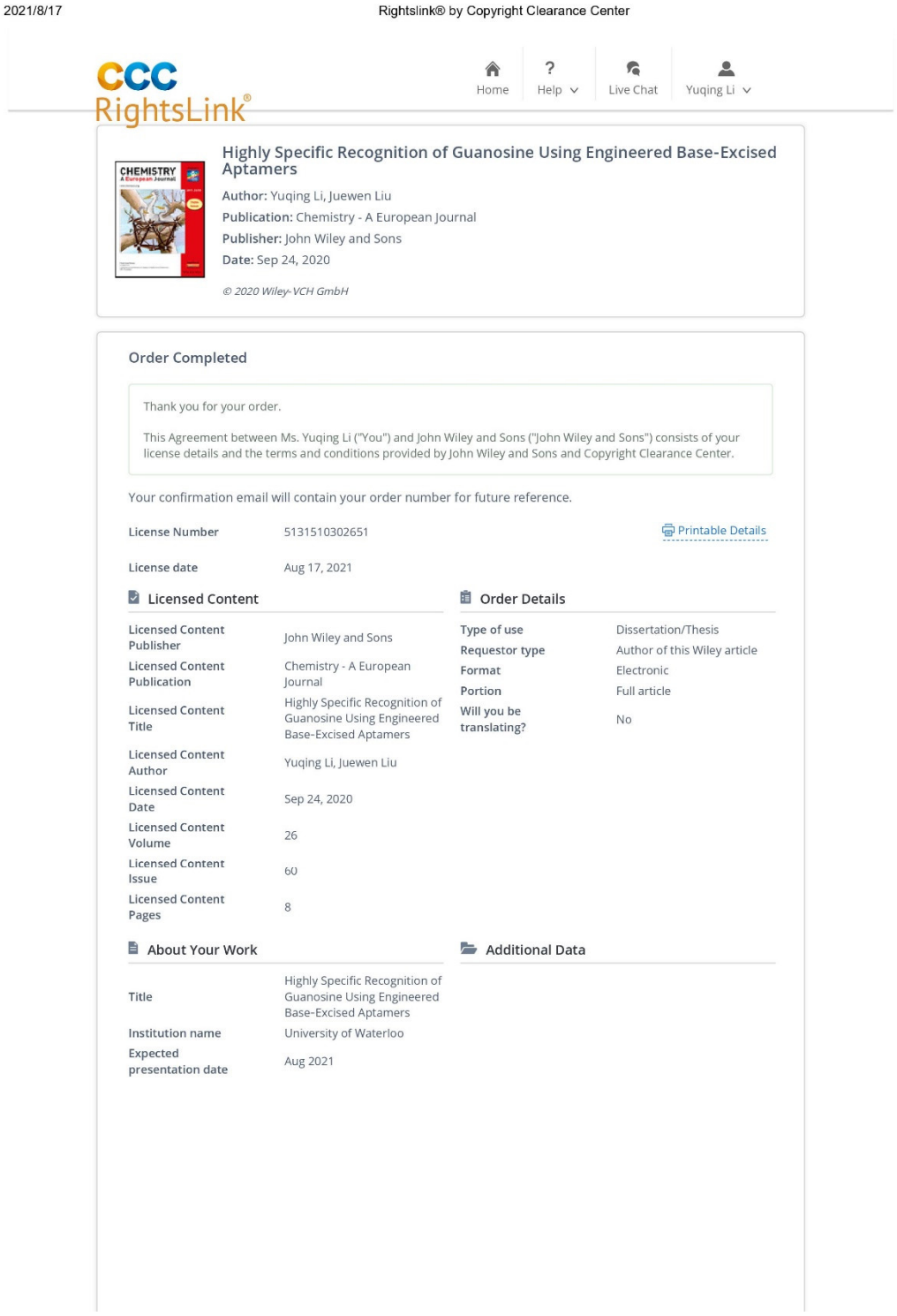

2021/8/17 Rightslink® by Copyright Clearance Center

CCC RightsLink®

Home | Help | Live Chat | Yuqing Li

Highly Specific Recognition of Guanosine Using Engineered Base-Excised Aptamers

Author: Yuqing Li, Juewen Liu
Publication: Chemistry - A European Journal
Publisher: John Wiley and Sons
Date: Sep 24, 2020

© 2020 Wiley-VCH GmbH

Order Completed

Thank you for your order.

This Agreement between Ms. Yuqing Li ("You") and John Wiley and Sons ("John Wiley and Sons") consists of your license details and the terms and conditions provided by John Wiley and Sons and Copyright Clearance Center.

Your confirmation email will contain your order number for future reference.

Printable Details

License Number	5131510302651
License date	Aug 17, 2021

Licensed Content

Licensed Content Publisher	John Wiley and Sons
Licensed Content Publication	Chemistry - A European Journal
Licensed Content Title	Highly Specific Recognition of Guanosine Using Engineered Base-Excised Aptamers
Licensed Content Author	Yuqing Li, Juewen Liu
Licensed Content Date	Sep 24, 2020
Licensed Content Volume	26
Licensed Content Issue	60
Licensed Content Pages	8

Order Details

Type of use	Dissertation/Thesis
Requestor type	Author of this Wiley article
Format	Electronic
Portion	Full article
Will you be translating?	No

About Your Work

Title	Highly Specific Recognition of Guanosine Using Engineered Base-Excised Aptamers
Institution name	University of Waterloo
Expected presentation date	Aug 2021

Additional Data

Requestor Location

Requestor Location	Ms. Yuqing Li 200 University Avenue West Quantum Nano Centre, 5611 Waterloo, ON N2L 3G1 Canada Attn: Yuqing Li

Tax Details

Publisher Tax ID	EU826007151

Price

Total	0.00 USD

Would you like to purchase the full text of this article? If so, please continue on to the content ordering system located here: Purchase PDF
If you click on the buttons below or close this window, you will not be able to return to the content ordering system.

Total: 0.00 USD

CLOSE WINDOW ORDER MORE

© 2021 Copyright - All Rights Reserved | Copyright Clearance Center, Inc. | Privacy statement | Terms and Conditions
Comments? We would like to hear from you. E-mail us at customercare@copyright.com

For paper published in chapter 4:

For paper published in chapter 5:

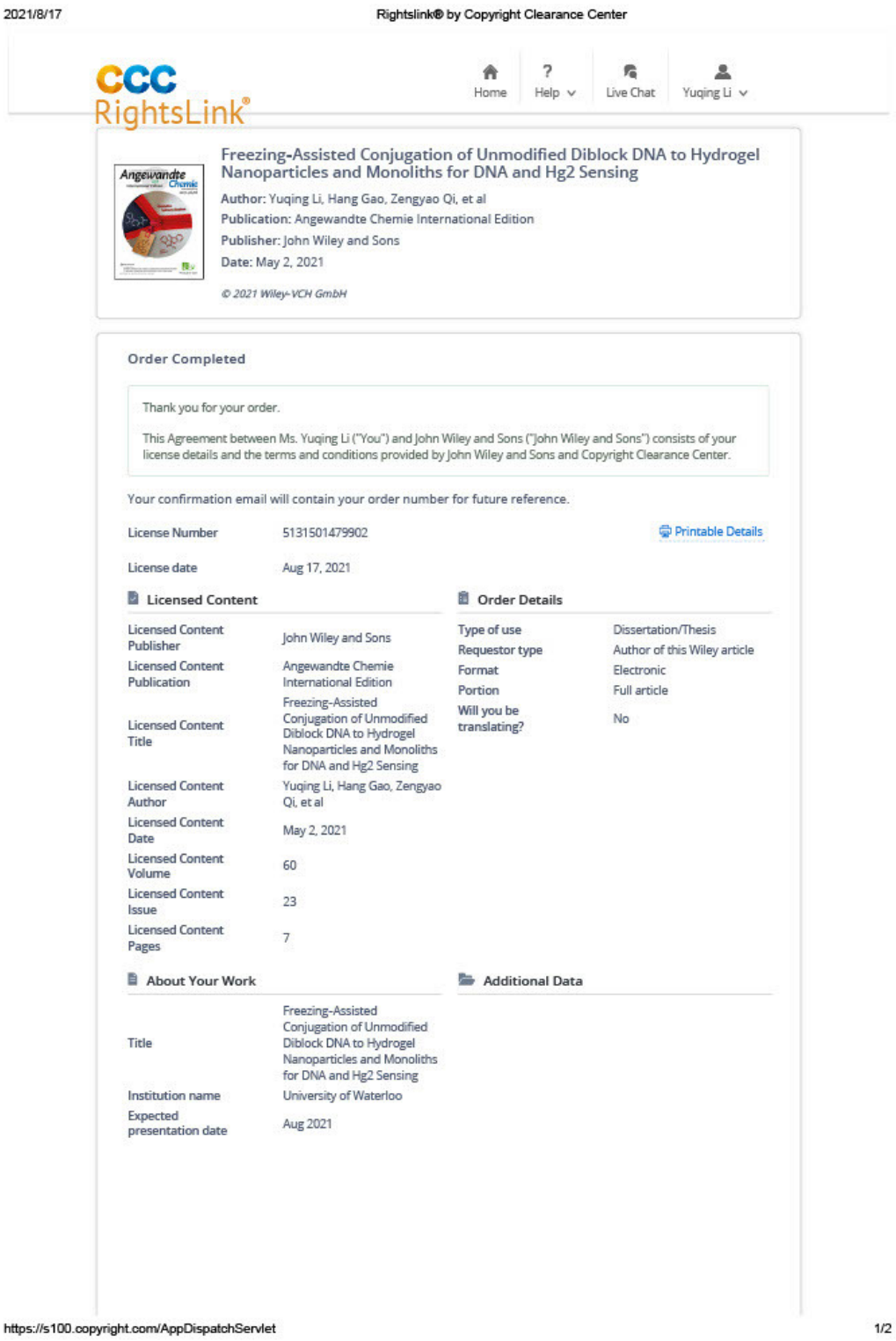

2021/8/17 Rightslink® by Copyright Clearance Center

CCC RightsLink®

Home | Help | Live Chat | Yuqing Li

Freezing-Assisted Conjugation of Unmodified Diblock DNA to Hydrogel Nanoparticles and Monoliths for DNA and Hg2 Sensing

Author: Yuqing Li, Hang Gao, Zengyao Qi, et al
Publication: Angewandte Chemie International Edition
Publisher: John Wiley and Sons
Date: May 2, 2021

© 2021 Wiley-VCH GmbH

Order Completed

Thank you for your order.

This Agreement between Ms. Yuqing Li ("You") and John Wiley and Sons ("John Wiley and Sons") consists of your license details and the terms and conditions provided by John Wiley and Sons and Copyright Clearance Center.

Your confirmation email will contain your order number for future reference.

Printable Details

License Number	5131501479902
License date	Aug 17, 2021

Licensed Content

Licensed Content Publisher	John Wiley and Sons
Licensed Content Publication	Angewandte Chemie International Edition
Licensed Content Title	Freezing-Assisted Conjugation of Unmodified Diblock DNA to Hydrogel Nanoparticles and Monoliths for DNA and Hg2 Sensing
Licensed Content Author	Yuqing Li, Hang Gao, Zengyao Qi, et al
Licensed Content Date	May 2, 2021
Licensed Content Volume	60
Licensed Content Issue	23
Licensed Content Pages	7

Order Details

Type of use	Dissertation/Thesis
Requestor type	Author of this Wiley article
Format	Electronic
Portion	Full article
Will you be translating?	No

About Your Work

Title	Freezing-Assisted Conjugation of Unmodified Diblock DNA to Hydrogel Nanoparticles and Monoliths for DNA and Hg2 Sensing
Institution name	University of Waterloo
Expected presentation date	Aug 2021

Additional Data

https://s100.copyright.com/AppDispatchServlet 1/2

Requestor Location

Requestor Location	Ms. Yuqing Li 200 University Avenue West Quantum Nano Centre, 5611 Waterloo, ON N2L 3G1 Canada Attn: Yuqing Li

Tax Details

Publisher Tax ID	EU826007151

Price

Total	0.00 USD

Would you like to purchase the full text of this article? If so, please continue on to the content ordering system located here: Purchase PDF
If you click on the buttons below or close this window, you will not be able to return to the content ordering system.

Total: 0.00 USD

CLOSE WINDOW ORDER MORE

© 2021 Copyright - All Rights Reserved | Copyright Clearance Center, Inc. | Privacy statement | Terms and Conditions
Comments? We would like to hear from you. E-mail us at customercare@copyright.com

References

1. Ellington, A. D.; Szostak, J. W., In vitro selection of RNA molecules that bind specific ligands. *Nature* **1990,** *346* (6287), 818-822.

2. Tuerk, C.; Gold, L., Systematic evolution of ligands by exponential enrichment: RNA ligands to bacteriophage T4 DNA polymerase. *Science* **1990,** *249* (4968), 505-510.

3. Yu, H.; Alkhamis, O.; Canoura, J.; Liu, Y.; Xiao, Y., Advances and challenges in small-molecule DNA aptamer isolation, characterization, and sensor development. *Angew. Chem. Int. Ed.* **2021**, https://doi.org/10.1002/anie.202008663.

4. Huizenga, D. E.; Szostak, J. W., A DNA aptamer that binds adenosine and ATP. *Biochemistry* **1995,** *34* (2), 656-665.

5. Stojanovic, M. N.; De Prada, P.; Landry, D. W., Aptamer-based folding fluorescent sensor for cocaine. *J. Am. Chem. Soc.* **2001,** *123* (21), 4928-4931.

6. Nutiu, R.; Li, Y., In vitro selection of structure-switching signaling atamers. *Angew. Chem., Int. Ed.* **2005,** *44* (7), 1061-1065.

7. Tan, W.; Donovan, M. J.; Jiang, J., Aptamers from cell-based selection for bioanalytical applications. *Chem. Rev.* **2013,** *113* (4), 2842-2862.

8. Sazani, P. L.; Larralde, R.; Szostak, J. W., A small aptamer with strong and specific recognition of the triphosphate of ATP. *J. Am. Chem. Soc.* **2004,** *126* (27), 8370-8371.

9. Liu, M.; Chang, D.; Li, Y., Discovery and biosensing applications of diverse RNA-cleaving DNAzymes. *Acc. Chem. Res.* **2017,** *50* (9), 2273-2283.

10. Li, X. M.; Zheng, K. W.; Zhang, J. Y.; Liu, H. H.; He, Y. D.; Yuan, B. F.; Hao, Y. H.; Tan, Z., Guanine-vacancy-bearing G-quadruplexes responsive to guanine derivatives. *Proc. Natl. Acad. Sci. U. S. A.* **2015,** *112* (47), 14581-14586.

11. Li, Y.; Liu, B.; Huang, Z.; Liu, J., Engineering base-excised aptamers for highly specific recognition of adenosine. *Chem. Sci.* **2020,** *11* (10), 2735-2743.

12. Li, Q.; Fei, Y.; Gao, L.; Yu, Y.; Zhou, Y.; Ye, T.; Zhou, X. S.; Shao, Y.; Yin, Z. Z., G-quadruplex DNA with an apurinic site as a soft molecularly imprinted sensing platform. *Anal. Chem.* **2018,** *90* (9), 5552-5556.

13. Kloor, D.; Yao, K.; Delabar, U.; Osswald, H., Simple and sensitive binding assay for measurement of adenosine using reduced S-adenosylhomocysteine hydrolase. *Clin. Chem.* **2000,** *46* (4), 537-542.

14. Lanznaster, D.; Dal-Cim, T.; Piermartiri, T. C.; Tasca, C. I., Guanosine: a neuromodulator with therapeutic potential in brain disorders. *Aging Dis.* **2016,** *7* (5), 657.

15. Dal-Cim, T.; Martins, W. C.; Thomaz, D. T.; Coelho, V.; Poluceno, G. G.; Lanznaster, D.; Vandresen-Filho, S.; Tasca, C. I., Neuroprotection promoted by guanosine depends on glutamine synthetase and glutamate transporters activity in hippocampal slices subjected to oxygen/glucose deprivation. *Neurotox. Res.* **2016,** *29* (4), 460-468.

16. Bettio, L. E.; Gil-Mohapel, J.; Rodrigues, A. L. S., Guanosine and its role in neuropathologies. *Purinergic Signal.* **2016,** *12* (3), 411-426.

17. Zhang, Y.; Dai, Y.; Wen, J.; Zhang, W.; Grenz, A.; Sun, H.; Tao, L.; Lu, G.; Alexander, D. C.; Milburn, M. V., Detrimental effects of adenosine signaling in sickle cell disease. *Nat. Med. (N. Y., NY, U. S.)* **2011,** *17* (1), 79-86.

18. Kawahara, Y.; Zinshteyn, B.; Sethupathy, P.; Iizasa, H.; Hatzigeorgiou, A. G.; Nishikura, K., Redirection of silencing targets by adenosine-to-inosine editing of miRNAs. *Science* **2007,** *315* (5815), 1137-1140.

19. Choudhary, R. K.; Capuco, A. V., In vitro expansion of the mammary stem/progenitor cell population by xanthosine treatment. *BMC Cell Biol.* **2012,** *13* (1), 1-8.

20. Willner, I.; Zayats, M., Electronic aptamer-based sensors. *Angew. Chem. Int. Ed.* **2007,** *46* (34), 6408-6418.

21. Liu, J.; Lu, Y., Preparation of aptamer-linked gold nanoparticle purple aggregates for colorimetric sensing of analytes. *Nat. Protoc.* **2006,** *1* (1), 246-252.

22. Li, Y.; Liu, J., Aptamer-based strategies for recognizing adenine, adenosine, ATP and related compounds. *Analyst* **2020,** *145* (21), 6753-6768.

23. Jhaveri, S. D.; Kirby, R.; Conrad, R.; Maglott, E. J.; Bowser, M.; Kennedy, R. T.; Glick, G.; Ellington, A. D., Designed signaling aptamers that transduce molecular recognition to changes in fluorescence intensity. *J. Am. Chem. Soc.* **2000,** *122* (11), 2469-2473.

24. Wachowius, F.; Höbartner, C., Probing essential nucleobase functional groups in aptamers and deoxyribozymes by nucleotide analogue interference mapping of DNA. *J. Am. Chem. Soc.* **2011,** *133* (38), 14888-14891.

25. Debiais, M.; Lelievre, A.; Smietana, M.; Müller, S., Splitting aptamers and nucleic acid enzymes for the development of advanced biosensors. *Nucleic Acids Res.* **2020,** *48* (7), 3400-3422.

26. Stojanovic, M. N.; de Prada, P.; Landry, D. W., Fluorescent sensors based on aptamer self-assembly. *J. Am. Chem. Soc.* **2000,** *122* (46), 11547-11548.

27. Nutiu, R.; Li, Y., Structure-switching signaling aptamers. *J. Am. Chem. Soc.* **2003,** *125* (16), 4771-4778.

28. Lopez, A.; Liu, J., Covalent and noncovalent functionalization of graphene oxide with DNA for smart sensing. *Adv. Intel. Sys.* **2020**, DOI:10.1002/aisy.202000123.

29. Zhang, F.; Wang, S.; Liu, J., Gold nanoparticles adsorb DNA and aptamer probes too strongly and a comparison with graphene Oxide for biosensing. *Anal. Chem.* **2019,** *91* (22), 14743-14750.

30. Wang, Y.; Li, Z.; Hu, D.; Lin, C.-T.; Li, J.; Lin, Y., Aptamer/graphene oxide nanocomplex for in situ molecular rrobing in living cells. *J. Am. Chem. Soc.* **2010,** *132* (27), 9274-9276.

31. Ma, Y.; Geng, F.; Wang, Y.; Xu, M.; Shao, C.; Qu, P.; Zhang, Y.; Ye, B., Novel strategy to improve the sensing performances of split ATP aptamer based fluorescent indicator displacement assay through enhanced molecular recognition. *Biosens. Bioelectron.* **2019,** *134*, 36-41.

32. Helwa, Y.; Dave, N.; Froidevaux, R.; Samadi, A.; Liu, J., Aptamer-functionalized hydrogel microparticles for fast visual detection of mercury (II) and adenosine. *ACS Appl. Mater. Interfaces* **2012,** *4* (4), 2228-2233.

33. Liu, J.; Lu, Y., Fast colorimetric sensing of adenosine and cocaine based on a general sensor design involving aptamers and nanoparticles. *Angew. Chem.* **2006,** *118* (1), 96-100.

34. Liu, B.; Liu, J., Interface-driven hybrid materials based on DNA-functionalized gold nanoparticles. *Matter* **2019,** *1* (4), 825-847.

35. Koo, K. M.; Sina, A. A.; Carrascosa, L. G.; Shiddiky, M. J.; Trau, M., DNA–bare gold affinity interactions: mechanism and applications in biosensing. *Anal. Methods* **2015,** *7* (17), 7042-7054.

36. Elbaz, J.; Moshe, M.; Shlyahovsky, B.; Willner, I., Cooperative multicomponent self-assembly of nucleic acid structures for the activation of DNAzyme cascades: a paradigm for DNA sensors and aptasensors. *Chem. Eur. J.* **2009,** *15* (14), 3411-3418.

37. Zhu, Z.; Wu, C.; Liu, H.; Zou, Y.; Zhang, X.; Kang, H.; Yang, C. J.; Tan, W., An aptamer cross-linked hydrogel as a colorimetric platform for visual detection. *Angew. Chem., Int. Ed.* **2010,** *49* (6), 1052-1056.

38. Liu, H.; Xiang, Y.; Lu, Y.; Crooks, R. M., Aptamer-based origami paper analytical device for electrochemical detection of adenosine. *Angew. Chem.* **2012,** *124* (28), 7031-7034.

39. Zhang, D.; Ma, J.; Meng, X.; Xu, Z.; Zhang, J.; Fang, Y.; Guo, Y., Electrochemical aptamer-based microsensor for real-time monitoring of adenosine in vivo. *Anal. Chim. Acta* **2019,** *1076*, 55-63.

40. Deng, C.; Chen, J.; Nie, L.; Nie, Z.; Yao, S., Sensitive bifunctional aptamer-based electrochemical biosensor for small molecules and protein. *Anal. Chem.* **2009,** *81* (24), 9972-9978.

41. Coria-Oriundo, L. L.; Ceretti, H.; Roupioz, Y.; Battaglini, F., Redox polyelectrolyte modified gold nanoparticles enhance the detection of adenosine in an electrochemical split-aptamer assay. *ChemistrySelect* **2020,** *5* (36), 11391-11398.

42. Li, X. m.; Zheng, K. w.; Hao, Y. h.; Tan, Z., Exceptionally selective and tunable sensing of guanine derivatives and analogues by structural complementation in a G-quadruplex. *Angew. Chem., Int. Ed.* **2016,** *128* (44), 13963-13968.

43. Wang, K.-B.; Dickerhoff, J.; Wu, G.; Yang, D., PDGFR-β promoter forms a vacancy G-Quadruplex that can be filled in by dGMP: Solution structure and molecular recognition of guanine metabolites and drugs. *J. Am. Chem. Soc.* **2020,** *142* (11), 5204-5211.

44. Li, Y.; Liu, J., Highly specific recognition of guanosine using engineered base-excised aptamers. *Chem. Eur. J.* **2020,** *26* (60), 13644-13651.

45. Liu, J., Oligonucleotide-functionalized hydrogels as stimuli responsive materials and biosensors. *Soft Matter* **2011,** *7* (15), 6757-6767.

46. Li, F.; Tang, J.; Geng, J.; Luo, D.; Yang, D., Polymeric DNA hydrogel: Design, synthesis and applications. *Prog. Polym. Sci.* **2019,** *98*, 101163.

47. Guan, Y.; Zhang, Y., PNIPAM microgels for biomedical applications: from dispersed particles to 3D assemblies. *Soft Matter* **2011,** *7* (14), 6375-6384.

48. Belali, S.; Savoie, H.; O'Brien, J. M.; Cafolla, A. A.; O'Connell, B.; Karimi, A. R.; Boyle, R. W.; Senge, M. O., Synthesis and characterization of temperature-sensitive and chemically cross-linked poly (N-isopropylacrylamide)/photosensitizer hydrogels for applications in photodynamic therapy. *Biomacromolecules* **2018,** *19* (5), 1592-1601.

49. Gao, W.; Gu, S.; Zhou, J.; Li, Y.; Zhao, Y.; Meng, J.; Zhang, W., Facile synthesis of poly N-isopropylacrylamide/acrylamide-quantum dots hybrid hydrogels and their fluorescence temperature sensitive behaviors. *Soft Mater.* **2020,** *18* (1), 101-110.

50. Kim, H.; Witt, H.; Oswald, T. A.; Tarantola, M., Adhesion of epithelial cells to PNIPAm treated surfaces for temperature-controlled cell-sheet harvesting. *ACS Appl. Mater. Interfaces* **2020,** *12* (30), 33516-33529.

51. Hu, H.; Wang, H.; Du, Q., Preparation of pH-sensitive polyacrylic acid hollow microspheres and their release properties. *Soft Matter* **2012,** *8* (25), 6816-6822.

52. Peppas, N. A.; Hilt, J. Z.; Khademhosseini, A.; Langer, R., Hydrogels in biology and medicine: from molecular principles to bionanotechnology. *Adv. Mater.* **2006,** *18* (11), 1345-1360.

53. Hendrickson, G. R.; Smith, M. H.; South, A. B.; Lyon, L. A., Design of multiresponsive hydrogel particles and assemblies. *Adv. Funct. Mater.* **2010,** *20* (11), 1697-1712.

54. Gačanin, J.; Synatschke, C. V.; Weil, T., Biomedical applications of DNA-based hydrogels. *Adv. Funct. Mater.* **2020,** *30* (4), 1906253.

55. Yang, H.; Liu, H.; Kang, H.; Tan, W., Engineering target-responsive hydrogels based on aptamer− target interactions. *J. Am. Chem. Soc.* **2008,** *130* (20), 6320-6321.

56. Shahbazi, M. A.; Bauleth-Ramos, T.; Santos, H. A., DNA hydrogel assemblies: bridging synthesis principles to biomedical applications. *Adv. Ther.* **2018,** *1* (4), 1800042.

57. Kahn, J. S.; Hu, Y.; Willner, I., Stimuli-responsive DNA-based hydrogels: From basic principles to applications. *Acc. Chem. Res.* **2017,** *50* (4), 680-690.

58. Ren, J.; Hu, Y.; Lu, C.-H.; Guo, W.; Aleman-Garcia, M. A.; Ricci, F.; Willner, I., pH-responsive and switchable triplex-based DNA hydrogels. *Chem. Sci.* **2015,** *6* (7), 4190-4195.

59. Yang, H.; Liu, H.; Kang, H.; Tan, W., Engineering target-responsive hydrogels based on aptamer− target interactions. *J. Am. Chem. Soc.* **2008,** *130* (20), 6320-6321.

60. Ren, J.; Hu, Y.; Lu, C.-H.; Guo, W.; Aleman-Garcia, M. A.; Ricci, F.; Willner, I., pH-responsive and switchable triplex-based DNA hydrogels. *Chem. Sci.* **2015,** *6* (7), 4190-4195.

61. Wackerlig, J.; Schirhagl, R., Applications of molecularly imprinted polymer nanoparticles and their advances toward industrial use: a review. *Anal. Chem.* **2016,** *88* (1), 250-261.

62. Byrne, M. E.; Park, K.; Peppas, N. A., Molecular imprinting within hydrogels. *Adv. Drug Delivery Rev.* **2002,** *54* (1), 149-161.

63. Zhang, Z.; Liu, J., Molecular imprinting with functional DNA. *Small* **2019,** *15* (26), 1805246.

64. Bai, W.; Gariano, N. A.; Spivak, D. A., Macromolecular amplification of binding response in superaptamer hydrogels. *J. Am. Chem. Soc.* **2013,** *135* (18), 6977-6984.

65. Shiang, Y. C.; Huang, C. C.; Wang, T. H.; Chien, C. W.; Chang, H. T., Aptamer-conjugated nanoparticles efficiently control the activity of thrombin. *Adv. Funct. Mater.* **2010,** *20* (18), 3175-3182.

66. Zhang, Z.; Liu, B.; Liu, J., Molecular imprinting for substrate selectivity and enhanced activity of enzyme mimics. *Small* **2017,** *13* (7), 1602730.

67. Mo, F.; Jiang, K.; Zhao, D.; Wang, Y.; Song, J.; Tan, W., DNA hydrogel-based gene editing and drug delivery systems. *Adv. Drug Deliv. Rev.* **2021,** *168*, 79-98.

68. Li, F.; Lyu, D.; Liu, S.; Guo, W., DNA hydrogels and microgels for biosensing and biomedical applications. *Adv. Mater.* **2020,** *32* (3), 1806538.

69. Kawai, R.; Tanaka, H.; Matsubara, S.; Ida, S.; Uchida, M.; Okumura, D., Implicit rule on the elastic function of a swollen polyacrylamide hydrogel. *Soft Matter* **2021,** *17* (19), 4979-4988.

70. Dave, N.; Chan, M. Y.; Huang, P.-J. J.; Smith, B. D.; Liu, J., Regenerable DNA-functionalized hydrogels for ultrasensitive, instrument-free mercury (II) detection and removal in water. *J. Am. Chem. Soc.* **2010,** *132* (36), 12668-12673.

71. Li, J.; Mo, L.; Lu, C.-H.; Fu, T.; Yang, H.-H.; Tan, W., Functional nucleic acid-based hydrogels for bioanalytical and biomedical applications. *Chem. Soc. Rev.* **2016,** *45* (5), 1410-1431.

72. Dunn, S. S.; Tian, S.; Blake, S.; Wang, J.; Galloway, A. L.; Murphy, A.; Pohlhaus, P. D.; Rolland, J. P.; Napier, M. E.; DeSimone, J. M., Reductively

responsive siRNA-conjugated hydrogel nanoparticles for gene silencing. *J. Am. Chem. Soc.* **2012,** *134* (17), 7423-7430.

73. Li, F.; Yu, W.; Zhang, J.; Dong, Y.; Ding, X.; Ruan, X.; Gu, Z.; Yang, D., Spatiotemporally programmable cascade hybridization of hairpin DNA in polymeric nanoframework for precise siRNA delivery. *Nat. Commun.* **2021,** *12* (1), 1-12.

74. Nishikawa, M.; Mizuno, Y.; Mohri, K.; Matsuoka, N.; Rattanakiat, S.; Takahashi, Y.; Funabashi, H.; Luo, D.; Takakura, Y., Biodegradable CpG DNA hydrogels for sustained delivery of doxorubicin and immunostimulatory signals in tumor-bearing mice. *Biomaterials* **2011,** *32* (2), 488-494.

75. Biniuri, Y.; Luo, G.-F.; Fadeev, M.; Wulf, V.; Willner, I., Redox-switchable binding properties of the ATP–aptamer. *J. Am. Chem. Soc.* **2019,** *141* (39), 15567-15576.

76. Sassanfar, M.; Szostak, J. W., An RNA motif that binds ATP. *Nature* **1993,** *364* (6437), 550-553.

77. Biniuri, Y.; Luo, G. F.; Fadeev, M.; Wulf, V.; Willner, I., Redox-switchable binding properties of the ATP-aptamer. *J. Am. Chem. Soc.* **2019**, *141* (39), 15567-15576.

78. Batey, R. T.; Gilbert, S. D.; Montange, R. K., Structure of a natural guanine-responsive riboswitch complexed with the metabolite hypoxanthine. *Nature* **2004,** *432* (7015), 411-415.

79. Ellington, A. D., RNA selection: aptamers achieve the desired recognition. *Curr. Biol.* **1994,** *4* (5), 427-429.

80. Torabi, S.-F.; Wu, P.; McGhee, C. E.; Chen, L.; Hwang, K.; Zheng, N.; Cheng, J.; Lu, Y., In vitro selection of a sodium-specific DNAzyme and its application in intracellular sensing. *Proc. Natl. Acad. Sci. U. S. A.* **2015,** *112* (19), 5903-5908.

81. Ma, L.; Kartik, S.; Liu, B.; Liu, J., From general base to general acid catalysis in a sodium-specific DNAzyme by a guanine-to-adenine mutation. *Nucleic Acids Res.* **2019,** *47* (15), 8154-8162.

82. Butz, K.; Denk, C.; Ullmann, A.; Scheffner, M.; Hoppe-Seyler, F., Induction of apoptosis in human papillomaviruspositive cancer cells by peptide aptamers targeting the viral E6 oncoprotein. *Proc. Natl. Acad. Sci. U. S. A.* **2000,** *97* (12), 6693-6697.

83. Russo Krauss, I.; Merlino, A.; Giancola, C.; Randazzo, A.; Mazzarella, L.; Sica, F., Thrombin–aptamer recognition: a revealed ambiguity. *Nucleic Acids Res.* **2011,** *39* (17), 7858-7867.

84. Wu, X.; Liu, H.; Han, D.; Peng, B.; Zhang, H.; Zhang, L.; Li, J.; Liu, J.; Cui, C.; Fang, S., Elucidation and structural modeling of CD71 as a molecular target for cell-specific aptamer binding. *J. Am. Chem. Soc.* **2019,** *141* (27), 10760-10769.

85. Iliuk, A. B.; Hu, L.; Tao, W. A., Aptamer in bioanalytical applications. *Anal. Chem.* **2011,** *83* (12), 4440-4452.

86. Zhou, W.; Huang, P. J.; Ding, J.; Liu, J., Aptamer-based biosensors for biomedical diagnostics. *The Analyst* **2014,** *139* (11), 2627-2640.

87. Song, Y.; Shi, Y.; Huang, M.; Wang, W.; Wang, Y.; Cheng, J.; Lei, Z.; Zhu, Z.; Yang, C., Bioinspired engineering of a multivalent aptamer-functionalized nanointerface to enhance the capture and release of circulating tumor cells. *Angew. Chem.* **2019,** *131* (8), 2258-2262.

88. Pang, X.; Cui, C.; Wan, S.; Jiang, Y.; Zhang, L.; Xia, L.; Li, L.; Li, X.; Tan, W., Bioapplications of cell-SELEX-generated aptamers in cancer diagnostics, therapeutics, theranostics and biomarker discovery: a comprehensive review. *Cancers* **2018,** *10* (2), 47.

89. Lin, C. H.; Patei, D. J., Structural basis of DNA folding and recognition in an AMP-DNA aptamer complex: distinct architectures but common recognition motifs for DNA and RNA aptamers complexed to AMP. *Chem. Biol.* **1997,** *4* (11), 817-832.

90. Nutiu, R.; Li, Y., In vitro selection of structure-switching signaling aptamers. *Angew. Chem., Int. Ed.* **2005,** *44* (7), 1061-1065.

91. Biniuri, Y.; Albada, B.; Willner, I., Probing ATP/ATP-aptamer or ATP-aptamer mutant complexes by microscale thermophoresis and molecular dynamics simulations: discovery of an ATP-aptamer sequence of superior binding properties. *J. Phys. Chem. B* **2018,** *122* (39), 9102-9109.

92. Zhang, Z.; Oni, O.; Liu, J., New insights into a classic aptamer: binding sites, cooperativity and more sensitive adenosine detection. *Nucleic Acids Res.* **2017,** *45* (13), 7593-7601.

93. Mosqueda-Garcia, R., Adenosine as a therapeutic agent. *Clin. Invest. Med.* **1992,** *15* (5), 445-455.

94. Rankin, A. C.; Brooks, R.; Ruskin, J. N.; McGovern, B. A., Adenosine and the treatment of supraventricular tachycardia. *Am. J. Med.* **1992,** *92* (6), 655-664.

95. Koizumi, M.; Breaker, R. R., Molecular recognition of cAMP by an RNA aptamer. *Biochemistry* **2000,** *39* (30), 8983-8992.

96. Özalp, V. C.; Pedersen, T. R.; Nielsen, L. J.; Olsen, L. F., Time-resolved measurements of intracellular ATP in the yeast saccharomyces cerevisiae using a new type of nanobiosensor. *J. Biol. Chem.* **2010,** *285* (48), 37579-37588.

97. Jhaveri, S.; Rajendran, M.; Ellington, A. D., In vitro selection of signaling aptamers. *Nat. Biotechnol.* **2000,** *18* (12), 1293-1297.

98. Qu, H.; Wang, L.; Liu, J.; Zheng, L., Direct screening for cytometric bead assays for adenosine triphosphate. *ACS Sens.* **2018,** *3* (10), 2071-2078.

99. Jiang, Y.; Pan, X.; Chang, J.; Niu, W.; Hou, W.; Kuai, H.; Zhao, Z.; Liu, J.; Wang, M.; Tan, W., Supramolecularly engineered circular bivalent aptamer for enhanced functional protein delivery. *J. Am. Chem. Soc.* **2018,** *140* (22), 6780-6784.

100. Zhang, J.; Lan, T.; Lu, Y., Molecular engineering of functional nucleic acid nanomaterials toward in vivo applications. *Adv. Healthcare Mater.* **2019,** *8* (6), 1801158.

101. Liu, B.; Liu, J., Freezing directed construction of bio/nano interfaces: reagentless conjugation, denser spherical nucleic acids, and better nanoflares. *J. Am. Chem. Soc.* **2017,** *139* (28), 9471-9474.

102. Xu, Z.; Morita, K.; Sato, Y.; Dai, Q.; Nishizawa, S.; Teramae, N., Label-free aptamer-based sensor using abasic site-containing DNA and a nucleobase-specific fluorescent ligand. *Chem. Commun.* **2009,** (42), 6445-6447.

103. Xu, Z.; Sato, Y.; Nishizawa, S.; Teramae, N., Signal-off and signal-on design for a label-free aptasensor based on target-induced self-assembly and abasic-site-binding ligands. *Chem. Eur. J.* **2009,** *15* (40), 10375-10378.

104. Li, X. m.; Zheng, K. w.; Hao, Y. h.; Tan, Z., Exceptionally selective and tunable sensing of guanine derivatives and analogues by structural complementation in a G-quadruplex. *Angew. Chem.* **2016,** *128* (44), 13963-13968.

105. Zhang, J.; Wang, L. L.; Hou, M. F.; Luo, L. P.; Liao, Y. J.; Xia, Y. K.; Yan, A.; Weng, Y. P.; Zeng, L. P.; Chen, J. H., Label-free fluorescent and electrochemical biosensors based on defective G-quadruplexes. *Biosens. Bioelectron.* **2018,** *118*, 1-8.

106. Sato, Y.; Nishizawa, S.; Yoshimoto, K.; Seino, T.; Ichihashi, T.; Morita, K.; Teramae, N., Influence of substituent modifications on the binding of 2-amino-1, 8-naphthyridines to cytosine opposite an AP site in DNA duplexes: thermodynamic characterization. *Nucleic Acids Res.* **2009,** *37* (5), 1411-1422.

107. Yoshimoto, K.; Nishizawa, S.; Minagawa, M.; Teramae, N., Use of abasic site-containing DNA strands for nucleobase recognition in water. *J. Am. Chem. Soc.* **2003,** *125* (30), 8982-8983.

108. Li, M.; Sato, Y.; Nishizawa, S.; Seino, T.; Nakamura, K.; Teramae, N., 2-Aminopurine-modified abasic-site-containing duplex DNA for highly selective detection of theophylline. *J. Am. Chem. Soc.* **2009,** *131* (7), 2448-2449.

109. Sharma, A. K.; Heemstra, J. M., Small-molecule-dependent split aptamer ligation. *J. Am. Chem. Soc.* **2011,** *133* (32), 12426-12429.

110. Yu, H.; Canoura, J.; Guntupalli, B.; Lou, X.; Xiao, Y., A cooperative-binding split aptamer assay for rapid, specific and ultra-sensitive fluorescence detection of cocaine in saliva. *Chem. Sci.* **2017,** *8* (1), 131-141.

111. Zhang, Z.; Liu, J., Molecularly imprinted polymers with DNA aptamer fragments as macromonomers. *ACS Appl. Mater. Interfaces* **2016,** *8* (10), 6371-6378.

112. Wang, Z.; Yu, H.; Canoura, J.; Liu, Y.; Alkhamis, O.; Fu, F.; Xiao, Y., Introducing structure-switching functionality into small-molecule-binding aptamers via nuclease-directed truncation. *Nucleic Acids Res.* **2018,** *46* (13), e81.

113. Canoura, J.; Wang, Z.; Yu, H.; Alkhamis, O.; Fu, F.; Xiao, Y., No Structure-Switching Required: A generalizable exonuclease-mediated aptamer-based assay for small-molecule detection. *J. Am. Chem. Soc.* **2018,** *140* (31), 9961-9971.

114. Wei, Y.; Chen, Y.; Li, H.; Shuang, S.; Dong, C.; Wang, G., An exonuclease I-based label-free fluorometric aptasensor for adenosine triphosphate (ATP) detection with a wide concentration range. *Biosens. Bioelectron.* **2015,** *63*, 311-316.

115. Kong, L.; Xu, J.; Xu, Y.; Xiang, Y.; Yuan, R.; Chai, Y., A universal and label-free aptasensor for fluorescent detection of ATP and thrombin based on SYBR Green I dye. *Biosens. Bioelectron.* **2013,** *42*, 193-197.

116. Xu, Y.; Xu, J.; Xiang, Y.; Yuan, R.; Chai, Y., Target-induced structure switching of hairpin aptamers for label-free and sensitive fluorescent detection of ATP via exonuclease-catalyzed target recycling amplification. *Biosens. Bioelectron.* **2014,** *51*, 293-296.

117. Zheng, D.; Seferos, D. S.; Giljohann, D. A.; Patel, P. C.; Mirkin, C. A., Aptamer nano-flares for molecular detection in living cells. *Nano Lett.* **2009,** *9* (9), 3258-3261.

118. Fong, L. K.; Wang, Z.; Schatz, G. C.; Luijten, E.; Mirkin, C. A., The role of structural enthalpy in spherical nucleic acid hybridization. *J. Am. Chem. Soc.* **2018,** *140* (20), 6226-6230.

119. Gunasekara, R. W.; Zhao, Y., A general method for selective recognition of monosaccharides and oligosaccharides in water. *J. Am. Chem. Soc.* **2017,** *139* (2), 829-835.

120. Walter, S. M.; Kniep, F.; Rout, L.; Schmidtchen, F. P.; Herdtweck, E.; Huber, S. M., Isothermal calorimetric titrations on charge-assisted halogen bonds: role of entropy, counterions, solvent, and temperature. *J. Am. Chem. Soc.* **2012,** *134* (20), 8507-8512.

121. Zuker, M., Mfold web server for nucleic acid folding and hybridization prediction. *Nucleic Acids Res.* **2003,** *31* (13), 3406-3415.

122. Traut, T. W., Physiological concentrations of purines and pyrimidines. *Mol. Cell. Biochem.* **1994,** *140* (1), 1-22.

123. Goyal, R. N.; Gupta, V. K.; Oyama, M.; Bachheti, N., Voltammetric determination of adenosine and guanosine using fullerene-C(60)-modified glassy carbon electrode. *Talanta* **2007,** *71* (3), 1110-1117.

124. Becker, S.; Thoma, I.; Deutsch, A.; Gehrke, T.; Mayer, P.; Zipse, H.; Carell, T., A high-yielding, strictly regioselective prebiotic purine nucleoside formation pathway. *Science* **2016,** *352* (6287), 833-836.

125. dos Santos Frizzo, M. E.; Lara, D. R.; de Souza Prokopiuk, A.; Vargas, C. R.; Salbego, C. G.; Wajner, M.; Souza, D. O., Guanosine enhances glutamate uptake in brain cortical slices at normal and excitotoxic conditions. *Cell. Mol. Neurobiol.* **2002,** *22* (3), 353-363.

126. Haskó, G.; Cronstein, B. N., Adenosine: an endogenous regulator of innate immunity. *Trends Immunol.* **2004,** *25* (1), 33-39.

127. Aird, K. M.; Zhang, R., Nucleotide metabolism, oncogene-induced senescence and cancer. *Cancer Lett.* **2015,** *356* (2), 204-210.

128. Nyhan, W. L., Disorders of purine and pyrimidine metabolism. *Mol. Genet. Metab.* **2005,** *86* (1-2), 25-33.

129. Tian, F.; Bibi, F.; Dale, N.; Imray, C. H., Blood purine measurements as a rapid real-time indicator of reversible brain ischaemia. *Purinergic Signal.* **2017,** *13* (4), 521-528.

130. Sebesta, I.; Stiburkova, B.; Krijt, J., Hereditary xanthinuria is not so rare disorder of purine metabolism. *Nucleos. Nucleot. Nucl.* **2018,** *37* (6), 324-328.

131. Brody, E. N.; Gold, L., Aptamers as therapeutic and diagnostic agents. *Mol. Biotechnol.* **2000,** *74* (1), 5-13.

132. Park, K. S., Nucleic acid aptamer-based methods for diagnosis of infections. *Biosens. Bioelectron.* **2018,** *102*, 179-188.

133. Meng, H.-M.; Fu, T.; Zhang, X.-B.; Tan, W., Cell-SELEX-based aptamer-conjugated nanomaterials for cancer diagnosis and therapy. *Natl. Sci. Rev.* **2015,** *2* (1), 71-84.

134. Alkhamis, O.; Canoura, J.; Yu, H.; Liu, Y.; Xiao, Y., Innovative engineering and sensing strategies for aptamer-based small-molecule detection. *Trends Analyt. Chem.* **2019**, 115699.

135. Ruscito, A.; DeRosa, M. C., Small-molecule binding aptamers: selection strategies, characterization, and applications. *Front. Chem.* **2016,** *4*, 14.

136. Noeske, J.; Richter, C.; Grundl, M. A.; Nasiri, H. R.; Schwalbe, H.; Wohnert, J., An intermolecular base triple as the basis of ligand specificity and affinity in the guanine- and adenine-sensing riboswitch RNAs. *Proc. Natl. Acad. Sci. U. S. A.* **2005,** *102* (5), 1372-1377.

137. Mandal, M.; Breaker, R. R., Adenine riboswitches and gene activation by disruption of a transcription terminator. *Nat. Struct. Mol. Biol.* **2004,** *11* (1), 29-35.

138. Kim, Y.-B.; Wacker, A.; Laer, K. v.; Rogov, V. V.; Suess, B.; Schwalbe, H., Ligand binding to 2′-deoxyguanosine sensing riboswitch in metabolic context. *Nucleic Acids Res.* **2017,** *45* (9), 5375-5386.

139. Fowler, C. C.; Sugiman-Marangos, S.; Junop, M. S.; Brown, E. D.; Li, Y., Exploring intermolecular interactions of a substrate binding protein using a riboswitch-based sensor. *Chem. Biol.* **2013,** *20* (12), 1502-1512.

140. Kellenberger, C. A.; Wilson, S. C.; Hickey, S. F.; Gonzalez, T. L.; Su, Y.; Hallberg, Z. F.; Brewer, T. F.; Iavarone, A. T.; Carlson, H. K.; Hsieh, Y.-F., GEMM-I riboswitches from geobacter sense the bacterial second messenger cyclic AMP-GMP. *Proc. Natl. Acad. Sci. U. S. A.* **2015,** *112* (17), 5383-5388.

141. Xiu, Y.; Jang, S.; Jones, J. A.; Zill, N. A.; Linhardt, R. J.; Yuan, Q.; Jung, G. Y.; Koffas, M. A. G., Naringenin-responsive riboswitch-based fluorescent biosensor module for escherichia coli co-cultures. *Biotechnol. Bioeng.* **2017,** *114* (10), 2235-2244.

142. Findeiß, S.; Etzel, M.; Will, S.; Mörl, M.; Stadler, P. F., Design of artificial riboswitches as biosensors. *Sensors* **2017,** *17* (9), 1990.

143. Lato, S. M.; Ozerova, N. D.; He, K.; Sergueeva, Z.; Shaw, B. R.; Burke, D. H., Boron-containing aptamers to ATP. *Nucleic Acids Res.* **2002,** *30* (6), 1401-1407.

144. Sharma, S.; Zajac, M.; Krishnan, Y., A DNA aptamer for cyclic adenosine monophosphate that shows adaptive recognition. *ChemBioChem.* **2020,** *21* (1-2), 157-162.

145. Kiga, D.; Futamura, Y.; Sakamoto, K.; Yokoyama, S., An RNA aptamer to the xanthine/guanine base with a distinctive mode of purine recognition. *Nucleic Acids Res.* **1998,** *26* (7), 1755-1760.

146. Davis, J. H.; Szostak, J. W., Isolation of high-affinity GTP aptamers from partially structured RNA libraries. *Proc. Natl. Acad. Sci. U. S. A.* **2002,** *99* (18), 11616-11621.

147. Carothers, J. M.; Oestreich, S. C.; Szostak, J. W., Aptamers selected for higher-affinity binding are not more specific for the target ligand. *J. Am. Chem. Soc.* **2006,** *128* (24), 7929-7937.

148. Mei, H.; Liao, J.-Y.; Jimenez, R. M.; Wang, Y.; Bala, S.; McCloskey, C.; Switzer, C.; Chaput, J. C., Synthesis and evolution of a threose nucleic acid aptamer bearing 7-Deaza-7-substituted guanosine residues. *J. Am. Chem. Soc.* **2018,** *140* (17), 5706-5713.

149. Connell, G.; Yarus, M., RNAs with dual specificity and dual RNAs with similar specificity. *Science* **1994,** *264* (5162), 1137-1141.

150. Sankaran, N. B.; Nishizawa, S.; Seino, T.; Yoshimoto, K.; Teramae, N., Abasic-site-containing oligodeoxynucleotides as aptamers for riboflavin. *Angew. Chem., Int. Ed.* **2006,** *118* (10), 1593-1598.

151. Zhou, W.; Ding, J.; Liu, J., A highly specific sodium aptamer probed by 2-aminopurine for robust Na^+ sensing. *Nucleic Acids Res.* **2016,** *44* (21), 10377-10385.

152. He, Y.; Chen, D.; Huang, P. J.; Zhou, Y.; Ma, L.; Xu, K.; Yang, R.; Liu, J., Misfolding of a DNAzyme for ultrahigh sodium selectivity over potassium. *Nucleic Acids Res.* **2018,** *46* (19), 10262-10271.

153. Zhou, W.; Zhang, Y.; Huang, P. J.; Ding, J.; Liu, J., A DNAzyme Requiring two different metal ions at two distinct sites. *Nucleic Acids Res.* **2016,** *44* (1), 354-363.

154. Zhou, W.; Saran, R.; Ding, J.; Liu, J., Two completely different mechanisms for highly specific Na^+ recognition by DNAzymes. *ChemBioChem.* **2017,** *18* (18), 1828-1835.

155. Mohanty, J.; Barooah, N.; Dhamodharan, V.; Harikrishna, S.; Pradeepkumar, P. I.; Bhasikuttan, A. C., Thioflavin T as an efficient inducer and selective fluorescent sensor for the human telomeric G-quadruplex DNA. *J. Am. Chem. Soc.* **2013,** *135* (1), 367-376.

156. Renaud de la Faverie, A.; Guedin, A.; Bedrat, A.; Yatsunyk, L. A.; Mergny, J. L., Thioflavin T as a fluorescence light-up probe for G4 formation. *Nucleic Acids Res.* **2014,** *42* (8), e65.

157. Khusbu, F. Y.; Zhou, X.; Chen, H.; Ma, C.; Wang, K., Thioflavin T as a fluorescence probe for biosensing applications. *Trends Analyt. Chem.* **2018,** *109*, 1-18.

158. Liu, B.; Kelly, E. Y.; Liu, J., Cation-size-dependent DNA adsorption kinetics and packing density on gold nanoparticles: an opposite trend. *Langmuir* **2014,** *30* (44), 13228-13234.

159. Vazin, M.; Huang, P. J.; Matuszek, Z.; Liu, J., Biochemical characterization of a lanthanide-dependent DNAzyme with normal and phosphorothioate-modified substrates. *Biochemistry* **2015,** *54* (39), 6132-6138.

160. Souliere, M. F.; Haller, A.; Rieder, R.; Micura, R., A powerful approach for the selection of 2-aminopurine substitution sites to investigate RNA folding. *J. Am. Chem. Soc.* **2011,** *133* (40), 16161-16167.

161. Li, Y.; Zhang, Z.; Liu, B.; Liu, J., Incorporation of boronic acid into aptamer-based molecularly imprinted hydrogels for highly specific recognition of adenosine. *ACS Appl. Bio Mater.* **2019,** *3* (5), 2568-2576.

162. Wang, K.-B.; Dickerhoff, J.; Wu, G.; Yang, D., PDGFR-β Promoter forms a vacancy G-quadruplex that can be filled in by dGMP: solution structure and molecular recognition of guanine metabolites and drugs. *J. Am. Chem. Soc.* **2020**, DOI: 10.1021/jacs.9b12770.

163. Hermann, T.; Patel, D. J., Adaptive recognition by nucleic Acid aptamers. *Science* **2000,** *287* (5454), 820-825.

164. Zhou, W.; Chen, Q.; Huang, P. J.; Ding, J.; Liu, J., DNAzyme hybridization, cleavage, degradation, and sensing in undiluted human blood serum. *Anal. Chem.* **2015,** *87* (7), 4001-4007.

165. Shi, H.; Jin, T.; Zhang, J.; Huang, X.; Tan, C.; Jiang, Y.; Tan, Y., A novel aptasensor strategy for protein detection based on G-quadruplex and exonuclease III-aided recycling amplification. *Chin. Chem. Lett.* **2020,** *31* (1), 155-158.

166. Arya, S. K.; Zhurauski, P.; Jolly, P.; Batistuti, M. R.; Mulato, M.; Estrela, P., Capacitive aptasensor based on interdigitated electrode for breast cancer detection in undiluted human serum. *Biosens. Bioelectron.* **2018,** *102*, 106-112.

167. Fang, X.; Tan, W., Aptamers generated from cell-SELEX for molecular medicine: a chemical biology approach. *Acc. Chem. Res.* **2010,** *43* (1), 48-57.

168. Hu, Q.; Li, H.; Wang, L.; Gu, H.; Fan, C., DNA nanotechnology-enabled drug delivery systems. *Chem. Rev.* **2019,** *119* (10), 6459-6506.

169. Mirts, E. N.; Bhagi-Damodaran, A.; Lu, Y., Understanding and modulating metalloenzymes with unnatural amino acids, non-native metal ions, and non-native metallocofactors. *Acc. Chem. Res.* **2019,** *52* (4), 935-944.

170. Zhou, W.; Saran, R.; Liu, J., Metal sensing by DNA. *Chem. Rev.* **2017,** *117* (12), 8272-8325.

171. Yang, Y.; Zhu, W.; Feng, L.; Chao, Y.; Yi, X.; Dong, Z.; Yang, K.; Tan, W.; Liu, Z.; Chen, M., G-quadruplex-based nanoscale coordination polymers to

modulate tumor hypoxia and achieve nuclear-targeted drug delivery for enhanced photodynamic therapy. *Nano Lett.* **2018,** *18* (11), 6867-6875.

172. Riechmann, L.; Clark, M.; Waldmann, H.; Winter, G., Reshaping human antibodies for therapy. *Nature* **1988,** *332* (6162), 323-327.

173. Rollenske, T.; Szijarto, V.; Lukasiewicz, J.; Guachalla, L. M.; Stojkovic, K.; Hartl, K.; Stulik, L.; Kocher, S.; Lasitschka, F.; Al-Saeedi, M.; Schroder-Braunstein, J.; von Frankenberg, M.; Gaebelein, G.; Hoffmann, P.; Klein, S.; Heeg, K.; Nagy, E.; Nagy, G.; Wardemann, H., Cross-specificity of protective human antibodies against klebsiella pneumoniae LPS O-antigen. *Nat. Immunol.* **2018,** *19* (6), 617-624.

174. Yang, Y.; Liu, J.; Sun, X.; Feng, L.; Zhu, W.; Liu, Z.; Chen, M., Near-infrared light-activated cancer cell targeting and drug delivery with aptamer-modified nanostructures. *Nano Res.* **2015,** *9* (1), 139-148.

175. Chen, L.; Wang, X.; Lu, W.; Wu, X.; Li, J., Molecular imprinting: perspectives and applications. *Chem. Soc. Rev.* **2016,** *45* (8), 2137-2211.

176. Baggiani, C.; Giovannoli, C.; Anfossi, L.; Passini, C.; Baravalle, P.; Giraudi, G., A connection between the binding properties of imprinted and nonimprinted polymers: a change of perspective in molecular imprinting. *J. Am. Chem. Soc.* **2012,** *134* (3), 1513-1518.

177. Haupt, K.; Mosbach, K., Molecularly imprinted polymers and their use in biomimetic sensors. *Chem. Rev.* **2000,** *100* (7), 2495-2504.

178. Andersson, L. I.; Müller, R.; Vlatakis, G.; Mosbach, K., Mimics of the binding sites of opioid receptors obtained by molecular imprinting of enkephalin and morphine. *Proc. Natl. Acad. Sci. U. S. A.* **1995,** *92* (11), 4788-4792.

179. Pan, J.; Chen, W.; Ma, Y.; Pan, G., Molecularly imprinted polymers as receptor mimics for selective cell recognition. *Chem. Soc. Rev.* **2018,** *47* (15), 5574-5587.

180. Dong, Y.; Li, W.; Gu, Z.; Xing, R.; Ma, Y.; Zhang, Q.; Liu, Z., Inhibition of HER2-positive breast cancer growth by blocking the HER2 signaling

pathway with HER2-glycan-imprinted nanoparticles. *Angew. Chem., Int. Ed.* **2019,** *58* (31), 10621-10625.

181. Shao, Y.; Jia, H.; Cao, T.; Liu, D., Supramolecular hydrogels based on DNA self-assembly. *Acc. Chem. Res.* **2017,** *50* (4), 659-668.

182. Lu, C.; Huang, Z.; Liu, B.; Liu, Y.; Ying, Y.; Liu, J., Poly-cytosine DNA as a high-affinity ligand for inorganic nanomaterials. *Angew. Chem., Int. Ed.* **2017,** *56* (22), 6208-6212.

183. Bai, W.; Spivak, D. A., A double-imprinted diffraction-grating sensor based on a virus-responsive super-aptamer hydrogel derived from an impure extract. *Angew. Chem., Int. Ed.* **2014,** *53* (8), 2095-2098.

184. Jolly, P.; Tamboli, V.; Harniman, R. L.; Estrela, P.; Allender, C. J.; Bowen, J. L., Aptamer–MIP hybrid receptor for highly sensitive electrochemical detection of prostate specific antigen. *Biosens. Bioelectron.* **2016,** *75*, 188-195.

185. Li, W.; Zhang, Q.; Wang, Y.; Ma, Y.; Guo, Z.; Liu, Z., Controllably prepared aptamer-molecularly imprinted polymer hybrid for high-specificity and high-affinity recognition of target proteins. *Anal. Chem.* **2019,** *91* (7), 4831-4837.

186. Zhang, Z.; Zhang, X.; Liu, B.; Liu, J., Molecular imprinting on inorganic nanozymes for hundred-fold enzyme specificity. *J. Am. Chem. Soc.* **2017,** *139* (15), 5412-5419.

187. Zhang, Z.; Liu, J., Intracellular Delivery of a Molecularly imprinted peroxidase mimicking DNAzyme for selective oxidation. *Mater. Horiz.* **2018,** *5* (4), 738-744.

188. Zhang, J.; Belardinelli, L.; Jacobson, K. A.; Otero, D. H.; Baker, S. P., Persistent activation by and receptor reserve for an irreversible A1-adenosine receptor agonist in DDT1 MF-2 cells and in guinea pig heart. *Mol. Pharmacol.* **1997,** *52* (3), 491-498.

189. Liu, Z.; He, H., Synthesis and applications of boronate affinity materials: from class selectivity to biomimetic specificity. *Acc. Chem. Res.* **2017,** *50* (9), 2185-2193.

190. Pan, G.; Guo, B.; Ma, Y.; Cui, W.; He, F.; Li, B.; Yang, H.; Shea, K. J., Dynamic introduction of cell adhesive factor via reversible multicovalent phenylboronic acid/cis-diol polymeric complexes. *J. Am. Chem. Soc.* **2014,** *136* (17), 6203-6206.

191. Liang, X.; Trentle, M.; Kozlovskaya, V.; Kharlampieva, E.; Bonizzoni, M., Carbohydrate sensing using water-soluble poly (methacrylic acid)-co-3-(acrylamido) phenylboronic acid copolymer. *ACS Appl. Polym. Mater.* **2019,** *1* (6), 1341-1349.

192. Gaballa, H.; Theato, P., Glucose-responsive polymeric micelles via boronic acid–diol complexation for insulin delivery at neutral pH. *Biomacromolecules* **2019,** *20* (2), 871-881.

193. Bie, Z.; Chen, Y.; Ye, J.; Wang, S.; Liu, Z., Boronate-affinity glycan-oriented surface imprinting: a new strategy to mimic lectins for the recognition of an intact glycoprotein and its characteristic fragments. *Angew. Chem., Int. Ed.* **2015,** *54* (35), 10211-20215.

194. Granot, E.; Tel-Vered, R.; Lioubashevski, O.; Willner, I., Stereoselective and enantioselective electrochemical sensing of monosaccharides using imprinted boronic acid-functionalized polyphenol films. *Adv. Funct. Mater.* **2008,** *18* (3), 478-484.

195. Chen, W.; Fu, M.; Zhu, X.; Liu, Q., A close-packed imprinted colloidal array for naked-eye detection of glycoproteins under physiological pH. *Biosens. Bioelectron.* **2019,** *142*, 111499.

196. Jiang, L.; Lu, R.; Ye, L., Towards detection of glycoproteins using molecularly imprinted nanoparticles and boronic acid-modified fluorescent probe. *Polymers* **2019,** *11* (1), 173.

197. Li, Y.; Zhang, Z.; Liu, B.; Liu, J., Adsorption of DNA oligonucleotides by boronic acid functionalized hydrogel nanoparticles. *Langmuir* **2019,** *35* (42), 13727-13734.

198. Ye, L.; Weiss, R.; Mosbach, K., Synthesis and characterization of molecularly imprinted microspheres. *Macromolecules* **2000,** *33* (22), 8239-8245.

199. Zhang, Z.; Liu, J., Improving molecularly imprinted nanogels by pH modulation. *RSC Adv.* **2015,** *5* (110), 91018-91025.

200. Zuo, X.; Xiao, Y.; Plaxco, K. W., High Specificity, Electrochemical sandwich assays based on single aptamer sequences and suitable for the direct detection of small-molecule targets in blood and other complex matrices. *J. Am. Chem. Soc.* **2009,** *131* (20), 6944-6945.

201. McKeague, M.; De Girolamo, A.; Valenzano, S.; Pascale, M.; Ruscito, A.; Velu, R.; Frost, N. R.; Hill, K.; Smith, M.; McConnell, E. M.; DeRosa, M. C., Comprehensive analytical comparison of strategies used for small molecule aptamer evaluation. *Anal. Chem.* **2015,** *87* (17), 8608-8612.

202. Gulbakan, B.; Barylyuk, K.; Schneider, P.; Pillong, M.; Schneider, G.; Zenobi, R., Native electrospray ionization mass spectrometry reveals multiple facets of aptamer-ligand interactions: from mechanism to binding constants. *J. Am. Chem. Soc.* **2018,** *140* (24), 7486-7497.

203. Yangyuoru, P. M.; Dhakal, S.; Yu, Z.; Koirala, D.; Mwongela, S. M.; Mao, H., Single-molecule measurements of the binding between small molecules and DNA aptamers. *Anal. Chem.* **2012,** *84* (12), 5298-5303.

204. Yetisen, A. K.; Jiang, N.; Fallahi, A.; Montelongo, Y.; Ruiz-Esparza, G. U.; Tamayol, A.; Zhang, Y. S.; Mahmood, I.; Yang, S. A.; Kim, K. S.; Butt, H.; Khademhosseini, A.; Yun, S. H., Glucose-sensitive hydrogel optical fibers functionalized with phenylboronic acid. *Adv. Mater.* **2017,** *29* (15), 1606380.

205. Guan, Y.; Zhang, Y., Boronic acid-containing hydrogels: synthesis and their applications. *Chem. Soc. Rev.* **2013,** *42* (20), 8106-8121.

206. Lin, C.; Chen, Y.; Cai, Z.; Zhu, Z.; Jiang, Y.; Yang, C. J.; Chen, X., A label-free fluorescence strategy for sensitive detection of ATP based on the ligation-triggered super-sandwich. *Biosens. Bioelectron.* **2015,** *63*, 562-565.

207. Kong, L.; Xu, J.; Xu, Y.; Xiang, Y.; Yuan, R.; Chai, Y., A universal and label-free aptasensor for fluorescent detection of ATP and thrombin based on SYBR Green Idye. *Biosens. Bioelectron.* **2013,** *42*, 193-197.

208. Jiang, S.; Ge, Z.; Mou, S.; Yan, H.; Fan, C., Designer DNA nanostructures for therapeutics. *Chem* **2021,** *7* (5), 1156-1179.

209. Li, L.; Xing, H.; Zhang, J.; Lu, Y., Functional DNA molecules enable selective and stimuli-responsive nanoparticles for biomedical applications. *Acc. Chem. Res.* **2019,** *52* (9), 2415-2426.

210. Hu, Y.; Cecconello, A.; Idili, A.; Ricci, F.; Willner, I., Triplex DNA nanostructures: from basic properties to applications. *Angew. Chem., Int. Ed.* **2017,** *56* (48), 15210-15233.

211. Dong, Y.; Yao, C.; Zhu, Y.; Yang, L.; Luo, D.; Yang, D., DNA functional materials assembled from branched DNA: design, synthesis, and applications. *Chem. Rev.* **2020,** *120* (17), 9420-9481.

212. Marras, A. E.; Zhou, L.; Su, H.-J.; Castro, C. E., Programmable motion of DNA origami mechanisms. *Proc. Natl. Acad. Sci. U.S.A.* **2015,** *112* (3), 713-718.

213. Kwak, M.; Herrmann, A., Nucleic acid/organic polymer hybrid materials: synthesis, superstructures, and applications. *Angew. Chem., Int. Ed.* **2010,** *49* (46), 8574-8587.

214. Liu, Y.; Zhang, H.; Du, Y.; Zhu, Z.; Zhang, M.; Lv, Z.; Wu, L.; Yang, Y.; Li, A.; Yang, L.; Song, Y.; Wang, S.; Yang, C., Highly sensitive minimal residual disease detection by biomimetic multivalent aptamer nanoclimber functionalized microfluidic chip. *Small* **2020,** *16* (20), 2000949.

215. Nagahara, S.; Matsuda, T., Hydrogel formation via hybridization of oligonucleotides derivatized in water-soluble vinyl polymers. *Polym. Gels Networks* **1996,** *4* (2), 111-127.

216. Li, F.; Wang, C.; Guo, W., Multifunctional poly-N-isopropylacrylamide/DNAzyme microgels as highly efficient and recyclable catalysts for biosensing. *Adv. Funct. Mater.* **2018,** *28* (10), 1705876.

217. Damase, T. R.; Ellington, A. D.; Allen, P. B., Purification of single-stranded DNA by co-polymerization with acrylamide and electrophoresis. *BioTechniques* **2017,** *62* (6), 275-282.

218. Poma, A.; Brahmbhatt, H.; Pendergraff, H. M.; Watts, J. K.; Turner, N. W., Generation of novel hybrid aptamer–molecularly imprinted polymeric nanoparticles. *Adv. Mater.* **2015,** *27* (4), 750-758.

219. Brahmbhatt, H.; Poma, A.; Pendergraff, H.; Watts, J.; Turner, N. W., Improvement of DNA recognition through molecular imprinting: hybrid oligomer imprinted polymeric nanoparticles (oligoMIP NPs). *Biomater. Sci.* **2016,** *4* (2), 281-287.

220. Hu, M.; Yuan, C.; Tian, T.; Wang, X.; Sun, J.; Xiong, E.; Zhou, X., Single-step, salt-aging-free, and thiol-free freezing construction of AuNP-based bioprobes for advancing CRISPR-based diagnostics. *J. Am. Chem. Soc.* **2020,** *142* (16), 7506-7513.

221. Pei, H.; Li, F.; Wan, Y.; Wei, M.; Liu, H.; Su, Y.; Chen, N.; Huang, Q.; Fan, C., Designed diblock oligonucleotide for the synthesis of spatially isolated and highly hybridizable functionalization of DNA–gold nanoparticle nanoconjugates. *J. Am. Chem. Soc.* **2012,** *134* (29), 11876-11879.

222. Zhang, X.; Liu, B.; Dave, N.; Servos, M. R.; Liu, J., Instantaneous attachment of an ultrahigh density of nonthiolated DNA to gold nanoparticles and its applications. *Langmuir* **2012,** *28* (49), 17053-17060.

223. Huang, Z.; Zhao, Y.; Liu, B.; Guan, S.; Liu, J., Stronger adsorption of phosphorothioate DNA oligonucleotides on graphene oxide by van der Waals forces. *Langmuir* **2020,** *36* (45), 13708-13715.

224. You, C.-C.; Chompoosor, A.; Rotello, V. M., The biomacromolecule-nanoparticle interface. *Nano Today* **2007,** *2* (3), 34-43.

225. Solomon, J. J.; Fedyk, J.; Mukai, F.; Segal, A., Direct alkylation of 2′-deoxynucleosides and DNA following in vitro reaction with acrylamide. *Cancer Res.* **1985,** *45* (8), 3465-3470.

226. Besaratinia, A.; Pfeifer, G. P., DNA adduction and mutagenic properties of acrylamide. *Mutat. Res.* **2005,** *580* (1-2), 31-40.

227. Atay, N. Z.; Çalgan, D.; Özakat, E.; Varnali, T., Acrylamide and glycidamide adducts of Guanine. *J. Mol. Struct.* **2005,** *728* (1-3), 249-251.

228. Nair, D. P.; Podgorski, M.; Chatani, S.; Gong, T.; Xi, W.; Fenoli, C. R.; Bowman, C. N., The thiol-Michael addition click reaction: a powerful and widely used tool in materials chemistry. *Chem. Mater.* **2014,** *26* (1), 724-744.

229. Chrambach, A.; Rodbard, D., Polyacrylamide gel electrophoresis. *Science* **1971,** *172* (3982), 440-451.

230. Steenken, S., Purine bases, nucleosides, and nucleotides: aqueous solution redox chemistry and transformation reactions of their radical cations and e-and OH adducts. *Chem. Rev.* **1989,** *89* (3), 503-520.

231. Dizdaroglu, M.; Jaruga, P., Mechanisms of free radical-induced damage to DNA. *Free Radic. Res.* **2012,** *46* (4), 382-419.

232. Vieira, A.; Steenken, S., Pattern of hydroxy radical reaction with adenine and its nucleosides and nucleotides. Characterization of two types of isomeric hydroxy adduct and their unimolecular transformation reactions. *J. Am. Chem. Soc.* **1990,** *112* (19), 6986-6994.

233. García, J. I.; García-Marín, H.; Pires, E., Glycerol based solvents: synthesis, properties and applications. *Green Chem.* **2014,** *16* (3), 1007-1033.

234. Jian, Y.; Handschuh-Wang, S.; Zhang, J.; Lu, W.; Zhou, X.; Chen, T., Biomimetic anti-freezing polymeric hydrogels: keeping soft-wet materials active in cold environments. *Mater. Horiz.* **2021,** *8* (2), 351-369.

235. Lane, L. B., Freezing points of glycerol and its aqueous solutions. *Ind. Eng. Chem.* **1925,** *17* (9), 924-924.

236. Chen, F.; Zhou, D.; Wang, J.; Li, T.; Zhou, X.; Gan, T.; Handschuh-Wang, S.; Zhou, X., Rational fabrication of anti-freezing, non-drying tough organohydrogels by one-pot solvent displacement. *Angew. Chem., Int. Ed.* **2018,** *130* (22), 6678-6681.

237. Rehman, F. N.; Audeh, M.; Abrams, E. S.; Hammond, P. W.; Kenney, M.; Boles, T. C., Immobilization of acrylamide-modified oligonucleotides by co-polymerization. *Nucleic Acids Res.* **1999,** *27* (2), 649-655.

238. Memic, A.; Colombani, T.; Eggermont, L. J.; Rezaeeyazdi, M.; Steingold, J.; Rogers, Z. J.; Navare, K. J.; Mohammed, H. S.; Bencherif, S. A., Latest advances in cryogel technology for biomedical applications. *Adv. Ther.* **2019,** *2* (4), 1800114.

239. Henderson, T. M.; Ladewig, K.; Haylock, D. N.; McLean, K. M.; O'Connor, A. J., Cryogels for biomedical applications. *J. Mater. Chem. B* **2013,** *1* (21), 2682-2695.

240. Kumar, A.; Srivastava, A., Cell separation using cryogel-based affinity chromatography. *Nat. Protoc.* **2010,** *5* (11), 1737-1747.

241. Kumar, A.; Mishra, R.; Reinwald, Y.; Bhat, S., Cryogels: Freezing unveiled by thawing. *Mater. Today* **2010,** *13* (11), 42-44.

242. Chen, X.; Sui, W.; Ren, D.; Ding, Y.; Zhu, X.; Chen, Z., Synthesis of hydrophobic polymeric cryogels with supermacroporous structure. *Macromol. Mater. Eng.* **2016,** *301* (6), 659-664.

243. O'Concubhair, R.; Sodeau, J. R., The effect of freezing on reactions with environmental impact. *Acc. Chem. Res.* **2013,** *46* (11), 2716-2724.

244. Takemoto, H.; Miyata, K.; Ishii, T.; Hattori, S.; Osawa, S.; Nishiyama, N.; Kataoka, K., Accelerated polymer–polymer click conjugation by freeze–thaw treatment. *Bioconjug. Chem.* **2012,** *23* (8), 1503-1506.

245. Agten, S. M.; Suylen, D. P.; Hackeng, T. M., Oxime catalysis by freezing. *Bioconjug. Chem.* **2016,** *27* (1), 42-46.

246. Yu, T.; Zhou, W.; Liu, J., An RNA-cleaving catalytic DNA accelerated by freezing. *ChemBioChem* **2018,** *19* (10), 1012-1017.

247. Hayes, O. G.; McMillan, J. R.; Lee, B.; Mirkin, C. A., DNA-encoded protein Janus nanoparticles. *J. Am. Chem. Soc.* **2018,** *140* (29), 9269-9274.

248. Knutson, S. D.; Sanford, A. A.; Swenson, C. S.; Korn, M. M.; Manuel, B. A.; Heemstra, J. M., Thermoreversible control of nucleic acid structure and function with glyoxal caging. *J. Am. Chem. Soc.* **2020,** *142* (41), 17766-17781.

249. Xu, Y.; Huang, K.; Lopez, A.; Xu, W.; Liu, J., Freezing promoted hybridization of very short DNA oligonucleotides. *Chem. Commun.* **2019,** *55* (69), 10300-10303.

250. Abou Assi, H.; Garavís, M.; González, C.; Damha, M. J., I-motif DNA: structural features and significance to cell biology. *Nucleic Acids Res.* **2018,** *46* (16), 8038-8056.

251. Zeraati, M.; Langley, D. B.; Schofield, P.; Moye, A. L.; Rouet, R.; Hughes, W. E.; Bryan, T. M.; Dinger, M. E.; Christ, D., I-motif DNA structures are formed in the nuclei of human cells. *Nat. Chem.* **2018,** *10* (6), 631-637.

252. Bochman, M. L.; Paeschke, K.; Zakian, V. A., DNA secondary structures: stability and function of G-quadruplex structures. *Nat. Rev. Genet.* **2012,** *13* (11), 770-780.

253. Phan, A. T. n.; Kuryavyi, V.; Luu, K. N.; Patel, D. J., Structure of two intramolecular G-quadruplexes formed by natural human telomere sequences in K+ solution. *Nucleic Acids Res.* **2007,** *35* (19), 6517-6525.

254. Du, X.; Bi, Y.; He, P.; Wang, C.; Guo, W., Hierarchically structured DNA-based hydrogels exhibiting enhanced enzyme-responsive and mechanical properties. *Adv. Funct. Mater.* **2020,** *30* (51), 2006305.

255. Matthews, B. M.; Maley, A. M.; Kartub, K. M.; Corn, R. M., Characterizing the incorporation of DNA into single NIPAm hydrogel nanoparticles with surface plasmon resonance imaging measurements. *J. Phys. Chem. C* **2019,** *123* (10), 6090-6096.

256. Kim, H. N.; Ren, W. X.; Kim, J. S.; Yoon, J., Fluorescent and colorimetric sensors for detection of lead, cadmium, and mercury ions. *Chem. Soc. Rev.* **2012,** *41* (8), 3210-3244.

257. Wang, Y.; Zhu, Y.; Hu, Y.; Zeng, G.; Zhang, Y.; Zhang, C.; Feng, C., How to construct DNA hydrogels for environmental applications: advanced water treatment and environmental analysis. *Small* **2018,** *14* (17), 1703305.

258. Miyake, Y.; Togashi, H.; Tashiro, M.; Yamaguchi, H.; Oda, S.; Kudo, M.; Tanaka, Y.; Kondo, Y.; Sawa, R.; Fujimoto, T.; Machinami, T.; Ono, A., Mercury^{II}-mediated formation of thymine−Hg^{II}−thymine base pairs in DNA duplexes. *J. Am. Chem. Soc.* **2006,** *128* (7), 2172-2173.

259. Ono, A.; Togashi, H., Highly selective oligonucleotide-based sensor for mercury (II) in aqueous solutions. *Angew. Chem., Int. Ed.* **2004,** *116* (33), 4400-4402.

260. Wang, J.; Liu, B., Highly sensitive and selective detection of Hg^{2+} in aqueous solution with mercury-specific DNA and Sybr Green I. *Chem. Commun.* **2008,** (39), 4759-4761.

261. Wang, D.; Hu, Y.; Liu, P.; Luo, D., Bioresponsive DNA hydrogels: beyond the conventional stimuli responsiveness. *Acc. Chem. Res.* **2017,** *50* (4), 733-739.

262. Lee, J. B.; Peng, S.; Yang, D.; Roh, Y. H.; Funabashi, H.; Park, N.; Rice, E. J.; Chen, L.; Long, R.; Wu, M.; Luo, D., A mechanical metamaterial made from a DNA hydrogel. *Nat. Nanotechnol.* **2012,** *7* (12), 816-820.

263. Yao, C.; Tang, H.; Wu, W.; Tang, J.; Guo, W.; Luo, D.; Yang, D., Double rolling circle amplification generates physically cross-linked DNA network for stem cell fishing. *J. Am. Chem. Soc.* **2020,** *142* (7), 3422-3429.

264. Zhang, Y.; Tu, J.; Wang, D.; Zhu, H.; Maity, S. K.; Qu, X.; Bogaert, B.; Pei, H.; Zhang, H., Programmable and multifunctional DNA-based materials for biomedical applications. *Adv. Mater.* **2018,** *30* (24), 1703658.

265. Chao, J.; Zhu, D.; Zhang, Y.; Wang, L.; Fan, C., DNA nanotechnology-enabled biosensors. *Biosens. Bioelectron.* **2016,** *76*, 68-79.

266. Ma, S.; Li, Y.; Ma, C.; Wang, Y.; Ou, J.; Ye, M., Challenges and advances in the fabrication of monolithic bioseparation materials and their applications in proteomics research. *Adv. Mater.* **2019,** *31* (50), 1902023.

267. Hui, L.; Zhang, Q.; Deng, W.; Liu, H., DNA-based nanofabrication: pathway to applications in surface engineering. *Small* **2019,** *15* (26), 1805428.